TECHNISCHE UNIVERSITÄT MÜNCHEN
TUM SCHOOL OF NATURAL SCIENCES

# *Breaking the Mirror: Development of New Photochemical Deracemization Reactions*

Johannes Josef Großkopf

Vollständiger Abdruck der von der TUM School of Natural Sciences zur Erlangung des akademischen Grades eines Doktors der Naturwissenschaften genehmigten Dissertation.

| | | |
|---|---|---|
| Vorsitz: | | Prof. Dr. Ulrich K. Heiz |
| Prüfer*innen der Dissertation: | 1. | Prof. Dr. Thorsten Bach |
| | 2. | apl. Prof. Dr. Wolfgang Eisenreich |
| | 3. | Prof. Dr. Patrick Nürnberger |

Die Dissertation wurde am 03.04.2023 bei der Technischen Universität München eingereicht und durch die TUM School of Natural Sciences am 25.04.2023 angenommen.

"*We are all born superstars!*"

from the song "Born This Way" by *Lady Gaga*

The data presented within this dissertation were obtained at the Chair of Organic Chemistry I at the Department of Chemistry of the School of Natural Sciences at the Technical University of Munich between December 2019 and March 2023 and supervised by Prof. Dr. Thorsten Bach.

**First Author Publications**

Plaza, M.*; Großkopf, J.*; Breitenlechner, S.; Bannwarth, C.; Bach, T. Photochemical Deracemization of Primary Allene Amides by Triplet Energy Transfer: A Combined Synthetic and Theoretical Study. *J. Am. Chem. Soc.* **2021**, *143*, 11209−11217.

Großkopf, J.*; Plaza, M.*; Seitz, A.*; Breitenlechner, S.; Storch, G.; Bach, T. Photochemical Deracemization at $sp^3$-Hybridized Carbon Centers *via* a Reversible Hydrogen Atom Transfer. *J. Am. Chem. Soc.* **2021**, *143*, 21241−21245.

Großkopf, J.; Kratz, T.; Rigotti, T.; Bach, T. Enantioselective Photochemical Reactions Enabled by Triplet Energy Transfer. *Chem. Rev.* **2022**, *122*, 1626−1653.

Kutta, R. J.*; Großkopf, J.*; van Staalduinen, N.; Seitz, A.; Pracht, P.; Breitenlechner, S.; Bannwart, C.; Nuernberger, P.; Bach, T. Multifaceted View on the Mechanism of a Photochemical Deracemization Reaction. *J. Am. Chem. Soc.* **2023**, *145*, 2354−2363.

**These authors contributed equally.*

**Conference Contributions**

22nd ORCHEM Lecture Conference 2022, Münster, Germany. "Deracemization of $sp^3$-Carbon Centers by Hydrogen Atom Transfer: En Route to Enantiopure Amino Acids" (Flash Talk and Poster)

ACS Meeting Spring 2022, San Diego, USA. "Overcoming the Equilibrium State: Development of Novel Photochemical Deracemization Reactions" (Presentation).

International CataLysis Networking Conference 2022, Kassel, Germany. "Photochemical Deracemization at $sp^3$-Hybridized Carbon Centers *via* Reversible Hydrogen Atom Transfer" (Poster).

Central European Conference on Photochemistry 2022, Bad Hofgastein, Austria. "Overcoming the Equilibrium State: Development of Novel Photochemical Deracemization Reactions" (Poster).

In this thesis, the relative configuration of racemates is represented by straight lines (bold or hashed). The absolute configuration of enantiomerically pure or enriched compounds is represented by wedge-shaped lines (bold or hashed).

racemate 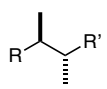


enantiomerically pure
or enantiomerically enriched 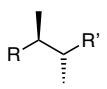

## Acknowledgements

First and foremost, I want to thank my doctoral advisor, *Prof. Dr. Thorsten Bach*, not only for supervising my dissertation but especially for his invaluable advice and tremendous support throughout my entire academic journey. During my B.Sc. and M.Sc. studies his classes inspired me to specialize in organic chemistry and to join his excellent research group focusing on photochemistry. Under his guidance, I was able to freely explore my interests and implement my ideas in our projects, teaching me how to tackle problems and especially how to overcome them. Moreover, he was the one encouraging me to pursue a career in academia and supported me in every way possible. For this mentorship, I will forever be deeply thankful, and I hope that we will stay in close contact even after I have left his group.

I gratefully acknowledge *Dr. Simone Stegbauer and Dr. Stefan Breitenlechner* and their great efforts in all matters concerning lab equipment, safety and management as well as teaching and student lab courses. Especially I want to thank *Stefan* for all his help regarding my projects. No matter if NMR titrations or KIE experiments, he always had an open ear for me and was always there for fruitful discussions.

I want to thank *Kerstin Voigt* for her help in all matters beyond chemistry including nice conversations and for helping me overcome bureaucratic burdens.

Furthermore, I warmly thank *Olaf Ackermann* for his continuous help with the HPLC and for handling the huge number of samples that piled up over the last years because of me.

I am indebted to the collaborators who made this work possible, including *Prof. Dr. Patrick Nürnberger*, *Prof. Dr. Christoph Bannwarth*, *Dr. Roger Jan Kutta*, *Nils van Staalduinen*, and *Philipp Pracht*. Their contributions were essential to the success of the herein presented projects.

Furthermore, I want to extend my gratitude to my former interns for their synthetic assistance as well as to *Dr. Manuel Plaza* and *Antonia Seitz* for their great teamwork and cooperation in pushing our projects.

I want to thank the whole Bach group for unforgettable moments in, but also outside the lab, and for friendships that will last far beyond our shared time in the lab. I will always remember our trips to California and Florence, skiing retreats, the Oktoberfest, Mattsee, and so much more. Especially, I will always cherish my awesome time in Box 3, which would not have been possible without my good friends *Noé Osorio Reineke* and *Dr. Noah*

*Jeremias*. I am convinced that working in the lab will not be the same without you guys, and I will miss you and our conversations.

A big thank you must go to the people who helped me correct this thesis and get the best out of it: *Dr. Anna Quitt, Dennis Meier, Dr. Lisa-Marie Mohr, Thilo Kratz,* and *Tim Langschwager*. Thank you very much for your thoughtful input and the discussions we had. The quality of this work was only possible because of your help.

Finally, I am forever grateful to my loving family including my mother *Jutta*, my father *Reinhold*, my sister *Anna* and our *Lilly,* as well as to my boyfriend *Dennis.* It is only because of them and their unconditional love and support that I am where I am right now in my life. They know me better than anyone else, and I can always count on them. No matter how hard the times, we stood together, and we will always stay together and be there for one another.

## Abstract

Photochemical deracemizations represent a newly developed reaction class that allows for the direct conversion of a racemic mixture into an enantiopure compound. For these reactions, that are impossible to be performed by a single catalyst on the ground state, photochemistry offers ways to overcome thermodynamic constraints and enables the successful realization of such a contra-thermodynamic transformation. Within the scope of this thesis, the broadening of the applicability of photochemical deracemizations, that only use a single chiral catalyst, was examined as well as the development of a new type of deracemization mechanism using hydrogen atom transfer (HAT).

The first successful deracemization of non-cyclic substrates was developed with primary allene amides as the substrate class of choice. By selective triplet energy transfer from a chiral thioxanthone catalyst, an efficient deracemization was observed that allowed for the enantiomeric enrichment of 19 allene amides with an enantiomeric excess of up to 93%. A thorough theoretical analysis unraveled the mechanism of the efficient differentiation between the two enantiomers by the chiral catalyst.

To allow for an expansion of addressable stereogenic elements for deracemizations, a new mode of action for the enantiomeric differentiation was developed that is based on selective HAT initiated by an excited chiral benzophenone catalyst. It was shown that by this approach, the $sp^3$-hybridized stereogenic center was deracemized in a variety of different hydantoins (27 examples) leading to an enantiomeric excess of up to 99%. Intrigued by the excellent catalytic performance and versatility of this approach, an in-depth mechanistic analysis was undertaken that combined preparative, spectroscopic and theoretical investigations allowing for a comprehensive understanding of the involved intermediates. This knowledge can be used for the development of future deracemizations of various substrate classes.

## Kurzzusammenfassung

Photochemische Deracemisierungen stellen eine neue Klasse an Reaktionen dar, die die direkte Umwandlung eines Racemats in eine enantiomerenreine Verbindung ermöglicht, ohne hierbei die Zusammensetzung der Verbindung zu ändern. Für diese Reaktionen, die mit einem einzigen Katalysator nicht unter thermischen Bedingungen realisierbar sind, ermöglicht der Einsatz der Photochemie die Überwindung thermodynamischer Beschränkungen und die Realisierung dieser contra-thermodynamischen Reaktionen. Im Rahmen dieser Dissertation wurde die Erweiterung der Anwendbarkeit von Deracemisierungen untersucht, welche durch einen einzigen chiralen Katalysator ermöglicht werden. Überdies konnte eine neue Deracemisierungsmethode entwickelt werden, die die Verwendung eines Wasserstoffatomtransfers zur Grundlage hat.

Die erste erfolgreiche Deracemisierung von azyklischen Substraten wurde entwickelt, wobei als Substrat primäre Allenamide gewählt wurden. Durch selektiven Triplett-Energietransfer, initiiert durch einen chiralen Thioxanthon-Katalysator, wurde eine effiziente Deracemisierung erreicht, die die Anreicherung eines Enantiomeres in 19 Fällen mit einem Enantiomerenüberschuss von bis zu 93% ermöglichte. Eine umfassende theoretische Analyse analysierte den Mechanismus der effizienten Differenzierung zwischen den beiden Enantiomeren durch den chiralen Katalysator.

Um eine Erweiterung der adressierbaren stereogenen Elementen für Deracemisierungen zu erreichen, wurde eine neue Differenzierungsmethode entwickelt, die auf einem selektivem Wasserstoffatomtransfer durch einen angeregten chiralen Benzophenon-Katalysator basiert. Es wurde gezeigt, dass durch diesen Ansatz das $sp^3$-hybridiserte Stereozentren einer Vielzahl von verschiedener Hydantoinen (27 Beispiele) deracemisiert wurde, wodurch ein Enantiomerenüberschuss von bis zu 99% erreicht werden konnte. Basierend auf der hervorragenden Leistung und Vielseitigkeit dieser Deracemisierung wurde eine umfassende mechanistische Analyse durchgeführt, die präparative, spektroskopische und theoretische Untersuchungen kombinierte und ein tieferes Verständnis des zugrundeliegenden Mechanismus ermöglichte. Dieses Wissen kann für die Entwicklung zukünftiger Deracemisierungen verschiedener weiterer Substratklassen herangezogen werden.

*Für meine Familie.*

## Table of Contents

# 1 Biological Homochirality and the Break in the Mirror

## 1.1 Biological Homochirality

With projected sales figures of USD 133.2 billion by 2026, the global market for chiral chemicals can be considered as one of the fastest growing sectors in chemical industry.[1] Especially their use in the synthesis of chiral pharmaceuticals, making up 56% of all small molecules currently used in therapy, stimulates this continuous positive trend.[2,3] Nevertheless, currently only 12% of chiral drugs are marketed as their single enantiomer, despite potentially superior pharmacokinetics and potency.[4] Recently, a growing number in requests for authorization of enantiopure pharmaceuticals by the Food and Drug Administration (FDA) has been registered, leading to an increasing number of newly, high-selling enantiopure drug molecules, including **1**-**4** (Figure 1).[5-11]

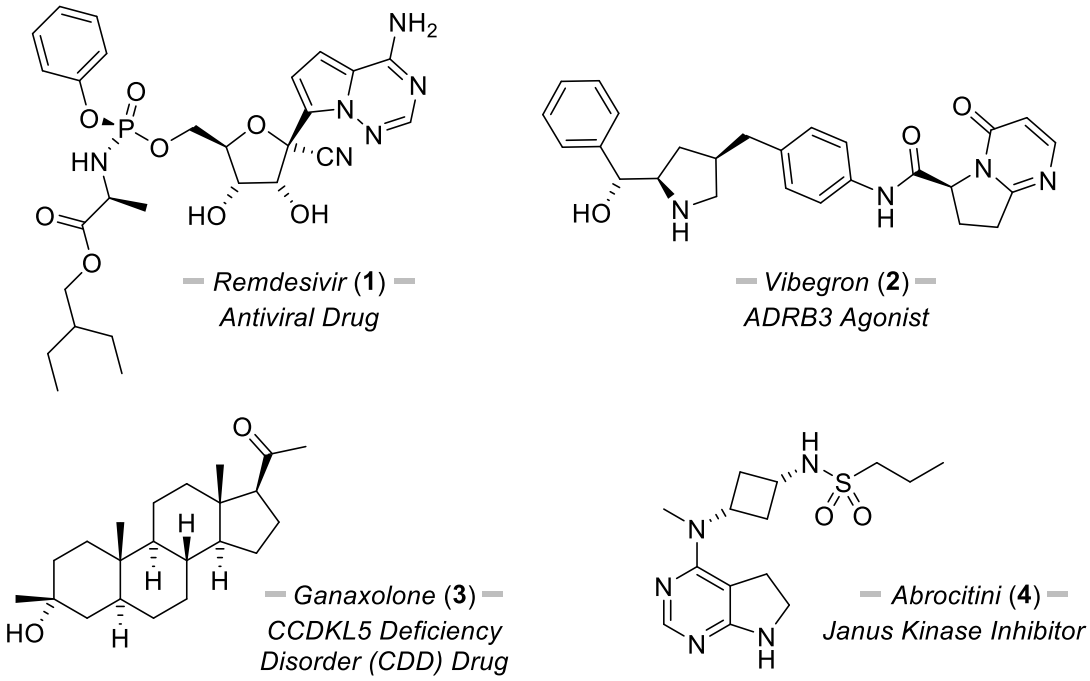


**Figure 1.** Selection of newly FDA-approved, high-selling enantiopure drugs and their pharmacological applications.

The increased potency of enantiopure compounds can be traced back to the, in many cases, inactivity of the compound's mirror image *in vivo*. This is the result of an important principle of how life is constructed on earth: *homochirality*. Organisms themselves are chiral and in most cases consist of only one of the two mirror images.[12-14] Therefore, an encounter between an organism's chiral receptors and a racemic drug molecule leads to the formation of two diastereomeric complexes with different, if not opposite, chemical properties.[15] Prime examples for this inherent chirality in biological systems are DNA and

enzymes, without which complex life would not have emerged (Figure 2). In these essential macromolecules one specific enantiomer is used selectively as a building block, such as 2-deoxy-D-ribose (**5**) in DNA or L-amino acids in enzymes[16], such as L-glutamic acid (**6**) in *Candida albicans Mtr2*.[17] Although biological homochirality is ubiquitous in biological chemistry, there is still a debate on how the *break in the mirror* initially occurred.

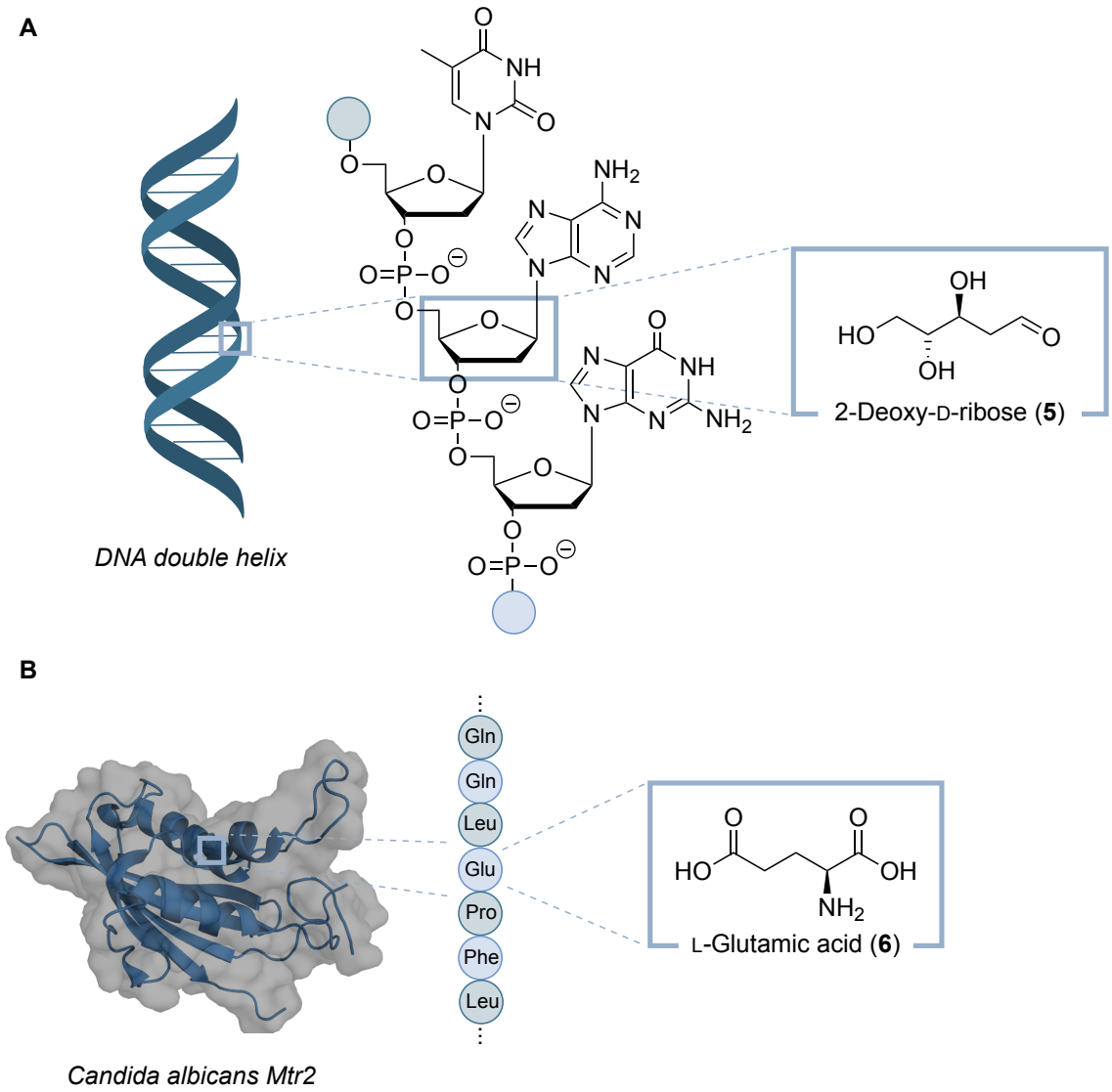


**Figure 2. A**: Exemplary molecular structure of a fragment of the right-handed DNA double helix with D-ribose (**5**) as its enantiopure core structure. **B**: Excerpt of the amino acid sequence of *Candida albicans Mtr2*, an example for a naturally occurring enzyme, exemplifying the use of L-amino acids such as L-glutamic acid (**6**) as building blocks.

## 1.2 The Origin of Asymmetry

Several theories on the emergence of biological homochirality have been established, two of which will be exemplified here: Over a long time period, it was common consensus that the natural laws and, thus, the universal interactions, *e.g.* gravitation and electromagnetism, are symmetric.[18] As a consequence, any event based on these interactions performed inversely, would result in the same outcome. Notably, the 4$^{th}$ fundamental interaction between bosons, the *weak force*, is indeed asymmetric.[19,20] Hence, this weak nuclear force can theoretically distinguish between enantiomers, manifested in the non-parity of the electron-spin during $\beta$-decay. It is, therefore, hypothesized that the resulting enantio-differentiating radiolysis or the photolysis of a racemate by circularly polarized electromagnetic radiation caused the preferential decay of one enantiomer, resulting in the initial imbalance in enantiomers.[21]

This deterministic explanation contrasts with a more stochastic approach towards the origin of asymmetry, which is based on *absolute asymmetric synthesis*.[22,23] This term classifies the spontaneous formation of enantiomerically enriched substrates without the intervention of an external optically active mediator. This phenomenon can be observed during the spontaneous formation of enantiopure crystals by *Ostwald* ripening out of a racemic solution,[24] which was already reported for tartaric acid by *Louis Pasteur* in 1848.[25,26] This might have caused the formation of catalytically active crystals, which had (auto)catalytic abilities allowing them to transfer their chirality onto other substrates.

The aforementioned theories share one key aspect in order to lead to homochirality: the need for chiral amplification after the initial breaking of symmetry. Thus, a suitable mechanism for amplifying the chiral information is key for the proliferation of chiral information and ultimately to a homochiral world.[27-29]

A concluding answer of how nature was able to initially take the step from racemic to homochiral still remains elusive. Nevertheless, synthetic organic chemistry can be a powerful tool for the elucidation of the mechanisms that might have been operational along the way. Especially the field of organocatalysis, awarded with the *Nobel Prize* in Chemistry for *David W. C. MacMillan* and *Benjamin List* in 2021,[30] employs simple chiral organic molecules as catalysts, *e.g.* L-proline (**7**) or imidazolidinone **8**, for creating defined chirality (Figure 3).

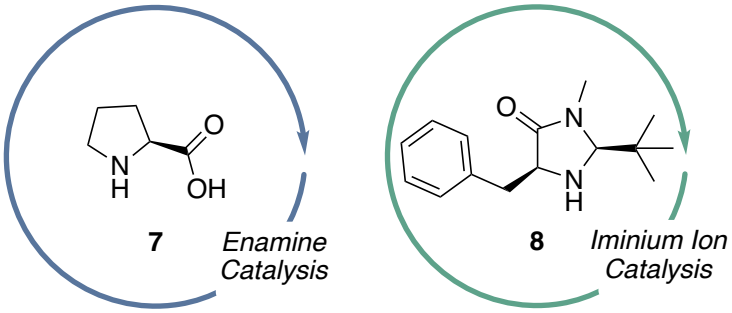


**Figure 3**. Prominent examples of potent chiral organocatalysts developed by *MacMillan* and *List* for enamine and iminium ion catalysis, respectively.

Hence, these reactions already approach ideal examples of chirality transfer and amplification.[31-34] However, thermal organocatalysis is not capable of breaking the enantiomeric parity of a given chiral substrate without changing its constitution. Photochemistry, however, has the potential to overcome intrinsic restriction of thermal chemistry in the ground state by unlocking novel reaction pathways otherwise inaccessible.[35]

The scope of the presented work comprises an outline of the prerequisites for reactions required to overcome thermal reaction equilibria. Furthermore, recent advances in the context of contra-thermodynamic reactions in the excited state are highlighted. The final part of this dissertation will elaborate how photochemistry enables the selective transformation of a racemate into one single enantiomer by breaking the mirror image. This reaction mode will eventually give rise to not only new avenues in the synthesis of valuable single-enantiomer drugs, but also can be applied to achieve a better understanding of how nature became what it is today – homochiral.

# 2 The Principle of Microscopic Reversibility

## 2.1 Reactions in the Ground State

In order to design a catalytic chemical reaction that is capable of overcoming thermodynamic constrains and of breaking the parity of enantiomers in a racemate, a fundamental principle of thermal chemistry has to be considered: microscopic reversibility.[36] The principle of microscopic reversibility is a direct consequence of transition state theory.[37] It states that, if a system is in equilibrium, any molecular process and the reverse of that process will take place averaged at the same rate.[38,39] This implies that, when considering the elementary steps of a reaction, the reaction path of the backward reaction must take exactly the same reaction pathway as the forward reaction, as it affords the least energy in both ways. Thus, microscopic reversibility can be set equal to the principle of *detailed balance*.[40] A chemical reaction at equilibrium, therefore, does not show reactivity on a macroscopic scale but on a microscopic scale with the elementary processes taking place in the forward and backward direction. In the following, an exergonic reaction from **A** to **B** *via* an intermediate (**IN**) is considered (Scheme 1).[36,41] At equilibrium, compounds **A**, **B** as well as **IN** are in balance with each other. Forward and backward reactions take place continuously with a constant ratio of their rate constants *via* the same transition state on the same potential energy surface. In this case, a thermodynamic product distribution is to be expected with a bias for **B** due to its lower *Gibbs* free energy $G^{\circ}$.

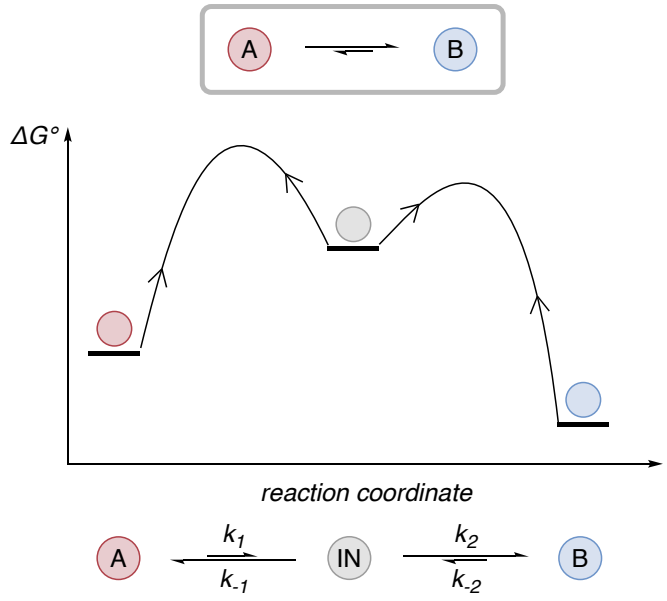


**Scheme 1.** Reaction profile of the reversible, exergonic reaction from **A** to **B** *via* intermediate **IN** at thermal equilibrium. The observed macroscopic reaction rate equals 0 whereas the individual microscopic reaction rates average out.

This equilibration towards the thermodynamically more favorable distribution between **A** and **B** renders the formation of the higher energetic substrate to be difficult in a closed system under thermal conditions in the case of endergonic reactions. Even if the energetic difference between **A** and **B** is small, microscopic reversibility will lead to a thermodynamic equilibration of the reaction network towards substrate **A**. A prime example of a reaction class with such an energetic profile are $E \rightarrow Z$ isomerizations of alkenes.[42,43] The formation of the *Z*-isomer (*Z*-**9**), if not thermoneutral ($\Delta G^{\circ} = 0$), is energetically unfavorable, leading to the preferred *E*-isomer (*E*-**9**) (Scheme 2). Overcoming this intrinsic thermodynamic directionality and creating the ability to dictate reaction outcomes of contra-thermodynamic reactions such as olefin isomerizations, is highly desirable.

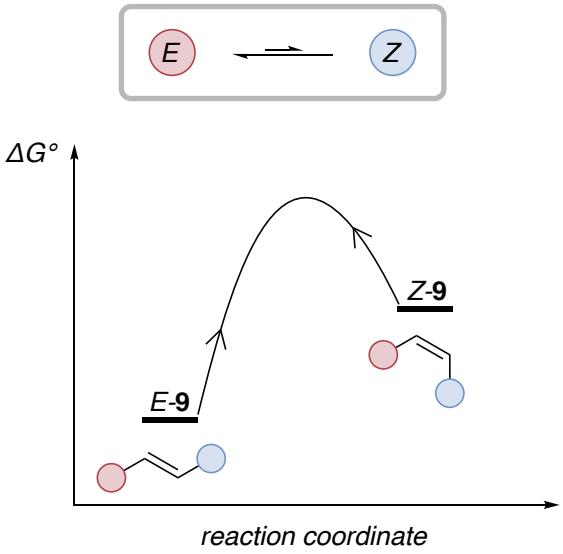


**Scheme 2.** Generic reaction profile for the isomerization reaction between an *E*- and *Z*-olefin, in favor for the more stable *E*-configured diastereoisomer *E*-**9**.

In the above-mentioned reaction archetype between two isomers **A** and **B** with different energies, the preferred formation of the more stable isomer is governed by thermodynamics. However, this is not the case for enantiomers, which are isoenergetic. If an interconversion between enantiomers, proceeding *via* a common achiral intermediate, is in equilibrium and forward and backward reaction follow the exact same pathway, a racemic mixture will always be the consequence (Scheme 3).[44] Due to the principle of microscopic reversibility, both reaction pathways will take place with the same rate constants since the activation barriers for the formation and energies of the enantiomers are equal.[45]

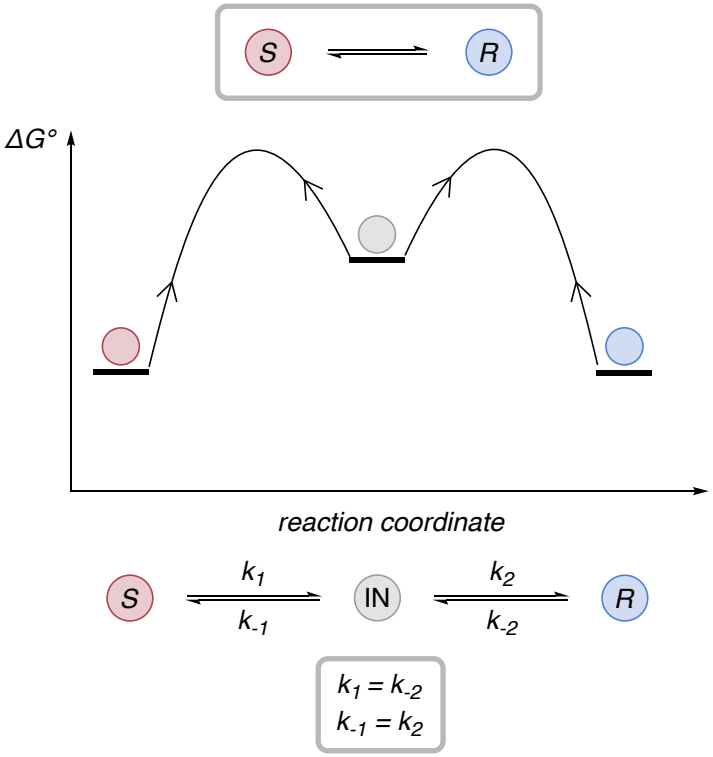


**Scheme 3**. Interconversion of the (*S*) and (*R*) enantiomer of the same compound *via* achiral intermediate **IN** at equilibrium state. A racemic mixture prevails with equal rate constants *k* for forward and backward reaction.

This is demonstrated when an enantiopure compound, such as ketone (*S*)-**10** with an α-stereogenic center, is subjected to a simple deprotonation/protonation sequence using a base ($NR_3$, Scheme 4), resulting in the formation of a racemic mixture *via* achiral enolate **11**.

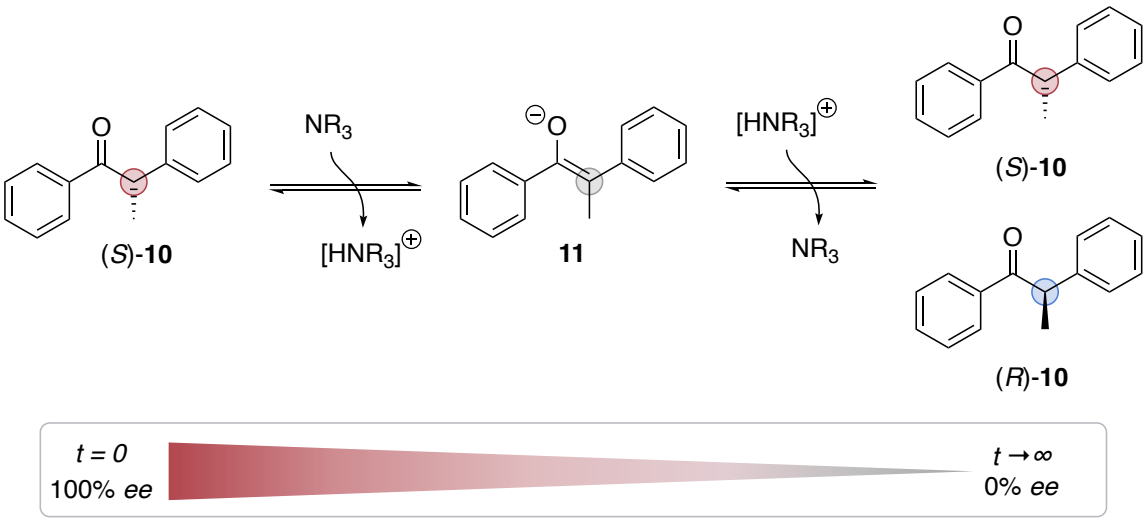


**Scheme 4.** Racemization of ketone (*S*)-**10** *via* achiral enolate **11** by deprotonation. In equilibrium, due to the racemate being entropically favored over the enantiopure compound, the chiral information is lost.

As soon as intermediate **11** is formed from either enantiomer, the chiral information is lost and no differentiation between the two enantiofaces is possible anymore. Thus, the racemization is governed by the inability of achiral intermediates to "remember" the chirality of their progenitor in an equilibrium. This ultimately leads to an increase in entropy within the system which can be determined as the actual driving force of racemization, with microscopic reversibility guaranteeing for a reversible reaction mechanism.[46,47]

In order to develop a method to break the parity of a racemate, *i.e.* to deracemize it, these issues have to be overcome. Taking ketone *rac*-**10** as a case study, the selective formation of an enolate out of one enantiomer, *e.g.* by a chiral *Lewis* acid **12**, appears to be feasible at first glance, as there is precedence for the stereoselective protonation of similar enolates (Scheme 5).[48-55] Nonetheless, due to microscopic reversibility, the reverse reaction of a catalytic step must proceed *via* the same catalytic path as the forward reaction. Consequently, it would be impossible to realize a deracemization under these conditions within a single operation,[36,56] as complexation with chiral *Lewis* acid **12** and subsequent deprotonation to enolate **13** might be favored for one enantiomer, *e.g.* (*R*)-**10**, but the same applies to the reverse reaction under equilibrium conditions due to an identical reaction pathway. Hence, the closed system will always maintain respectively equilibrate towards its entropically favored state, the racemate.[36]

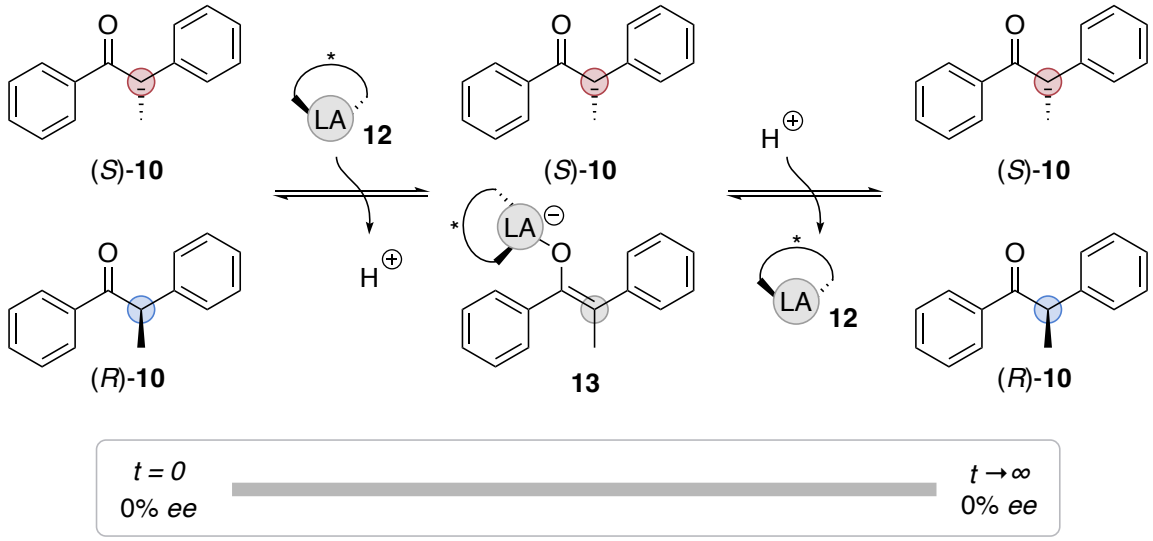


**Scheme 5.** Enolization/protonation sequence of a chiral ketone *rac*-**10** using a chiral *Lewis* acid **12**. The enantiomeric excess does not change over the course of the reaction as the elementary steps of the closed catalytic system are in full equilibrium with each other.

## 2.2 Reactions in the Excited State

The previously mentioned restrictions regarding the formation of contra-thermodynamic products as well as achieving a deracemization under thermal conditions, make photochemistry an elegant solution to overcome these issues.[41,57] Upon photoexcitation, a substrate or a photocatalyst is excited into a higher lying potential energy surface. By subsequent relaxation along the energy surface respectively by activation of another substrate, metastable intermediate **IN** can be accessed (Scheme 6).[58] The distinct difference between the thermal and the photochemical reaction pathway is the irreversibility of the latter.[59,60] Using photonic energy as the exogenous driving force, a high energy barrier would have to be overcome thermally by the intermediate in order to reform the initial substrate **A**. Moreover, excitation, bond formation and bond breaking processes can take place along different potential energy surfaces with different multiplicity, *i.e.* singlet and triplet states, which cannot simply proceed in the reverse direction.[41,61,62]

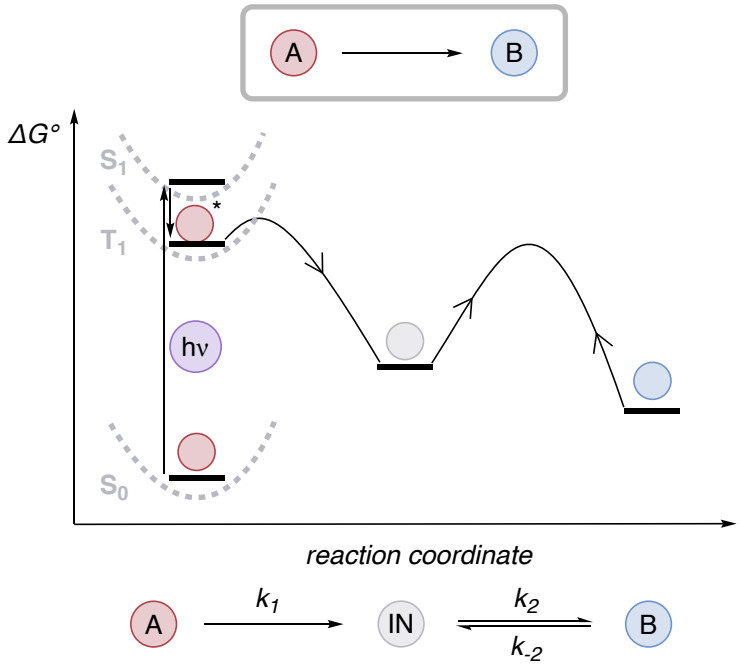


**Scheme 6.** Energy profile of a photochemical reaction initiated by the excitation of **A** leading to the formation of **B** *via* intermediate **IN**. The potential energy surfaces of the ground state ($S_0$), the first excited singlet state ($S_1$) and the first excited triplet state ($T_1$) are shown.

The subsequent thermal reaction, which is the formation of product **B** from intermediate **IN**, is again under the regime of microscopic reversibility. Accordingly, the key idea of contra-thermodynamic reactions is to decouple the irreversible photochemical elementary step from reversible thermal steps.[63] This allows bypassing the constraints of microscopic

reversibility that prevail for ground state chemistry by establishing an equilibrium under photochemical conditions, the photostationary state.[64,65]

This concept can be applied for catalytic as well as non-catalytic reactions. In order to obtain high selectivities in non-catalytic reactions a prerequisite is that at a given wavelength only starting material **A** shows absorbance whereas product **B** is ideally transparent. This approach is especially prominent in the context of photoswitches that use *e.g.* azobenzenes as structural motives.[66-68] The concept utilizes the relatively large difference in the absorption maxima between the two isomeric forms of azobenzene (Scheme 7), with *E*-azobenzene (*E*-**14**) showing absorption in the near-UV (320 nm ≤ λ ≤ 380 nm), whereas *Z*-azobenzene (*Z*-**14**) absorbs in the blue range of the visible spectrum (400 nm ≤ λ ≤ 450 nm).[69]

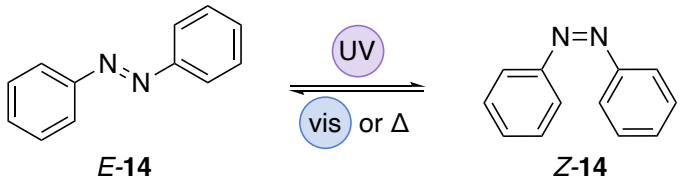


**Scheme 7.** *E*→*Z* isomerization of azobenzene under photochemical and thermal conditions. The *Z*-isomer can only be accessed by light irradiation whereas the *E*-isomer can be formed thermally.

Thus, a judicious choice of the applied wavelength is crucial for a successful reaction outcome in the case of direct excitation which requires a sufficient gap between the absorption maxima of the starting material and product. For that reason, reaction design can be a challenge as for most diastereoisomers[70] this difference is relatively low[42] and even non-existent for enantiomers. Therefore, catalytic systems which do not depend on the absorption properties of the substrates but rather on the different interactions of the substrates with a catalyst need to be developed.

# 3 Contra-Thermodynamic Stereochemical Editing

## 3.1 The Concept of Stereochemical Editing

The term *molecular editing* became increasingly popular during recent years sparked by seminal publications of the groups of *Levin*[71] and *Sarpong*[72] that described efficient ways of altering the skeletal connectivity of various heterocycles. The concept behind these editing strategies is the selective modification of existing molecular scaffolds to allow for the fast access and diversification of molecules that would need extensive *de novo* syntheses otherwise.[73] This concept can not only be applied for skeletal alterations but also for the creation of a defined configuration. Traditional approaches towards stereoselective syntheses involve several bond forming and bond breaking events and are often in need of specifically planned stereoselectivity-determining reactions. Consequently, late-stage introduction of a stereogenic center often requires a newly devised retrosynthetic analysis and, consequently, a new synthetic route. In contrast, *stereochemical editing* separates the connectivity phase, responsible for the molecular complexity, from the configuration phase in which the stereochemistry is defined (Figure 4).[63,74] Essentially, this allows for the flexible modification of different (stereo)isomers as well as the interconversion of enantiomers resulting in modular and more efficient synthetic routes.

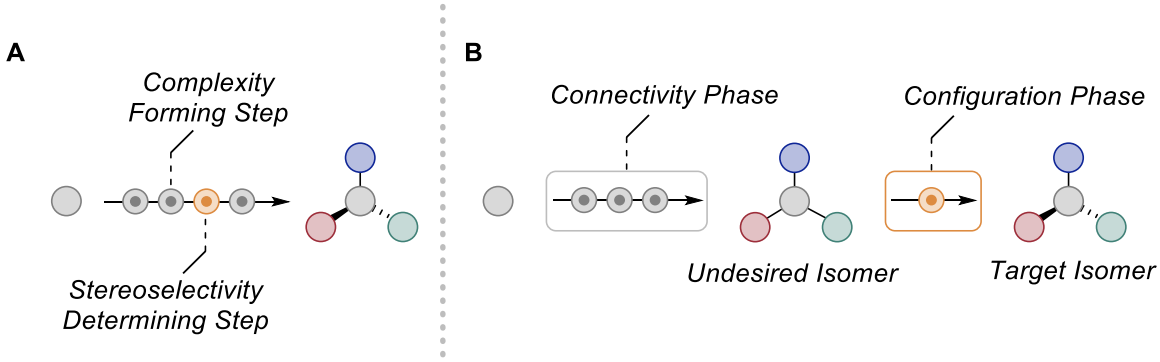


**Figure 4**. Stereoselective synthesis of a target compound by different approaches. **A**: Classical approach using a series of bond forming and breaking steps including a stereoselectivity determining transformation as key step. **B**: Stereochemical editing logic with the connectivity phase creating molecular complexity and the configuration phase forming the desired (stereo)isomer.

The stereochemical editing steps mostly require contra-thermodynamic conditions, *i.e.* catalyzed reactions in the excited state, as in most cases, the thermodynamically more stable product is formed in the connectivity phase. The following section examines recently developed, important methods for the catalytic, contra-thermodynamic stereochemical editing of diastereoisomers and positional isomers under photochemical conditions.

## 3.2 Geometric Isomerization of Olefins

The contra-thermodynamic isomerization of olefins is an elegant way of transferring C–C double bonds to the more energetic, desired isomer.[42] In contrast to azobenzenes (*vide supra*), for structurally abundant styrene derivatives[75] the two isomers hardly differ in their absorption maxima, but show significantly different triplet energies for the *E*- and *Z*-form. Due to the allylic strain-induced rotation of the aryl moiety in the *Z*-isomer, the conjugation of the π-system is disrupted, leading to a higher triplet energy than for the *E*-isomer. By judicious choice of an appropriate triplet sensitizer (*sens.*), a selective excitation of isomer *E*-**15** is possible, which results in triplet state **15-1** with diradical character (Scheme 8).[58,76] Upon rotation around the C–C bond, **15-1** converts to **15-2** and **15-3**, which ultimately results in the formation of isomer *Z*-**15** after intersystem crossing and double bond formation. In the photostationary state *Z*-**15** is accumulated due to the more efficient sensitization of *E*-**15**.

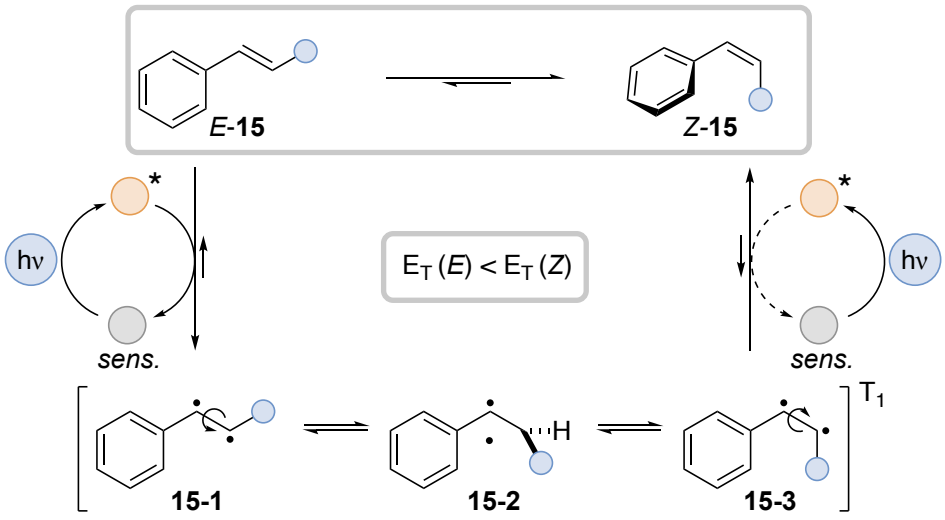


**Scheme 8.** General mechanism of the geometric isomerization of a styrene C-C double bond by triplet sensitization.

Despite this well-known mode of action,[77-83] the work of *Weaver* and coworkers on the *E*→Z isomerization of styrenyl ally amines *E*-**16** sparked new interest in this field (Scheme 9). A combination of $Ir(ppy)_3$ as the triplet sensitizer with DIPEA as a base was

used to transfer an array of *E*-styrenyl based compounds, including those without an amine moiety (*Z*-**17**), to the corresponding *Z*-isomer under blue LED irradiation. Although a photoredox process had been anticipated involving an $\alpha$-amino radical, the complete retention of configuration at the $\alpha$-position of *Z*-**16b** contradicted this mechanism.

*Weaver (2014)*

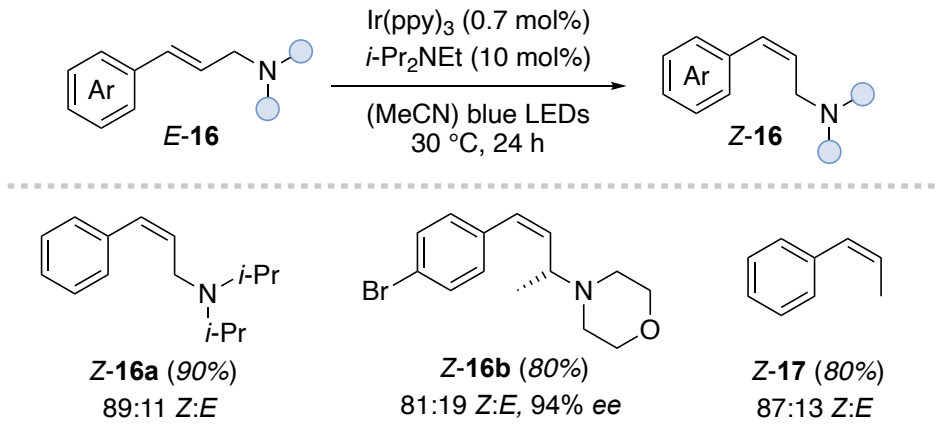


**Scheme 9.** Photochemical *E*→*Z* isomerization of cinnamyl amines (**16**) and styrene derivatives (**17**) using $Ir(ppy)_3$ as a triplet sensitizer.

Based on the photochemical isomerization of retinal by (–)-riboflavin (**19**),[84,85] the group of *Gilmour* adapted this activation strategy and applied it to the isomerization of cinnamic acid derivatives *E*-**18** with excellent yields and selectivities (Scheme 10).[86] The presence of a substituent at the $\beta$-carbonyl position was crucial, boosting the selectivity for the *Z*-isomer. This was reasoned with an increase in allylic strain in *Z*-**18** resulting in pronounced deconjugation.

*Gilmour (2015)*

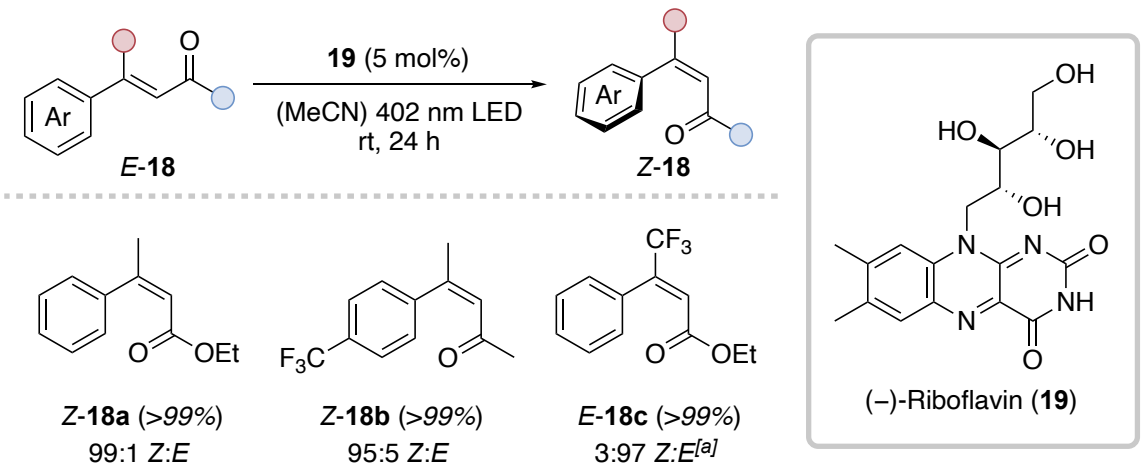


[a]*E*/*Z* ratio is inverted to account for the higher IUPAC priority of fluorine than carbon.

**Scheme 10.** Bioinspired use of (–)-riboflavin (**19**) as triplet sensitizer for the *E*→*Z* isomerization of cinnamic derivatives *E*-**18**.

The same conditions were applied to the isomerization of cinnamonitriles *E*-**20** with moderate to good selectivities (Scheme 10).[87] The effect of the substitution on the allylic strain was especially pronounced for systems with an exocyclic double bond. The bigger the ring size (*Z*-**20a** < *Z*-**20b** < *Z*-**20c**), the more degrees of freedom the aryl ring possesses to twist out of plane, leading to a decreased sensitization efficiency.

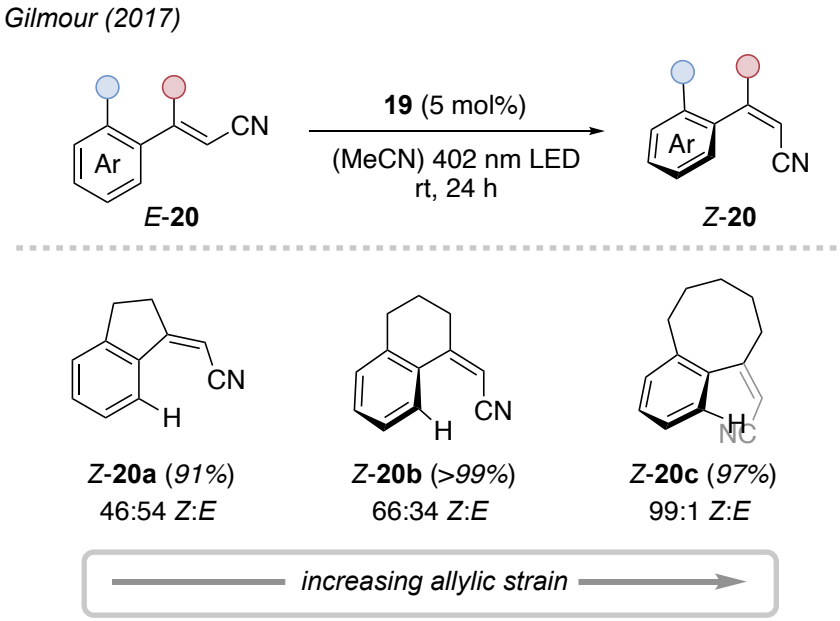


**Scheme 11.** Influence of the allylic strain on the selectivity of sensitized *E*→*Z* isomerizations of cinnamonitriles *E*-**20**.

*β*-Ionyl derivatives could also be addressed and successfully isomerized to the corresponding *Z*-isomer by triplet sensitization.[88] For this compound class reports by *Liu* and *Ramamurthy* were already published in the 1970s.[89-92] Instead of a twisted aryl group, the deconjugation of the two double bonds in the course of the isomerization was the reason for the success of the reaction.

A prerequisite of previously examined isomerization approaches was the existence of an aryl group or an additional double bond in conjugation to the targeted double bond. In order to overcome this limitation, the group of *Gilmour* recently developed two methods that aim at the isomerization of *β*-borylacrylates *E*-**21**[93] and fumarates *E*-**23**[94] (Scheme 12). The resulting contra-thermodynamic *Z*-products (*Z*-**21**/*Z*-**23**) contained (boronic) ester moieties which can act as exit vectors for the stereoselective synthesis of important structural motives such as polyenes.

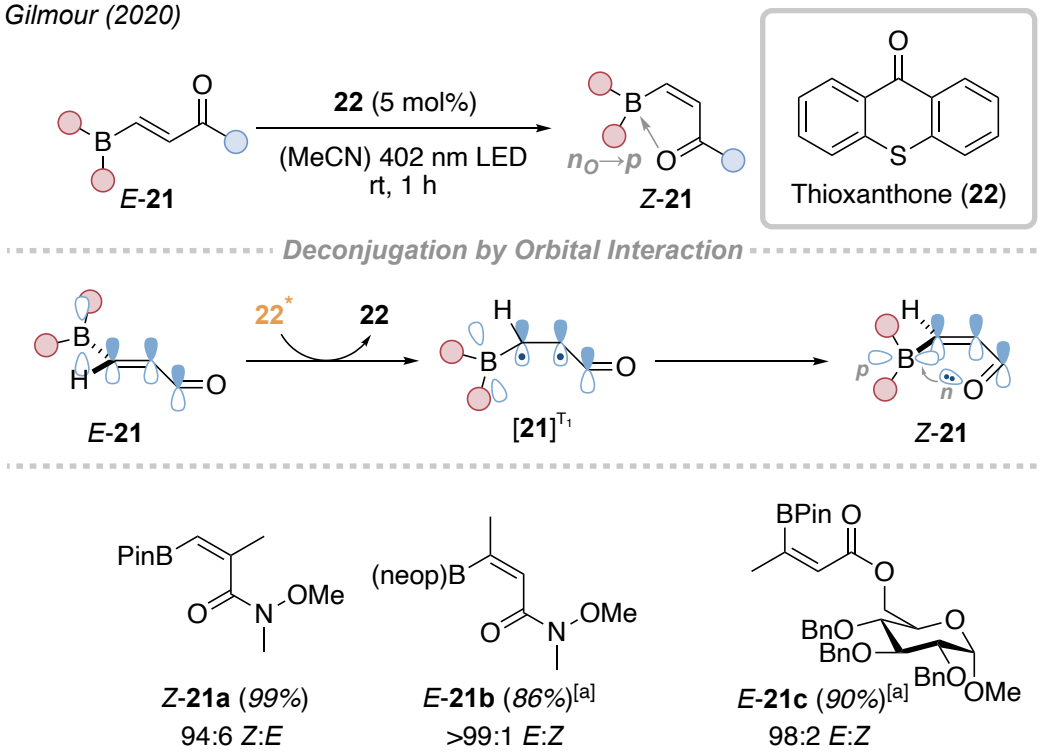


**Scheme 12.** Geometrical *E*→*Z* Isomerization of *β*-boronic ester derivatives *E*-**21** and fumarates *E*-**23** by triplet sensitization exploiting intramolecular orbital interactions.

The key mechanistic feature allowing for high *Z*-selectivity in both cases is the pronounced deconjugation caused by intramolecular orbital interactions. In the case of *E*-**21**, the boron p-orbital is in conjugation with the π-orbitals of the *α,β*-unsaturated ester, making it amenable for triplet sensitization by thioxanthone (**22**). In the triplet state $[\mathbf{21}]^{T_1}$ this conjugation is disrupted, and the system becomes twisted. The dihedral angle increases further in *Z*-**21** because of the population of the p-orbital by the ester oxygen lone pair.[93] The same concept applies for fumarates *E*-**23**, where the triplet sensitization and

subsequent isomerization leads to the through-space interaction of the oxygen lone pair with the π*-orbital of the other carbonyl group of the formed maleate (*Z*-**23**).[94]

Both methods can be applied to a broad variety of structurally diverse substrates which can be further diversified by subsequent transformations that make use of the configuration as well as the high kinetic activity of the newly *Z*-configured double bond.

### 3.3 Positional Isomerization of Olefins

Aside from the geometrical isomerization of C–C double bonds, the development of synthetic strategies to achieve the controlled, positional isomerization of olefins under mild reaction conditions has been a longstanding research field.[43,95] Under thermal conditions, using metal-based catalysts, internal double bonds are generated from terminal double bonds, *e.g.* by *chain-walking* mechanisms.[96,97] Despite these developments, overcoming the thermodynamic bias that dictates the relocation of a double bond remained challenging. Early strategies that allowed monoisomerizations did not lead to the contra-thermodynamic product, but rather to a local thermodynamic minimum in contrast to the global minimum.[98-100]

Based on early work by *Pete*,[101,102] the group of *Gilmour* and *Morack* developed an improved protocol for the positional isomerization of $\alpha,\beta$-unsaturated esters **24** to the $\beta,\gamma$-isomer **26** or *ent*-**26** by employing an amino alcohol catalyst **25** (Scheme 13).[103] The mechanistic framework comprises an initial $E \rightarrow Z$ isomerization of the conjugated double bond to the corresponding geometrical isomer *Z*-**24**. Due to 1,3-allylic strain, the methine hydrogen atom is positioned in a way that makes it amenable for a 1,5-hydrogen atom transfer (HAT) upon re-excitation by a vinylogous *Norrish* type II pathway.[104] This results in dienol **27** with a sufficiently high basicity at the $\alpha$-position to be irreversibly protonated by **25**. The reaction can be rendered enantioselective when using quinine (**25a**) or quinidine (**25b**) respectively, as the chiral proton transfer catalyst. The deconjugation of product **26** or *ent*-**26** enables this contra-thermodynamic process due to a distinct reaction path for the forward and backward reaction, microscopic reversibility is circumvented.

*Gilmour/Morack (2021)*

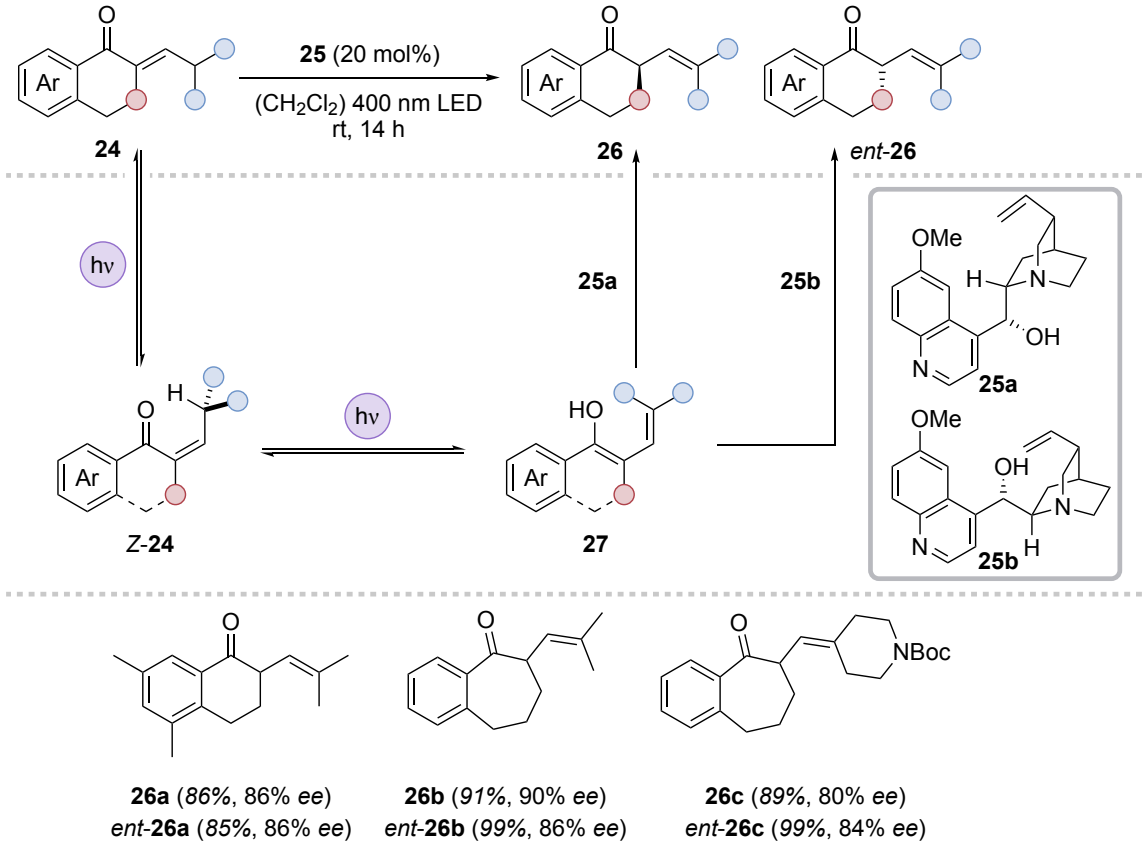


**Scheme 13.** Enantioselective, contra-thermodynamic positional isomerization of $\alpha,\beta$-unsaturated esters **24**.

A drawback of the previously described method consists in its limited substrate scope for positional isomerization which is partly due to the need for direct excitation of the chromophore. The use of a photocatalyst circumvents this prerequisite, therefore, broadening the addressable scope. Recently, two independently developed approaches by the groups of *Knowles*[105] and *Wendlandt*[106] were published that tackle this issue by employing photoredox catalysis. Despite a similar reaction outcome, that is the positional isomerization of an internal double bond to a terminal one for a diverse range of substrates, the reaction pathways clearly differ.

The method by *Knowles* uses oxidizing photoredox catalysts (**PC-1** – **PC-4**) to transfer the electron rich internal double bond of substrates **28** into the corresponding radical cation **28-1** (Scheme14).[105] 4,4′-Di-*tert*-butyl-2,2′-dipyridine (dtbbpy), initially employed as a ligand, acts as the *Brønsted* base required for deprotonation of **28-1** generating allylic radical **28-2**. This reactive species is trapped by the chromium(II) catalyst affording an allylchromium(III) intermediate. By ligation with methanol a six-membered transition state **28-3** for the regioselective protodemetalation can be accessed, releasing terminal olefin **29** and the oxidized chromium(III) methanolate species. After subsequent reduction by the

reduced photocatalyst $\mathbf{PC}^{-\bullet}$ and final protonation, the necessary chromium(II) species and methanol are regenerated. Due to the higher reduction potential of **29** in comparison to **28**, the product is not amenable for oxidation by the photocatalysts rendering a reverse reaction disfavored.

***Method A:*** *Knowles (2022)*

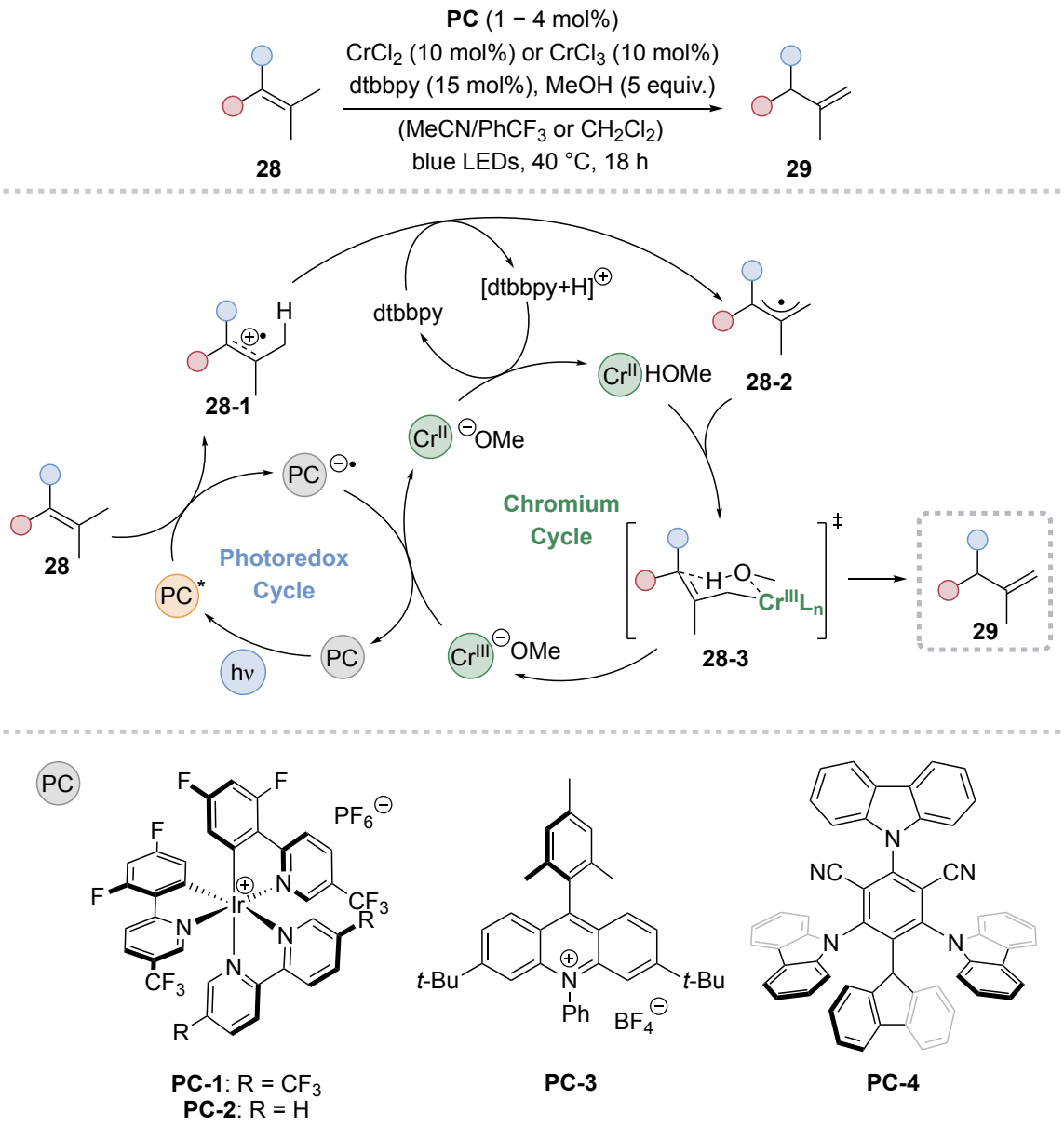


**Scheme 14.** Contra-thermodynamic positional isomerization of olefins **28** using a combination of oxidizing photocatalysts (**PC**) and a chromium(II) active species.

In contrast to the stepwise formation of the allylic radical **28-2** by oxidation and subsequent deprotonation, the group of *Wendlandt* used sodium or tetrabutylammonium decatungstate (DT) catalysts for direct HAT.[106] Due to the steric bulk of the DT anion, the hydrogen abstraction takes place at the lowest substituted allylic position of olefin **30** which is the terminal position, leading to allylic radical **30-1**. Regeneration of the ground state

photocatalyst is achieved by HAT between $[HW_{10}O_{32}]^{4-}$ and the *in situ* formed thiol radical TripS• generating the corresponding aryl thiol. The fate of intermediate **30-1** is governed by an *in situ* generated cobaloxime(II) species **31-1** which captures the radical to form complex **30-2**. It was shown that this complex undergoes a regioselective vinylogous bimolecular homolytic substitution ($S_H2'$)[107-109] with the thiol by HAT or proton-coupled electron transfer (PCET), releasing product **32** and catalyst **31-1**. In those cases, where no thiol is added as a hydrogen atom shuttle, the $S_H2'$ reaction is initiated by the reduced form of the tungsten catalyst or **31-1** itself.[110,111] In this approach, a possible reversibility of the process is circumvented by the incapability of the DT anion to abstract a hydrogen atom at the higher substituted carbon atom of **32**.

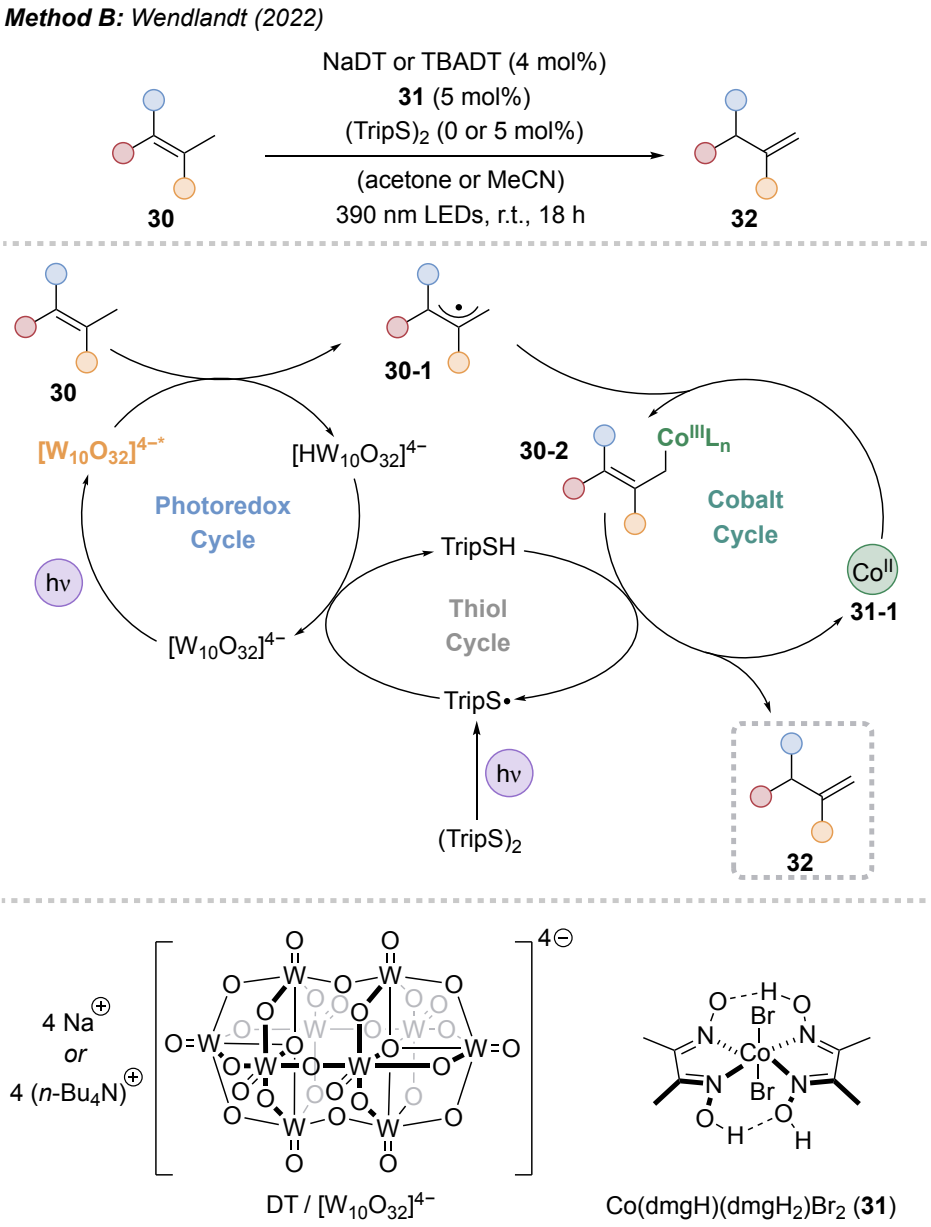


**Scheme 15.** Contra-thermodynamic positional isomerization of olefins **30** using a decatunstate catalyst for HAT and a cobaloxime catalyst **31**.

Both methods cover a wide range of differently substituted C−C bonds including silyl enol ethers as well as enamines and are complementary to each other (Scheme 16).

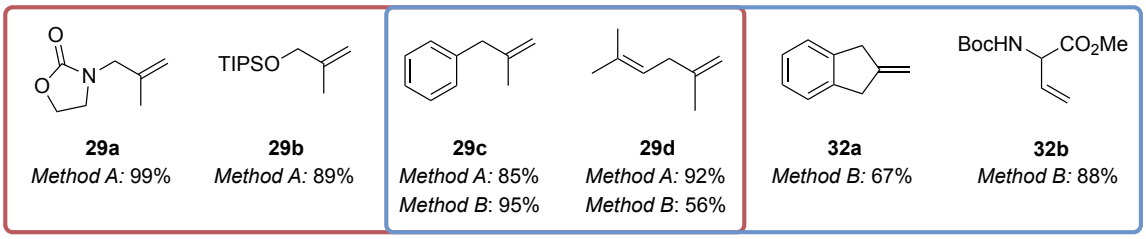


**Scheme 16.** Selected examples of the scope of the positional isomerization approaches by *Knowles* and *Wendlandt*.

## 3.4 Epimerizations

Tetrahedral $sp^3$-stereogenic centers represent the most prominent structural element in stereochemistry, typically formed by stereoselective C–C bond formations. In order to allow for the selective manipulation of the stereogenic information at a distinct $sp^3$- center in a complex molecular scaffold, photochemically driven epimerizations have emerged as a powerful synthetic tool. The main challenge of contra-thermodynamic epimerizations lies within the potential rapid interconversion of the two isomers and the, therefore, challenging selection of the desired epimer from a dynamic equilibrating system.[63] So far, two methods have been reported that use different approaches to address this challenge by either transient thermodynamic control or the use of kinetically favored pathways.

*MacMillan* and coworkers disclosed an epimerization technique for *trans*-1,2-diols (*trans*-**33**) that relies on the interplay of a HAT catalyst, specifically a DT photocatalyst, *in situ* generated thiophenol and methyl boronic acid (Scheme 17).[112] Both epimeric forms of **33** are in equilibrium with each other *via* radical intermediate **33-1** generated upon HAT initiated by the excited DT catalyst. The boronic acid is intended to remove the *cis*-diol *cis*-**33** from the dynamic equilibrium by creating transient thermodynamic control. Due to lower ring strain of boronic ester *cis*-**34** in contrast to *trans*-**34**, a thermodynamic sink is created by the reversal of the intrinsic energetic profile of the two diol epimers. Therefore, *cis*-**34** is accumulated in the photostationary state and upon subsequent cleavage of the boronic ester, *cis*-**33** is released, which results in a two-step-one-pot procedure to obtain the desired contra-thermodynamic diol.

*MacMillan (2022)*

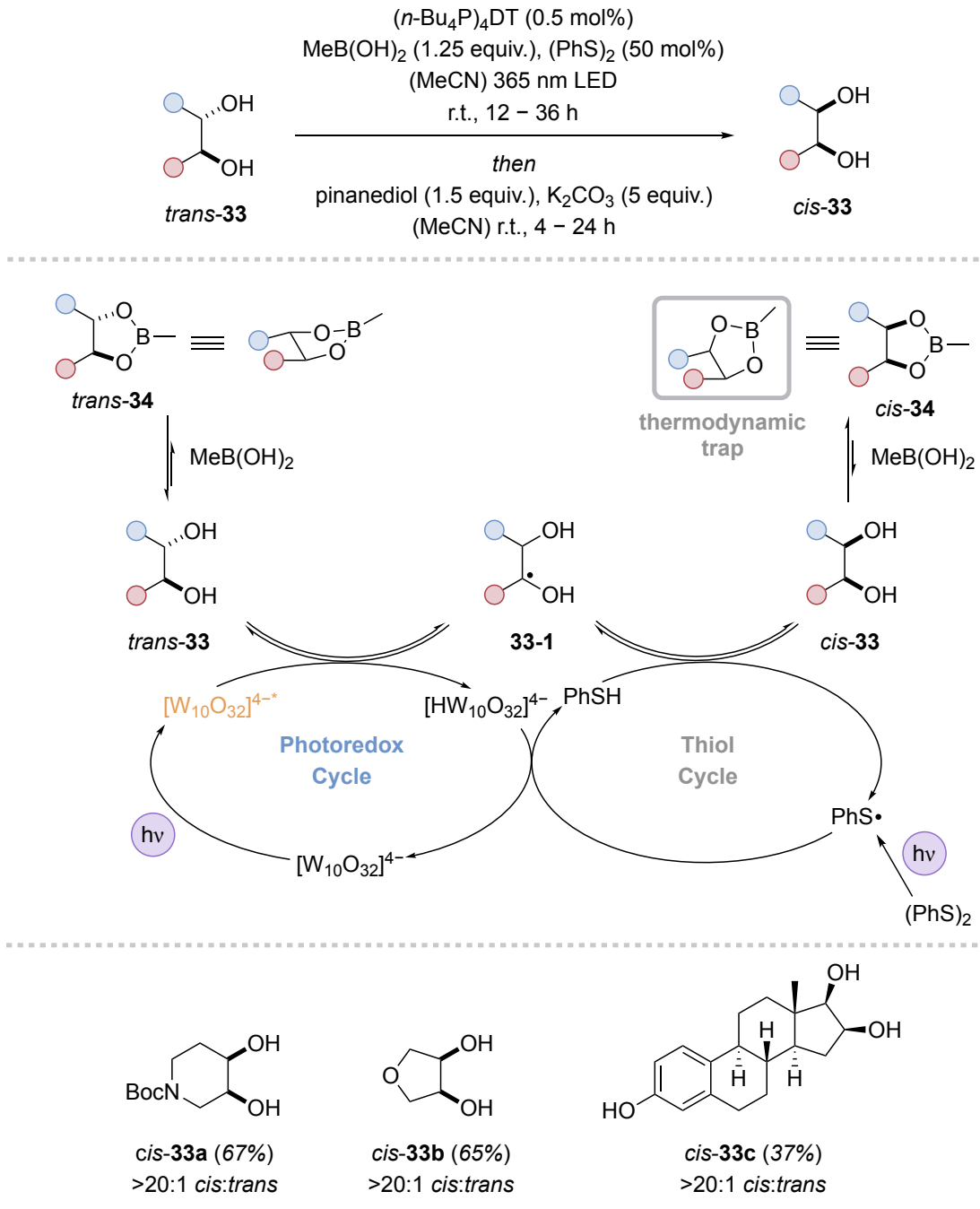


**Scheme 17.** Application of transient thermodynamic control for the contra-thermodynamic epimerization of diols *trans*-**33**.

A different approach was taken by the group of *Wendlandt* that aimed at the epimerization of biomass derived sugar derivatives to their rare sugar epimers (Scheme 18).[113] A previously established combination of photoredox catalyst **PC-4** and quinuclidine[114] was used to generate the corresponding amine radical cation ($R_3N^{+\bullet}$) capable of abstracting an $\alpha$-hydrogen atom from substrate **35** furnishing radical intermediate **35-1**. Bulky adamantanethiol (AdSH) as the co-catalyst donates its hydrogen atom stereoselectively from the most accessible equatorial side to the substrate, generating *epi*-**35**. Mechanistic

data support the formation of hydrogen bonds from the benzoate base to the substrate influencing the observed selectivity. Despite the possibility of both epimers to undergo HAT to $\alpha$-hydroxy radical **35-1**, under the given conditions, preferably the kinetically favored epimer *epi*-**35** is formed, due to the irreversible diastereoselective HAT from the thiol.

*Wendlandt (2020)*

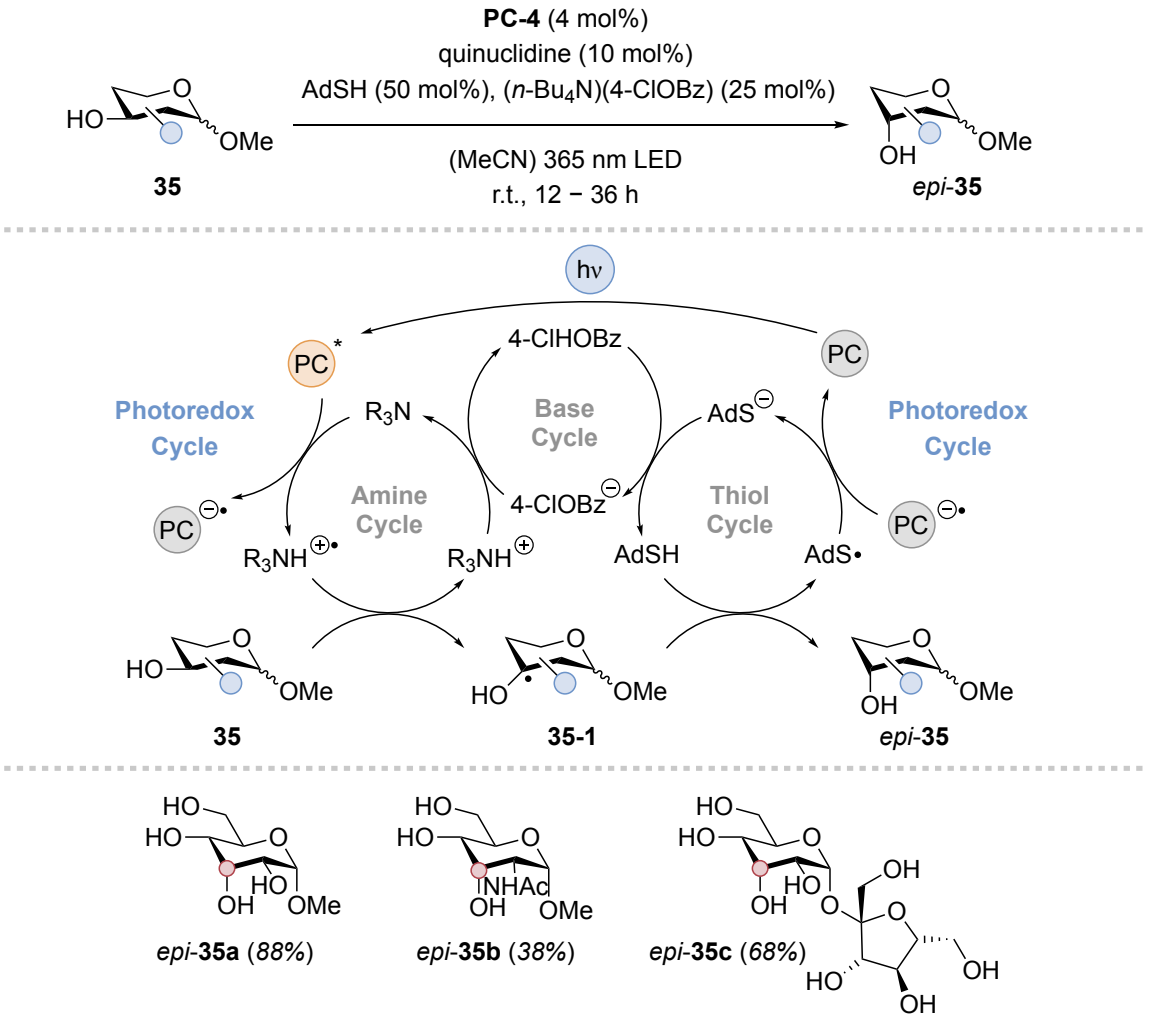


**Scheme 18.** Contra-thermodynamic epimerization of biomass sugars **35** by stepwise HAT to the corresponding epimeric rare sugars *epi*-**35**.

Apart from the presented contra-thermodynamic epimerizations, recent progress in this field focused on the development of other photochemically driven epimerization reactions. Despite similar mechanisms including the use of hydrogen atom transfer, these reactions deliver the thermodynamic product and will not be elaborated further in the scope of this thesis.[115-117]

# 4 Stereochemical Editing by Photochemical Deracemizations

## 4.1 Mechanistic Blueprints for Photochemical Deracemizations

In general, deracemizations refer to a type of reaction "in which a racemate is made non-racemic by increasing the quantity of one enantiomer at the expense of the other".[118] In contrast to (dynamic) kinetic resolutions, during deracemization reactions the constitution and scaffold of the substrate do not change which results ideally in quantitative yield and an enantiopure compound. In the past, several methods were developed that were able to fulfill these criteria by using a kinetic resolution cycling process with an external stochiometric reagent to drive the cycle.[56,119,120] An example for such a classical approach is the deracemization of amines involving the selective oxidation of one enantiomer and a subsequent unselective reduction, *e.g.* the combination of a type-II monoamine oxidase and borane-ammonia complex.[121]

Despite these developments, a catalytic deracemization of a closed system remained elusive until recently.[122] As pointed out before, the main obstacle of realizing a thermal catalytic deracemization is the inherent entropic bias for the racemate to which the system will always equilibrate due to microscopic reversibility (*vide supra*). The key to realize a deracemization comprises the division of the overall reaction into a photochemical and a thermal step that are decoupled from each other and with at least one of them being irreversible (Figure 5).[36] In any case, the reaction must proceed *via* an achiral intermediate **IN** to allow for the inversion of configuration.

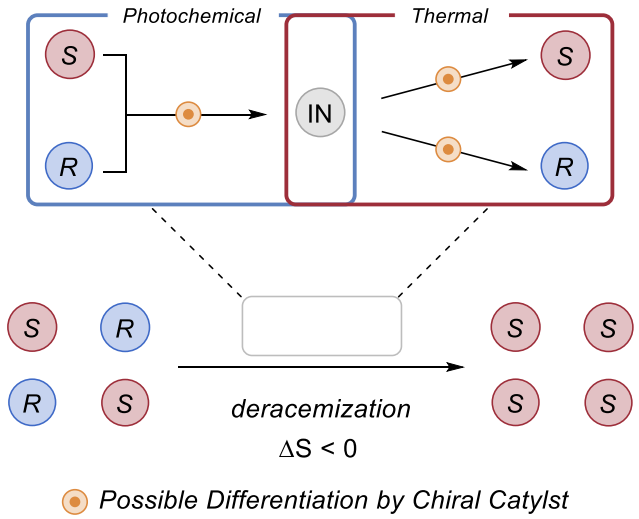


**Figure 5.** General outline of a catalytic photochemical deracemization reaction. The enantiomeric differentiation can occur by selective transformation in the photochemical step or by selective formation of one enantiomer from achiral intermediate **IN**.

The concept is comparable to the strategies for contra-thermodynamic editing of diastereoisomers with the difference that one of the employed catalysts must be chiral in order to allow for a differentiation of the enantiomers. For this differentiation two approaches can be considered:[63] A chiral photocatalyst which interacts differently with each of the two enantiomers can be employed to render the stereoablative step, *i.e.* the formation of the achiral intermediate, stereoselective. This results in the preferential conversion of one enantiomer over the other. A subsequent unselective thermal reaction eventually leads to the formation of both enantiomers. By continuous repetition of this cycle, an enrichment of one enantiomer on the expense of the other is the result. (Figure 6A). Another possibility is the selective transformation of the achiral intermediate to one enantiomer by a chiral catalyst in a thermal reaction. For this approach, chiral catalysts that are used for enantioselective ground state reactions can be employed (Figure 6B). Due to the need for a, at least, dual catalytic system in this scenario, the two catalytic cycles have to be compatible with each other in order to allow for several turnovers.

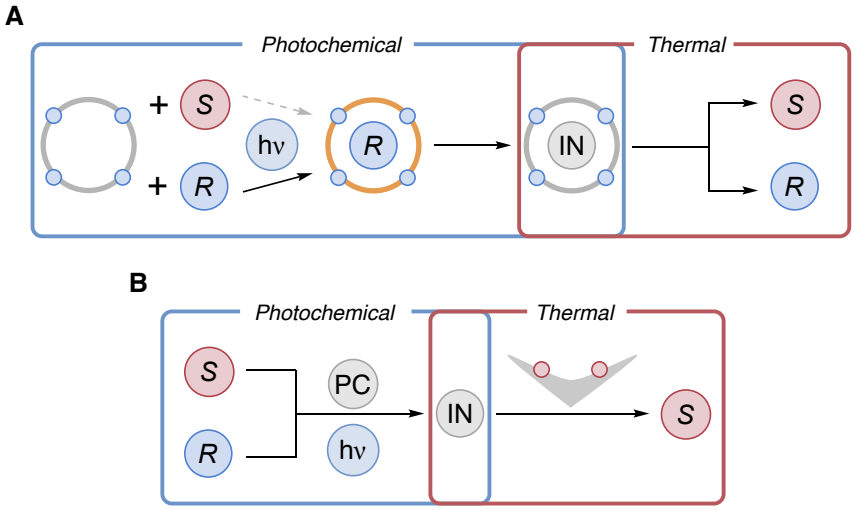


**Figure 6.** Two approaches for achieving a catalytic photochemical deracemization by either differentiation in the photochemical (**A**) or the thermal (**B**) step by a chiral (photo)catalyst.

## 4.2 Deracemizations by a Chiral Photocatalyst

The first successful catalytic deracemization of a closed system was reported by our group demonstrating that the use of a chiral thioxanthone triplet sensitizer (**38**) enables the deracemization of an array of differently substituted six- (**36**) and five-membered (**37**) lactams in high yields and excellent enantioselectivities (Scheme 19).[122,123]

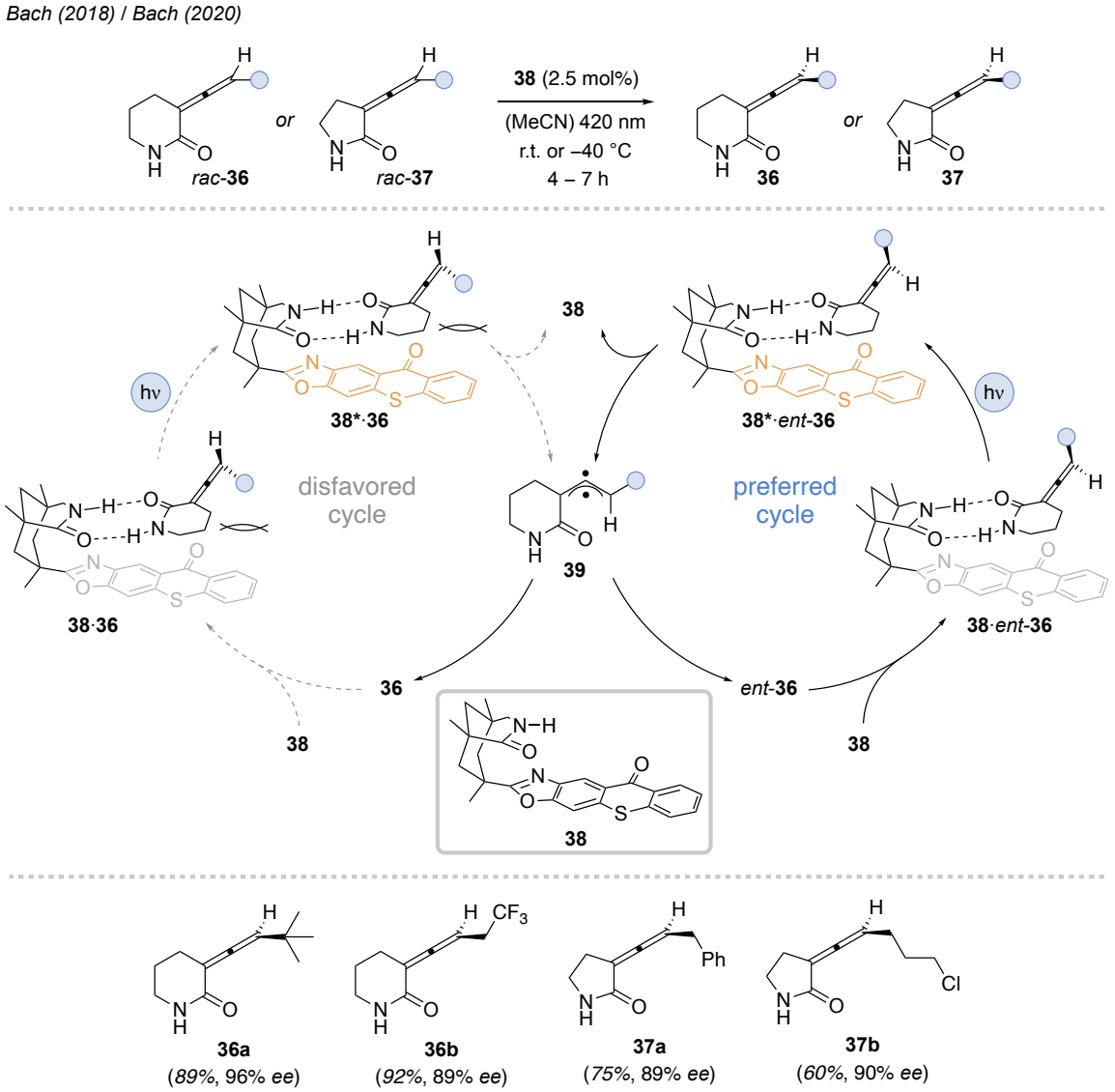


**Scheme 19.** Deracemization of axially chiral allenes *rac*-**36** and *rac*-**37** by triplet energy transfer using chiral thioxanthone catalyst **38** and exemplified mechanism for the conversion of *rac*-**36**.

The employed catalyst possesses the ability of establishing hydrogen bonds with the lactam moiety of the substrate allowing for a precise positioning of the allene in the substrate/catalyst complex (**38**·**36** and **38**·*ent*-**36**). The differentiation between the enantiomers occurs upon complexation with catalyst **38**. The *mismatched* enantiomer **36** shows lower association to the catalyst than *ent*-**36** due to steric repulsions between the bulky terminal residue and **38** (**38**·**36**). Therefore, a higher concentration of the *matched*

diastereomeric complex **38**·*ent*-**36** prevails in solution. Moreover, upon excitation of the thioxanthone moiety, triplet energy transfer preferentially occurs within the *matched* complex, as the distance between the catalyst's chromophore and the allene is lower as compared to the *mismatched* complex. Consequently, the conversion of *ent*-**36** to the corresponding achiral diradical **39** occurs faster. The triplet intermediate features two unpaired electrons in orthogonal orbitals which leads to the ablation of the stereogenic information. Subsequently, intermediate **39** dissociates from the catalyst and relaxes to the two enantiomers upon electron recombination in the ground state. Due to the preferential procession of *ent*-**36** over **36**, a profound enantiomeric excess of **36** is observed in the photostationary state.

Despite their importance in material science,[124,125] the enantioselective synthesis of axially chiral alkenes remains challenging. By translating the previously developed deracemization strategy based on selective triplet energy transfer, our group was able to obtain tetra-substituted alkylidencycloalkanes **40** with high enantioselectivities and excellent yields when sensitizer *ent*-**38** was applied (Scheme 20).[126]

*Bach (2022)*

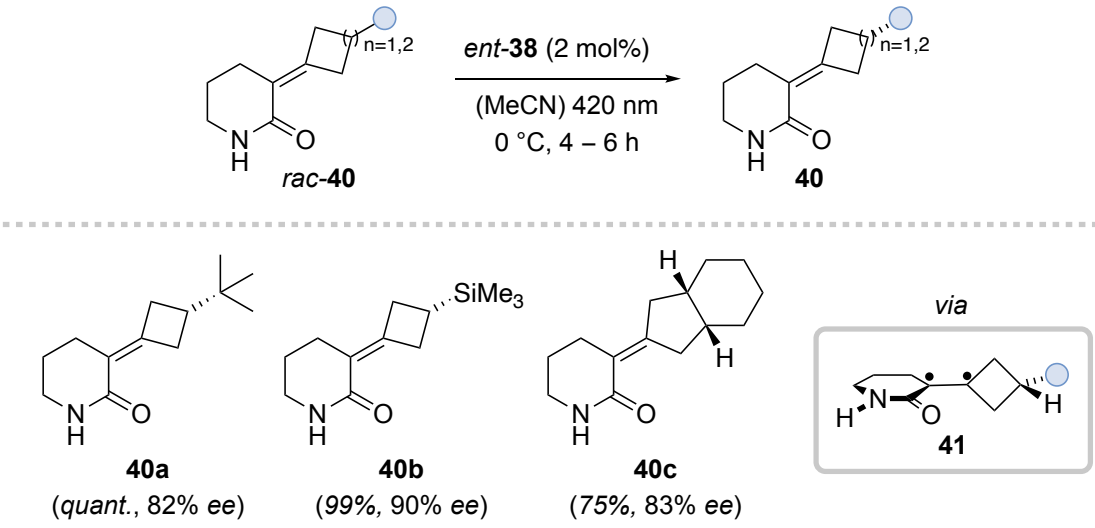


**Scheme 20.** Deracemization of axially chiral alkenes *rac*-**38** *via* achiral diradical **41** by means of selective triplet energy transfer.

The underlying principle of the deracemization *rac*-**40** → **40** follows a similar mechanism as for allenes **36** and takes place *via* diradical **41**. However, excited state density functional theory (DFT) calculations revealed that the main difference in the sensitization rate between the *matched* and *mismatched* catalyst/substrate complex is rooted in the energetic difference of the complexes' triplet states. Due to a lower energetic barrier for sensitization,

the *matched* complex exhibits a faster sensitization rate leading to the preferred procession *ent*-**40** → **41**.

Using selective triplet sensitization as the activation mode not only enables the excitation of C–C double bonds, but also the cleavage of C–C single bonds. The orbital structure of cyclopropanes in the excited state shows high similarity to that of double bonds[127] and their triplet energy is low enough to be addressed by common triplet sensitizers[58]. Inspired by studies of *Hammond* and *Cole*[128] as well as work of *Ouannès*[129], our group expanded the strategy of using triplet sensitization for deracemizations to spirocyclopropyl oxindoles *rac*-**42** (Scheme 21).[130] Depending on the substitution of the cyclopropane and, thus, the triplet energy of the substrate, either chiral thioxanthone **38** or xanthone **43**, which exhibits a higher triplet energy, was applied. In this case, for the first time, the achiral intermediate of a deracemization, diradical **44**, was detected by transient absorption (TA) spectroscopy with a lifetime of $\tau = 22$ µs in acetonitrile. Combining the results of the TA measurements and the association behavior of **42** and *ent*-**42** towards the catalyst, a coherent picture of the deracemization mechanism similar to the allene deracemization (*vide supra*) was obtained.

*Bach (2020)*

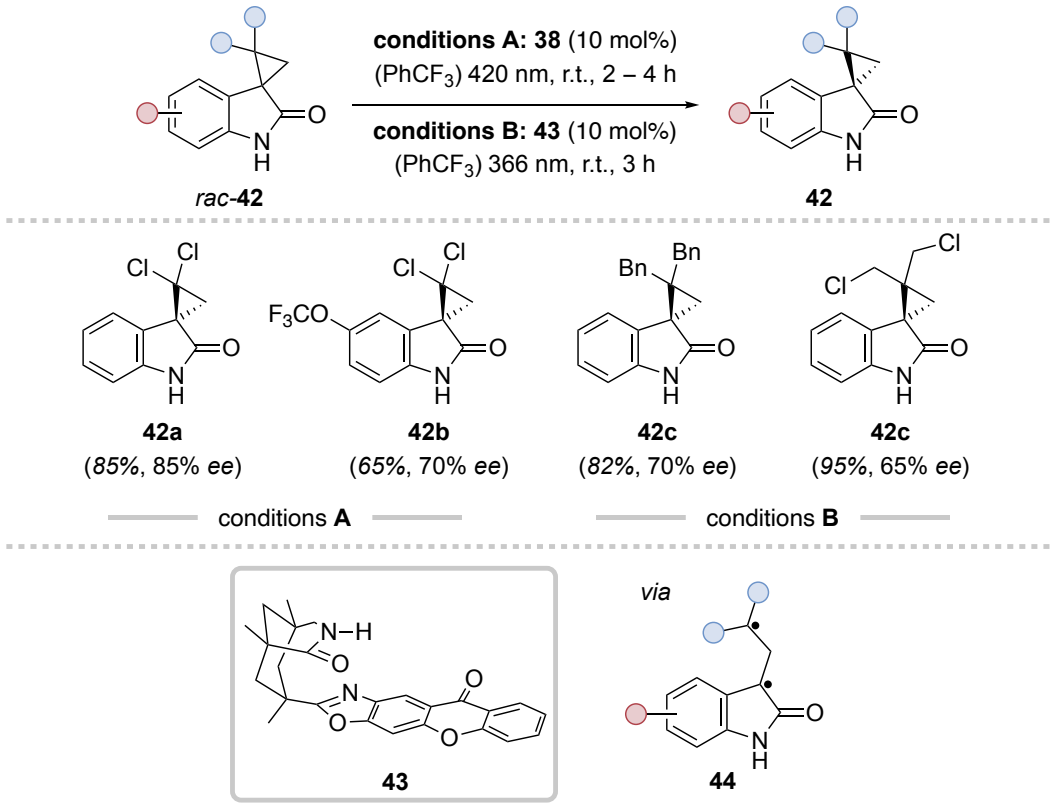


**Scheme 21.** Deracemization of spirooxindoles *rac*-**42** using thioxanthone **38** or xanthone **43**. The intermediacy of **44** was detected by TA spectroscopy.

Moreover, this strategy was successfully combined with an upstream di-π-methane rearrangement for the synthesis of enantioenriched cyclopropanes from 3-allylquinolones using sensitizer **38**.[131]

Chiral sulfoxides are known to be configurationally labile under irradiation conditions and are amenable for sensitization which results in the loss of the stereogenic information at the sulfur atom.[132,133] Therefore, our group used xanthone *ent*-**43** to enable the deracemization of sulfoxides *rac*-**45**, which led to moderate enantioselectivities (Scheme 22).[134] The relatively low selectivity was traced back to the little steric difference between the free electron pair at the sulfur atom and the oxygen atom, which is responsible for the enantiomeric differentiation by the catalyst. As an intermediate, diradical **46** was postulated, which is likely the result of $\alpha$-cleavage of the labile C($sp^3$)–S bond.

*Bach (2019)*

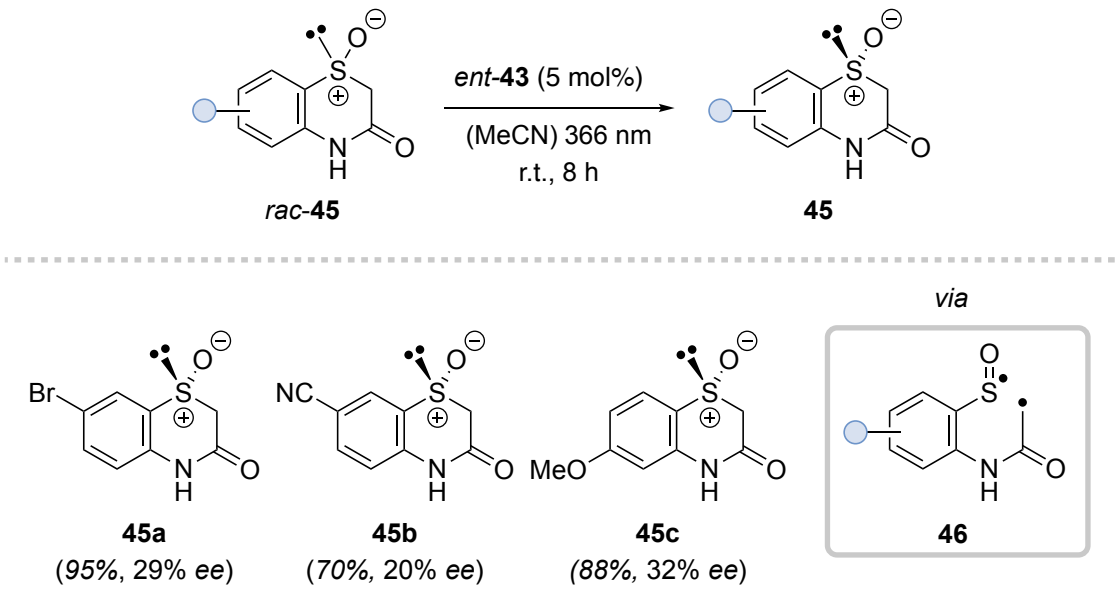


**Scheme 22.** Deracemization of chiral sulfoxides *rac*-**45** by selective triplet energy transfer. The stereoablation is expected to take place *via* $\alpha$-cleavage generating intermediate **46**.

## 4.3 Deracemizations by Thermal Differentiation

The selective procession of one enantiomer in the stereoablative step relies on the use of well-designed, chiral photocatalyst that make use of the different geometries of the transient diastereomeric complexes that are formed prior to excitation. The combination of differentiation and excitation makes it possible to use only one specifically designed catalyst, albeit this renders these systems less flexible. By transferring both enantiomers to the achiral intermediate in an unselective photochemical reaction and introducing enantioselectivity subsequently, combinations of catalyst can be used that have already found prior use in photochemistry respectively ground state chemistry and are well established.

Based on their previous studies,[135] the group of *Luo* developed a deracemization method for aryl-substituted aldehydes *rac*-**47** bearing an $\alpha$-stereogenic center.[136] As for the previous methods, it relies on the use of a triplet sensitizer but instead of a chiral photocatalyst, $Ir(ppy)_3$ in combination with chiral organocatalyst **48** is employed (Scheme 23). Primary amine **48**, assisted by a catalytic amount of benzoic acid, preferentially forms the corresponding *E*-enamine *E*-**49** when reacting with *ent*-**47** which has a lower triplet energy than corresponding *Z*-**49**, generated from **47**. Subsequent selective, triplet sensitized $E \rightarrow Z$ isomerization (*vide supra*) leads to the enrichment of *Z*-**49**, which forms the desired enantiomer **47** upon catalyst release.

*Luo (2022)*

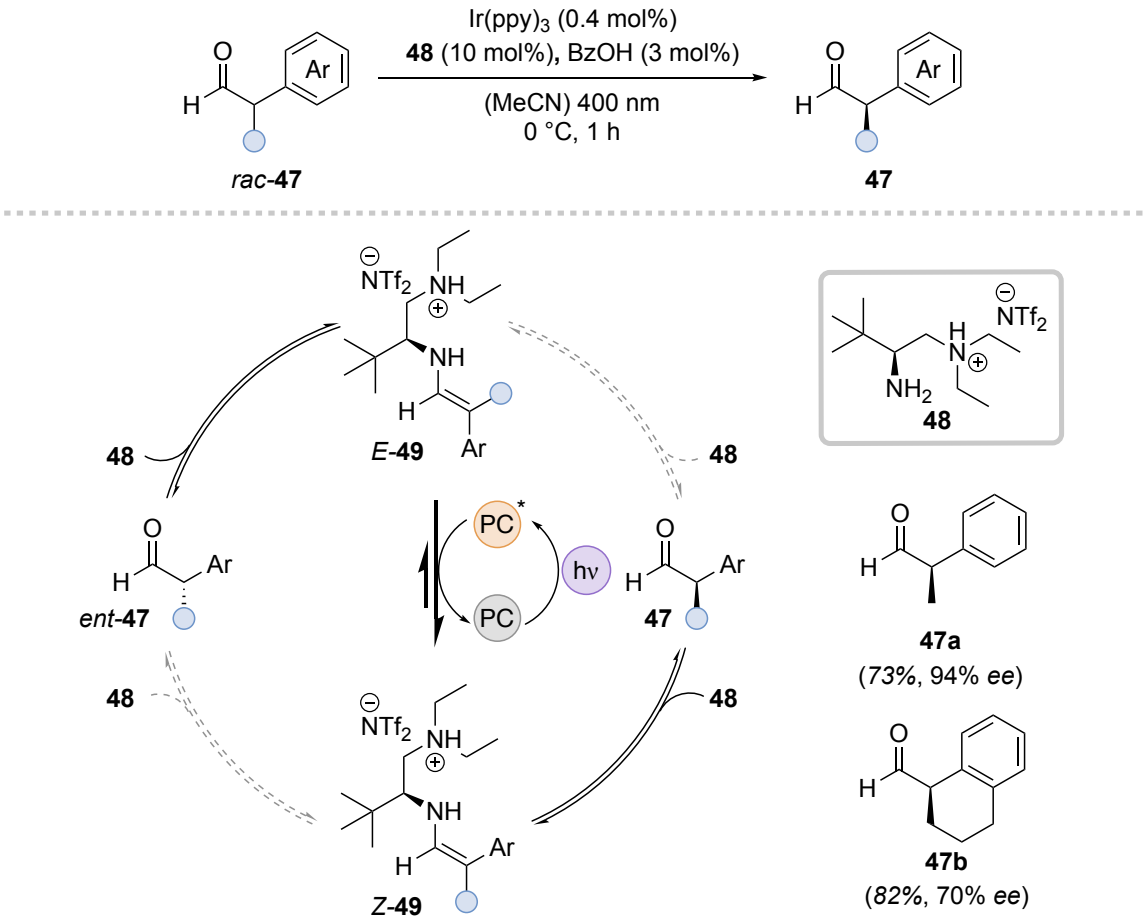


**Scheme 23.** Deracemization of *α*-branched aromatic aldehydes *rac*-**47** by using a dual catalytic approach combining a photosensitizer and chiral amine **48**.

Apart from triplet sensitization, the use of photoredox chemistry has proved to be an efficient way of generating the necessary chiral intermediate *via* a stepwise ablation of the stereoinformation. *Knowles* and *Miller* presented a deracemization of cyclic ureas *rac*-**50** based on the use of a photoredox catalyst **PC-2**, a chiral *Brønsted* base **51** and a chiral peptide-derived thiol **52** (Scheme 24).[137] The achiral intermediate is formed by stepwise non-stereoselective oxidation of *rac*-**50** by the excited photocatalyst to amino radical cation **50-1** and *ent*-**50-1**, followed by deprotonated by base **51** to generate radical intermediate **53**. As the deprotonation of *ent*-**50-1** is kinetically favored, **50-1** remains and regenerates the photocatalyst by being reduced. Upon enantioselective HAT from thiol **52** to radical **53**, enantiomer **50** is formed as the major enantiomer in the photostationary state. Despite the observation of a notable enantiomeric excess when only one chiral catalyst was employed, only dual stereoselective differentiation in the photointermediate *rac*-**50-1** as well as in the achiral intermediate **53** led to excellent selectivities for enantiomer **50**.

*Knowles/Miller (2019)*

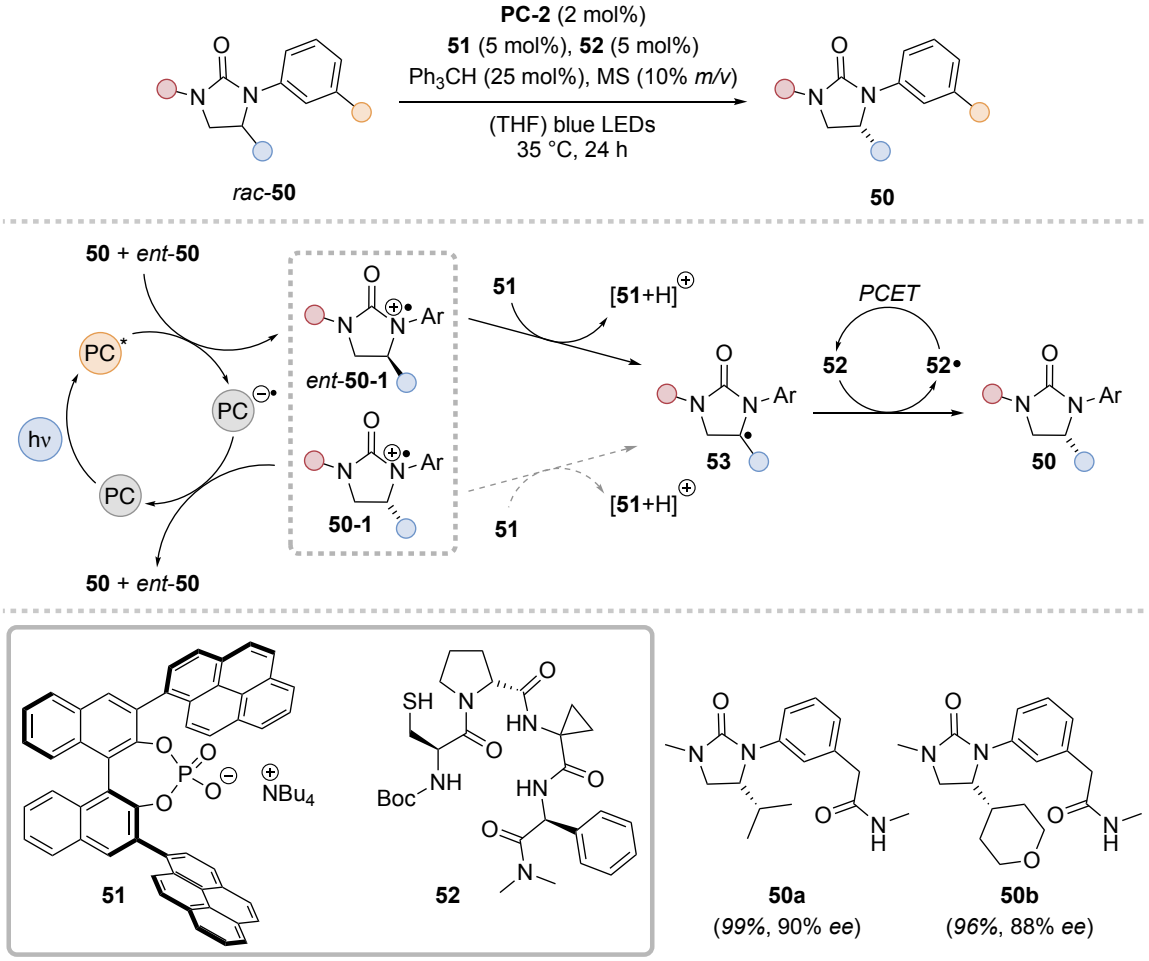


**Scheme 24.** Double differentiation by using a chiral base **51** and a chiral thiol **52** in combination with a photoredox catalyst leads to the successful deracemization of cyclic ureas *rac*-**50**.

The regeneration of base and thiol takes place in a concerted PCET event involving **PC-2**$^{-\bullet}$ which regenerates the ground state photocatalyst.

A similar strategy was designed by the group of *Jiang* who implemented a protocol for the deracemization of $\alpha$-amino acid derivatives *rac*-**54**.[138] In contrast to the previous method, in this case only one chiral catalyst, that is chiral *Brønsted* acid **55**, was needed in combination with photocatalyst **PC-5** (Scheme 25). The overall mechanism involves the generation of an amino radical cation *rac*-**54-1** which, upon deprotonation by the reduced photocatalyst, forms the corresponding *N*-centered radical *rac*-**54-2** which can abstract the $\alpha$-hydrogen atom of a substrate molecule (*rac*-**54)** leading to the generation of the *C*-centered radical **56**. Subsequent PCET, initiated by the photocatalyst species **PC-5-H•**, results in the formation of enol **57**. Based on established methods for the enantioselective protonation of enols,[139,140] chiral acid **55** enantioselectively protonates enol **57** furnishing the $\alpha$-amino acid-derived enantiomer **54**.

*Jiang (2022)*

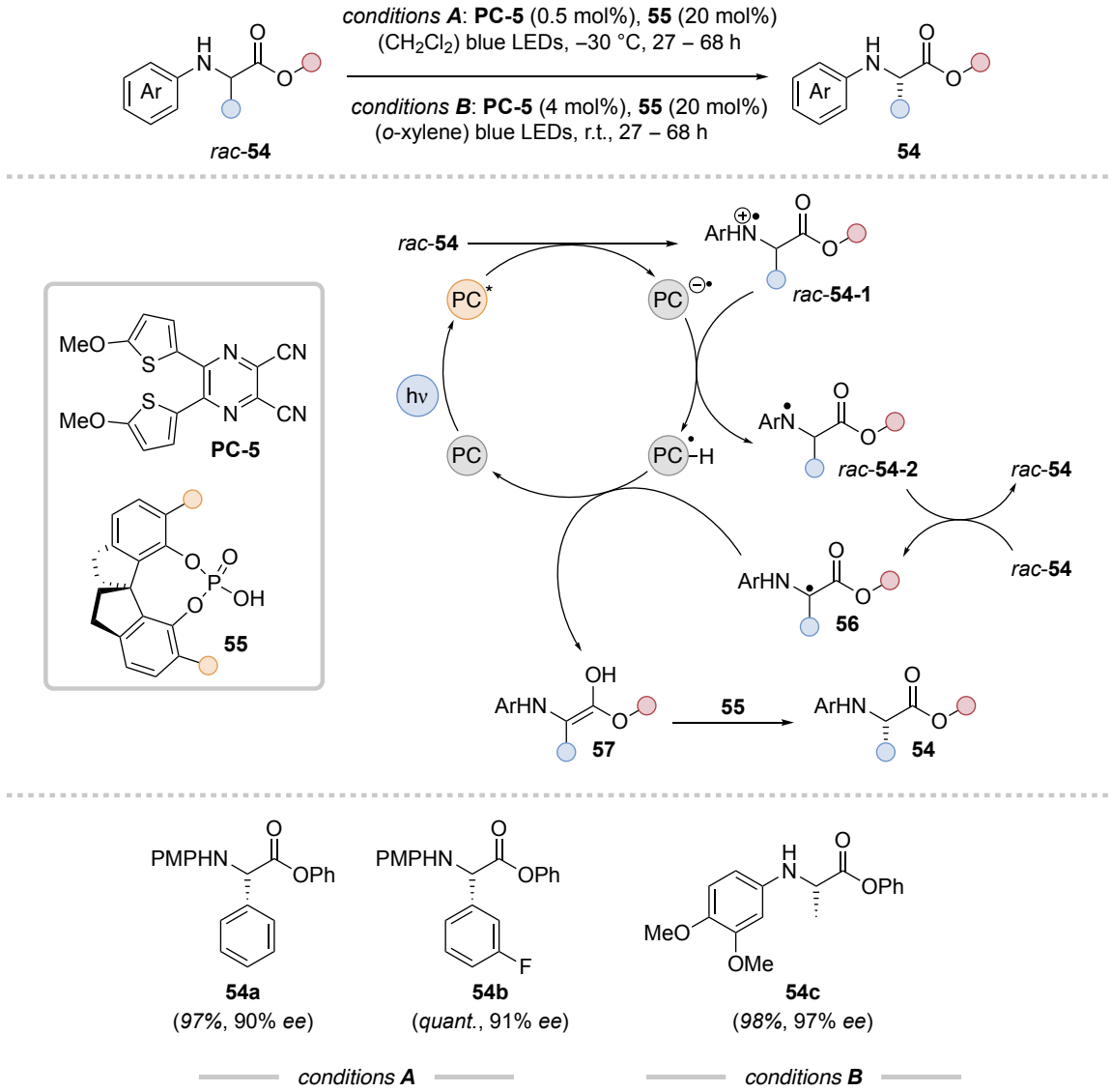


**Scheme 25.** Deracemization of *α*-amino acid derivatives *rac*-**54** by sequential photoredox and chiral *Brønsted* acid catalysis.

Despite the advantages of multicatalytic systems, such as high flexibility and broad applicability, an issue is the need for the individual catalytic cycles to be compatible with each other. Therefore, the use of a single catalyst can be advantageous, not only when the differentiation occurs in the photochemical step but also when the achiral intermediate is enantioselectivly processed.

In this regard, *Meggers* and *Chen* established a platform for the deracemization of pyridylketones *rac*-**58** that makes use of the previously developed chiral-at-metal rhodium catalyst **59** (Scheme 26).[55,141] The active photocatalyst is formed upon coordination of the substrate to the catalyst forming two diastereomeric complexes **61** and *ent*-**61**, which possess a significantly higher absorbance than the sole metal complex. Upon excitation,

the added amine base **60** is oxidized, generating the ketyl-metal complex **62**, of which the oxidized base **62-1** can abstract a hydrogen atom leading to achiral enolate **63**. The subsequent protonation by **62-2** takes place diastereoselectivly due to the shielding of one diastereotopic face by the rhodium complex. Final dissociation of **61** leads to the release of the desired enantiomer **58** and the regeneration of the catalyst.

*Meggers/Chen (2021)*

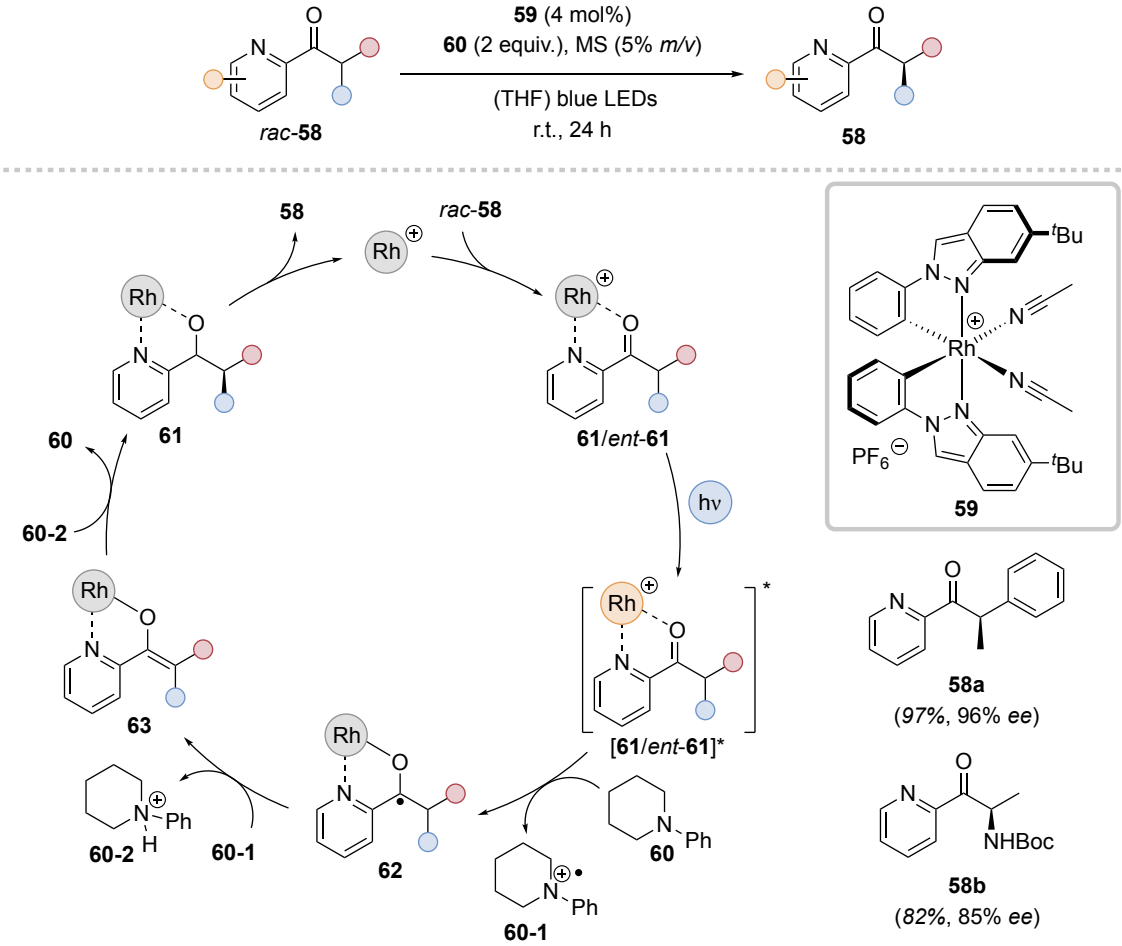


**Scheme 26.** Deracemization of 2-pyridylketones *rac*-**58** by chiral-at-metal rhodium catalyst **59** in a single catalytic system.

An example for the use of another chiral photoredox catalyst in photochemical deracemizations was recently presented by *Gilmour*. Chiral aluminum-salen complex **65**, whose optical properties are well defined,[142] was applied for the deracemization of cyclopropanes *rac*-**64**.[143] Due to the LUMO-lowering activation of the metal center acting as a *Lewis* acid, upon coordination (**66**/*ent*-**66**) and subsequent excitation, transient ketyl radical **67** is formed from both diastereomeric complexes, similarly to the previously elaborated mechanism. Subsequently, ring opening of the cyclopropane leads to achiral enolate **68**. The anew closure of the cyclopropane ring represent the selectivity determining step of the deracemization as the chiral aluminum complex governs the diastereo-

selectivity. Final back SET, supported by tetrabutylammonium chloride, and dissociation of the substrate/catalyst complex **66** furnishes enantiomer **64**.

*Gilmour (2022)*

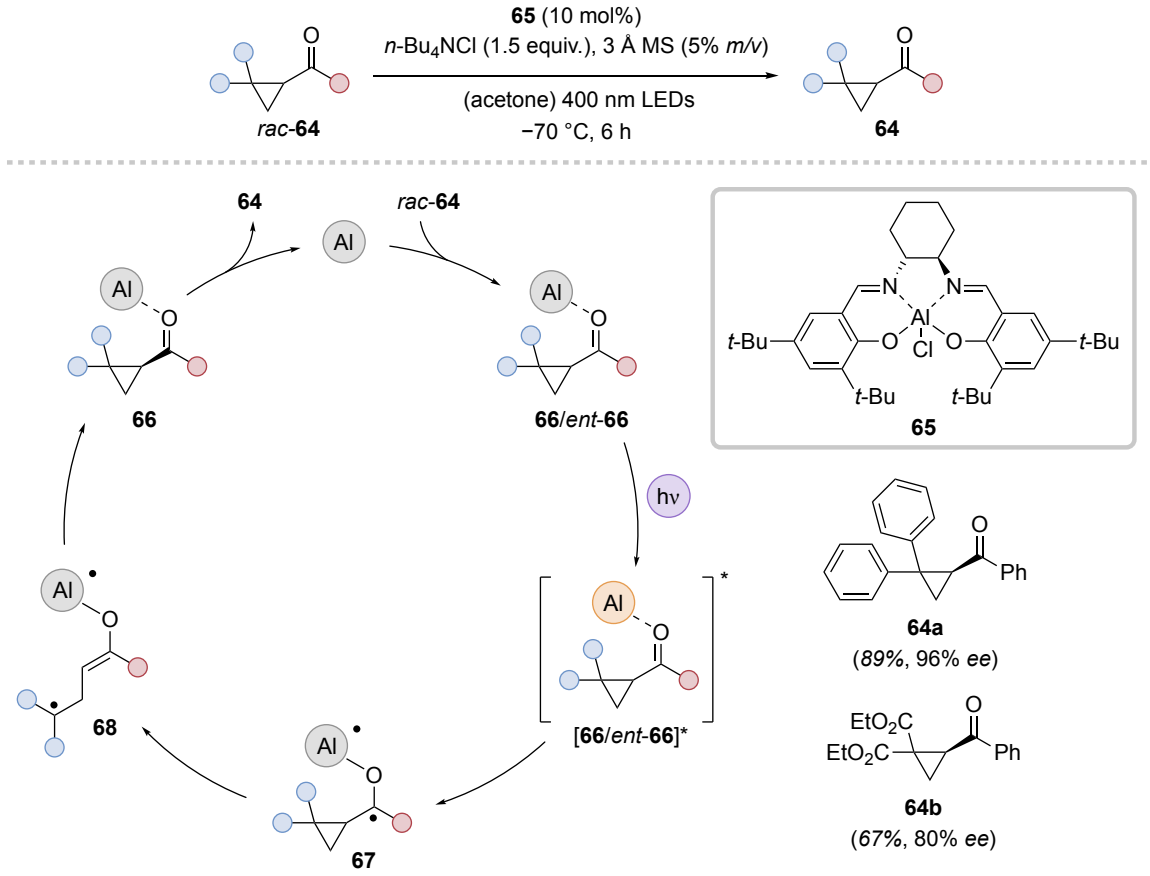


**Scheme 27.** Deracemization of cyclopropyl ketones *rac*-**64** by using chiral aluminum catalyst **65** *via* a photoredox-triggered ring opening/closing mechanism.

# 5 Project Scope

Within the scope of this dissertation, the focus was set on the advancement of existing mono-catalytic deracemization techniques as well as on the development of novel deracemization pathways that allow for a broader application of this type of stereochemical editing to a more diverse range of substrates and stereogenic centers.

## 5.1 Deracemization of Primary Allene Amides

Despite the tremendous success of generating enantiopure allenes by using chiral thioxanthone **38** *via* selective triplet energy transfer (see chapter 4.2),[122,123] these reactions rely on of the inherent rigidity of the substrate structure. Due to the relatively limited degrees of freedom, a defined positioning of the substrate within the substrate/catalyst complex can be realized which allows for a straightforward prediction of the reaction outcome. Unfortunately, the requirement for a lactam moiety within an aliphatic ring restricted to a certain extent the applicability of these allenes.

Therefore, we envisioned the use of allenes bearing a primary amide (*rac*-**69**) to be a suitable solution for this issue and an important advancement regarding the applicability of our deracemization approach (Scheme 28A). Being highly abundant in nature and with a propensity for hydrogen bonding interactions, primary allene amides poses an ideal recognition site for chiral sensitizer **38**.[144,145] A challenge that accompanies primary amides is the existence of at least one rotatable bond, which can potentially prevent a substantial enantioface differentiation by the catalyst. Previous studies have shown that, despite a successful binding, the high number of rotational degrees of freedom only led to moderate selectivities compared to their lactam counterparts.[146]

To overcome this drawback, a set of axially chiral primary allene amides had to be designed that would preferentially prevail only in one major conformation (*rac*-**69'**), rooted in their substitution pattern (Scheme 28B). By that, these substrates would become amenable for deracemization by triplet energy transfer, making them the first class of acyclic substrates being addressable by this reaction type. It was envisioned, that by performing ground and excited state DFT calculations, potential substrates and their binding conformations to the catalyst could be identified, which would further allow for an unprecedented in-depth study of the underlying mechanism of the triplet sensitized deracemization.

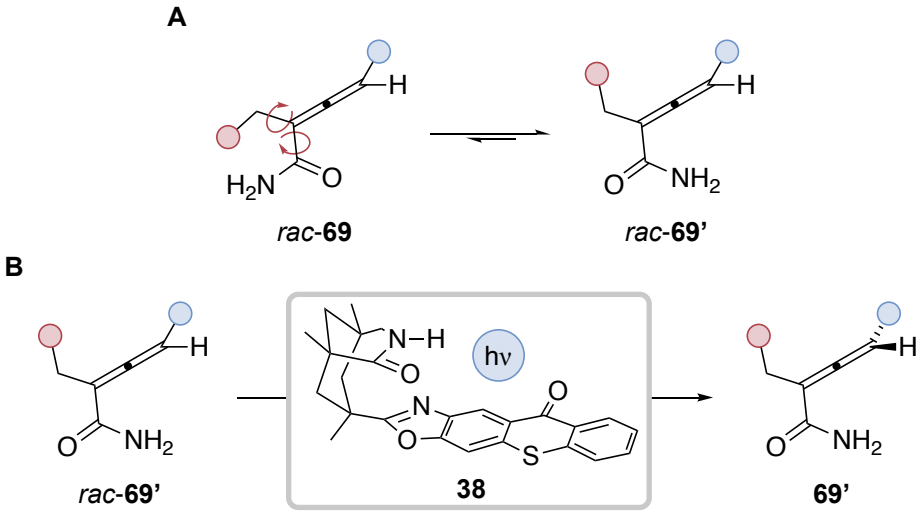


**Scheme 28. A:** Single bond rotations in primary allene amides *rac*-**69** and a potential preferred major conformation of *rac*-**69'** with defined orientation of the binding motif. **B:** Triplet sensitized deracemization of major conformer *rac*-**69'** by sensitizer **38** furnishing the enrichment of **69'** in the photostationary state.

## 5.2 Deracemization of sp$^3$-Hybridized Carbon Centers by Hydrogen Atom Transfer

Our previous approaches for successful deracemizations relied on the presence of a substrate chromophore that could be excited by triplet sensitization. Albeit, achieving great success, these methods were limited to specific substrate classes with suitable triplet energies. We recognized that sp$^3$-hybridized tertiary carbon centers, ubiquitous in both nature and pharmacologically active compounds,[147] represented an attractive target for photochemical deracemization. A single chiral catalyst was envisioned to be used that could differentiate between the two enantiomers and perform hydrogen atom transfer.

Based on their inherent importance in nature, $\alpha$-amino acid-derived compounds (*ent*-**70** and **70**) are interesting targets to test the feasibility of this approach. General prerequisites for this method included that the employed catalyst to have a bias for HAT from one enantiomer (*ent*-**70**), ideally only from one enantiomer but not the other (Scheme 29). Moreover, a back-HAT event from the employed catalyst to potential intermediate **70-1** would have to be energetically as well as geometrically feasible in order to allow for a catalyst turnover and the formation of both enantiomers.

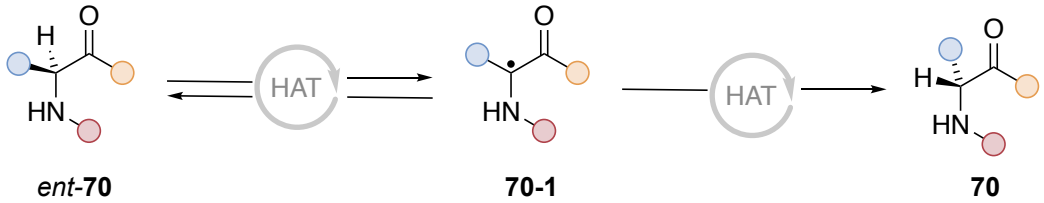


**Scheme 29.** Mechanistic considerations for the successful realization of a HAT-based deracemization technique in amino acid derived substrates.

Owing to their prominence in pharmaceuticals and their direct synthetic and structural relation to $\alpha$-amino acids,[148] hydantoins (*rac*-**71**) were selected as proof-of-principle substrates. Due to their cyclic structure, they possess a constrained conformation allowing for precise positioning by a chiral catalyst *via* hydrogen bonding interactions. Furthermore, the bond dissociation energy of the C($sp^3$)–H bond at the stereogenic center is low enough to make it amenable for abstraction by known HAT catalysts.[149] Based on previous studies on enantioselective, photoinduced electron transfer,[150] chiral benzophenone **72** was chosen as the HAT catalyst as the benzophenone moiety is well-known for its capability of abstracting hydrogen atoms[151-153] (Scheme 30).

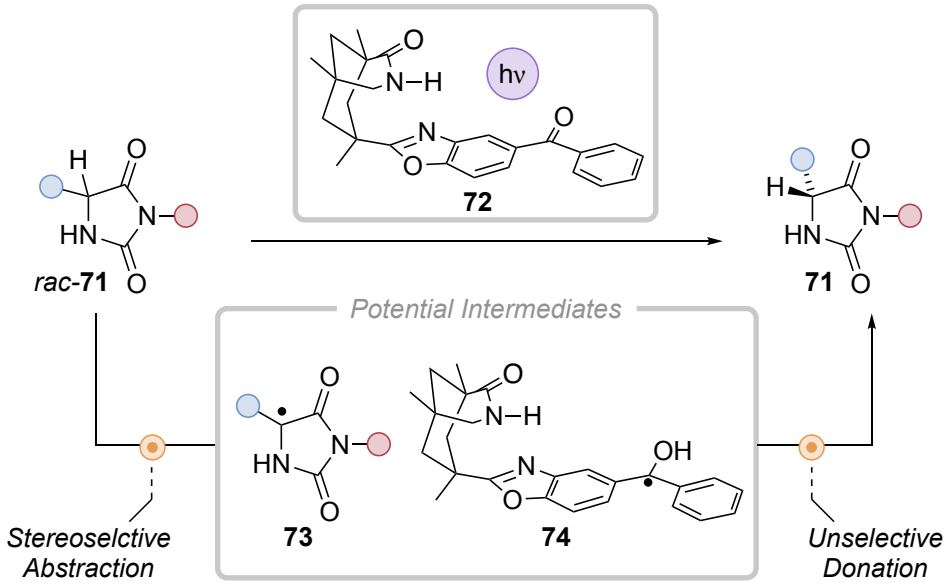


**Scheme 30.** Potential transient intermediates of a HAT initiated deracemization of hydantoins *rac*-**71** catalyzed by chiral benzophenone **72**.

Although the initial HAT step appeared straightforward, the mechanism of the subsequent backdonation of the hydrogen atom to a potential radical intermediate **73** from the transient protonated ketyl radical **74** remained unclear. Therefore, we planned to undertake a comprehensive mechanistic analysis involving synthetic, spectroscopic, and theoretical investigations. This would enable us to predict the prerequisites for other substrate classes

compatible with this type of deracemization, leading to a significant expansion of the applicability of photochemical deracemization reactions for stereochemical editing of complex molecules.

# 6 Photochemical Deracemization of Primary Allene Amides by Triplet Energy Transfer: A Combined Synthetic and Theoretical Study

**Title:** "Photochemical Deracemization of Primary Allene Amides by Triplet Energy Transfer: A Combined Synthetic and Theoretical Study"

**Status:** Article, published online July 19, 2021

**Journal:** *Journal of the American Chemical Society* **2021**, *143*, 11209–11217.

**Publisher:** American Chemical Society

**DOI:** 10.1021/jacs.1c05286

**Authors:** Manuel Plaza*, Johannes Großkopf*, Stefan Breitenlechner, Christoph Bannwarth, Thorsten Bach (*These authors contributed equally.)

**Content**: In this publication, the challenging photochemical deracemization of non-cyclic primary allene amides was investigated, both experimentally and theoretically. A chiral thioxanthone catalyst was employed as a triplet sensitizer with a two-point hydrogen bonding site. Upon irradiation at $\lambda = 420$ nm in the presence of only 2.5 mol % catalyst at −10 °C, a photostationary state was reached, in which one enantiomer prevailed with up to quantitative yield and 93% enantiomeric excess (*ee*) (19 examples). Luminescence spectroscopy and DFT calculations supported a selective energy transfer from the thioxanthone to the allene amides as well as the presence of a transient achiral triplet allene intermediate. NMR titration studies revealed a different association behavior of the two enantiomers to the catalyst. Moreover, a significant difference in the binding properties of the two diastereomeric substrate/catalyst complexes was detected by DFT calculations. Noncovalent dispersion interaction between the substrate residues and the thioxanthone moiety govern the distance of the two chromophores and, therefore, the different rates of triplet energy transfer, responsible for the observed enantiomeric enrichment.

J. Großkopf and M. Plaza planned and executed all experiments (50% each). J. Großkopf recorded all luminescence data and M. Plaza performed NMR titration studies. C. Bannwarth conducted all DFT calculations. J. Großkopf, M. Plaza, C. Bannwarth and T. Bach wrote the manuscript. S. Breitenlechner helped with NMR titration studies and proof reading of the manuscript. All work was performed under the supervision of T. Bach.

JACS
JOURNAL OF THE AMERICAN CHEMICAL SOCIETY
pubs.acs.org/JACS
Article

# Photochemical Deracemization of Primary Allene Amides by Triplet Energy Transfer: A Combined Synthetic and Theoretical Study

Manuel Plaza,[‖] Johannes Großkopf,[‖] Stefan Breitenlechner, Christoph Bannwarth,* and Thorsten Bach*

Cite This: *J. Am. Chem. Soc.* 2021, 143, 11209−11217
Read Online
ACCESS | Metrics & More | Article Recommendations | Supporting Information

**ABSTRACT:** The photochemical deracemization of 2,4-disubstituted 2,3-butadienamides (allene amides) was investigated both experimentally and theoretically. The reaction was catalyzed by a thioxanthone which is covalently linked to a chiral 1,5,7-trimethyl-3-azabicyclo[3.3.1]nonan-2-one skeleton providing a U-shaped arrangement of the sensitizing unit relative to a potential hydrogen-bonding site. Upon irradiation at $\lambda$ = 420 nm in the presence of the sensitizer (2.5 mol %), the amides reached at −10 °C a photostationary state in which one enantiomer prevailed. The enantioenriched allene amides (70−93% ee) were isolated in 74% to quantitative yield (19 examples). Based on luminescence data and DFT calculations, energy transfer from the thioxanthone to the allene amides is thermodynamically feasible, and the achiral triplet allene intermediate was structurally characterized. Hydrogen bonding of the amide enantiomers to the sensitizer was monitored by NMR titration. The experimental association constants ($K_a$) were similar (59.8 vs 25.7 L·mol$^{-1}$). DFT calculations, however, revealed a significant difference in the binding properties of the two enantiomers. The major product enantiomer exhibits a noncovalent dispersion interaction of its arylmethyl group to the external benzene ring of the thioxanthone, thus moving away the allene from the carbonyl chromophore. The minor enantiomer displays a CH−$\pi$ interaction of the hydrogen atom at the terminal allene carbon atom to the same benzene ring, thus forcing the allene into close proximity to the chromophore. The binding behavior explains the observed enantioselectivity which, as corroborated by additional calculations, is due to a rapid triplet energy transfer within the substrate-catalyst complex of the minor enantiomer.

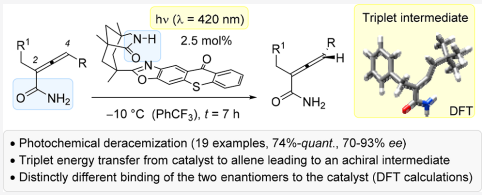


## INTRODUCTION

Hydrogen bonds represent one of the most powerful tools in the diversified repertoire of noncovalent bonds available to nature.[1] Recent years have witnessed a continuous increase in synthetic studies which aim to use hydrogen-bonding interactions for position- and enantioselective catalytic processes.[2,3] The directionality of one (or ideally more than one) hydrogen bond[4] enables a spatially defined coordination of a substrate at a hydrogen-bonding catalyst, while the reversible, noncovalent character of the interaction facilitates a desirable turn over.[5] Despite the fact that a manifold of binding motifs has been employed in hydrogen-bond-mediated catalysis, there are functional groups which have received very little or no attention. The primary amide functional group (−$CONH_2$) represents an example of a group which enables hydrogen bonding and is abundant in nature[6] but has seen very few applications in enantioselective transformations.[7] The high propensity of primary amides for inter- and intramolecular hydrogen bonding is a well-documented property which has been used for the formation of crystal lattice structures[8] but is potentially prohibitive for hydrogen bonding to other molecules. Even if binding to a catalyst or a template occurs, primary amides exhibit at least one rotatable bond in $\alpha$-position which renders an enantioface differentiation difficult. Attempts by our group to employ primary amides as substrates in hydrogen-bond mediated enantioselective reactions have not met the success encountered with prochiral lactams.[2b] Amide **1**, for example, was used in a radical cyclization reaction which was meant to be directed by chiral template **2** (Scheme 1, DCPNO = 2,6-dichloropyridine-*N*-oxide, Mes = mesityl). Although the latter template had enabled highly enantioselective, even catalytic radical cyclization reactions with lactam substrates,[2b,9] the enantioselectivity (ee = enantiomeric excess) in the reaction to product **3** remained low.[7a] Likewise, chiral ruthenium catalyst **5** with a hydrogen-bonding site was found to process 3-alkenylquinolones in an enantioselective epoxidation with >90% ee but failed to deliver the same degree of enantioselectivity on prochiral alkene amides, for example, in the transformation **4** → **6**.[7b] Against this background, it appeared challenging to discover reactions of primary amides

**Received:** May 22, 2021
**Published:** July 19, 2021





https://doi.org/10.1021/jacs.1c05286
*J. Am. Chem. Soc.* 2021, 143, 11209−11217

**Scheme 1. Previous Studies Employing Prochiral Amides 1 and 4 in Enantioselective Transformations Mediated by Hydrogen Bonding to Chiral Lactams**

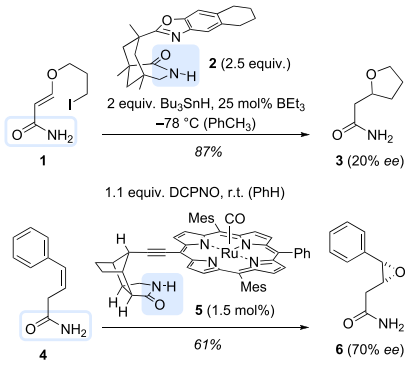


which occur with high enantioselectivity and which involve hydrogen bonding to molecules related to compounds **2** and **5**.

Our interest in primary amides was kindled by the recent discovery that chiral thioxanthone **7** differentiates between the two enantiomers of a given lactam with the generic structure **I** and *ent*-**I**. Although this property had been described for template **2** some time ago,[10] it becomes synthetically relevant if the lactam can be excited via triplet energy transfer from the thioxanthone unit and if it racemizes upon excitation. In such a scenario, it was shown that a preferred triplet energy transfer within complex **7**·*ent*-**I** vs complex **7**·**I** leads to a significant enrichment of compound **I**. As a consequence, a product mixture is obtained in which one enantiomer is formed at the expense of the other enantiomer.[11] Deracemization reactions following this mechanistic scheme have been described for lactams containing an allene,[12,13] a sulfoxide,[14] or a cyclopropyl group.[15]

We have now prepared a set of chiral substituted 2,3-butadienamides (allene amides)[16] in racemic form and subjected them to a photochemical deracemization[17] using chiral thioxanthone **7** as catalyst. Remarkably, these primary amides were found to undergo the process with an enantioselectivity unprecedented[18] for acyclic substrates (up to 93% ee). In this article, we provide full details on the development of the reaction, on its scope, and on its mechanism. Extended quantum chemical calculations were employed to shed light on the involved triplet intermediates and on the enantiodifferentiation in the excited state.

## RESULTS AND DISCUSSION

**Initial Considerations and Preparation of Starting Materials.** As seen from the general picture shown in Figure 1, a differentiation between the two lactam enantiomers **I** and *ent*-**I** depends on a repulsion between a sterically bulky entity R and the thioxanthone backbone of **7**, which in the former case induces (a) an unfavorable binding and (b) in complex **7**·**I** a larger distance between the thioxanthone and the lactam chromophore. We hypothesized that an acyclic amide would also be amenable to a related differentiation if there was a conformational preference in which a similar situation would arise, that is, a large substituent R would point either towards or away from the thioxanthone chromophore. Calculations[19]

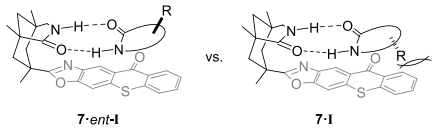


**Figure 1.** Differentiation of chiral lactams **I** and *ent*-**I** by chiral sensitizer **7**: Pauli repulsion disfavors the formation of complex **7**·**I** as compared to **7**·*ent*-**I**.

indicated that 2,4-disubstituted 2,3-butadienamide *rac*-**8a** adopts a preferred conformation in which the amide bond is locked with the amino group and the allene group being *cis*-positioned (*syn*-periplanar). The C−H bonds of the methylene group at carbon atom C2 bisect the carbonyl plane so that the aryl group is positioned *anti*-periplanar (*trans*) to the amide group (Scheme 2). This conformation was identified to be

**Scheme 2. Preferred Conformation *rac*-8a′ of Allene Amide *rac*-8a: The Position of the *tert*-Butyl Substituent Is Locked Relative to the Plane Formed by the Amide Group and the Allene Axis**

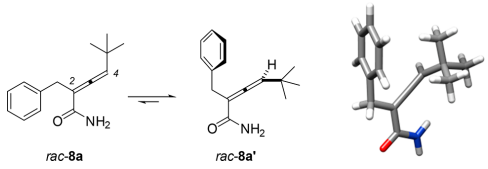


dominant by conformational sampling at the semiempirical GFN2-xTB level and subsequent refinement using density functional theory (DFT) calculations (see SI for details).[20]

Compounds *rac*-**8** with various substituents in 2- and 4-position of a 2,3-butadienamide core are readily accessible in a modular fashion from commercially available ethyl (triphenylphosphoranylidene)acetate (**9**).[21] The stable ylide **9** is sufficiently nucleophilic at its carbon atom to attack activated alkyl halides in a nucleophilic substitution reaction (Scheme 3).

**Scheme 3. Modular Synthesis of Primary Allene Amides *rac*-8 by Two Consecutive C−C Bond Formation Reactions at Ethyl (Triphenylphosphoranylidene)acetate (9)**

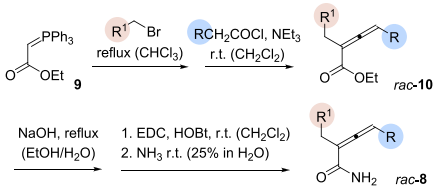


Benzylic ($R^1$ = aryl) and allylic ($R^1$ = alkenyl) bromides are particularly good electrophiles and delivered smoothly the respective phosphonium salts under reflux conditions.[22] The salts were taken without isolation in the next step which involved a Wittig reaction with an *in situ* generated ketene. To this end, an excess triethyl amine was used as a base which induces a 1,2-elimination of acyl chlorides and which simultaneously generates reactive phosphorus ylides from the phosphonium salts.[23] The Wittig reaction delivered ethyl 2,3-butadienoates


https://doi.org/10.1021/jacs.1c05286
J. Am. Chem. Soc. 2021, 143, 11209−11217

*rac*-**10** which were isolated and purified (for yields and further details, see the SI).

Saponification with sodium hydroxide in aqueous ethanol led to the respective acids which were subsequently converted into primary amides *rac*-**8**. In most cases, the crude allene acid was sufficiently pure to be utilized in the next step without further purification. The amide formation was performed with aqueous ammonia after activation of the carboxyl group.[24] In the course of our studies, it turned out that 1-ethyl-3-(3-(dimethylamino)-propyl)carbodiimide (EDC) in combination with 1-hydroxy-benzotriazole (HOBt) gave higher yields than *N*,*N*′-dicyclohexylcarbodiimide (DCC) which had been initially used. The synthesis of allene *rac*-**8s** ($R^1$ = H, R = *tert*-butyl) was accomplished by a Wittig reaction of commercially available (1-ethoxycarbonylethyliden)-triphenylphosphorane. In this instance, the substituent in the $\alpha$-position of the allenoate was not introduced by alkylation but was already incorporated into the phosphorus ylide.

**Optimization of Reaction Conditions and Substrate Scope.** Before subjecting the complete set of allene amides to a deracemization protocol, it was secured that a triplet energy transfer to allenes is feasible. To this end, the two enantiomers of compound *rac*-**8a** were separated by semipreparative HPLC on a chiral stationary phase. A single separated enantiomer was irradiated in the presence of achiral thioxanthen-9-one. The triplet energy $E_T$ of this sensitizer ($E_T$ = 268 kJ mol$^{-1}$ in EtOH)[25] is close to the triplet energy of compound **7** ($E_T$ = 263 kJ mol$^{-1}$ in $PhCF_3$).[12] A successful racemization of an enantiopure sample thus indicates that energy transfer is feasible under the chosen conditions. In the present case, irradiation of enantiopure compound **8a** was performed at $\lambda$ = 420 nm in acetonitrile solution and led in the presence of thioxanthen-9-one (50 mol %) to a complete racemization after 8 h. In the next step, a deracemization was attempted. Screening of reaction conditions was performed initially in the same solvent at $\lambda$ = 420 nm with a substrate concentration of $c$ = 10 mM (Table 1). Chiral thioxanthone **7** was used as the catalyst which was meant to act by establishing a nonthermodynamic equilibrium between the two enantiomers (photostationary state). Previous studies with allenes had shown that a low catalyst loading of 2.5 mol % is sufficient to achieve high enantioselectivities.[12] In the present case, irradiation for 4 h at 0 °C allowed for isolation of the allene amide in 87% yield (entry 1) which already displayed a notable enantiomeric excess (61% ee). Since we suspected that the photostationary state had not yet been reached, a second experiment was performed with a longer irradiation time (entry 2) which led to an improved enantioselectivity. A temperature decrease (entries 3 and 4) to −10 °C was beneficial to the enantioselectivity (up to 81% ee). The enantioselectivity dropped at −25 °C, in which case the photostationary state was likely not reached, even after 8 h (entry 5).[26] In addition, yields were lower after extended irradiation most likely due to unwanted side reactions. A lower substrate concentration led to a decrease in selectivity (entry 6 vs entry 4), while a higher concentration led to a sluggish reaction, potentially associated with solubility issues. A solvent change to dichloromethane did not improve the selectivity (entry 7), but the nonpolar solvent $\alpha,\alpha,\alpha$-trifluorotoluene ($PhCF_3$) gave a better result than acetonitrile. The allene amide was isolated in high yield and with 82% ee after an irradiation time of 4 h (entry 8) and with 85% ee after 8 h (entry 9). A further decrease of the reaction temperature was precluded by the poor solubility of the allene amide in $PhCF_3$.

**Table 1. Optimization of the Reaction Conditions for the Deracemization of Allene Amide *rac*-8a by Triplet Energy Transfer from Chiral Thioxanthone 7**

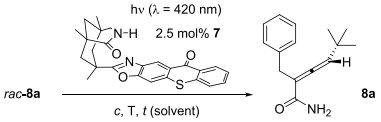


| entry[a] | solvent | $c$ (mM) | $T$ (°C) | $t$ (h) | ee[b] (%) | yield[c] (%) |
|---|---|---|---|---|---|---|
| 1 | MeCN | 10 | 0 | 4 | 61 | 87 |
| 2 | MeCN | 10 | 0 | 8 | 76 | 94 |
| 3 | MeCN | 10 | −10 | 4 | 68 | 89 |
| 4 | MeCN | 10 | −10 | 8 | 81 | 80 |
| 5 | MeCN | 10 | −25 | 8 | 61 | n.d.[d] |
| 6 | MeCN | 5 | −10 | 8 | 70 | 82 |
| 7 | $CH_2Cl_2$ | 10 | −10 | 8 | 64 | 83 |
| 8 | $PhCF_3$ | 10 | −10 | 4 | 82 | 94 |
| 9 | $PhCF_3$ | 10 | −10 | 8 | 85 | 91 |

[a]A degassed solution of the allene amide (11.4 mg, 50 $\mu$mol) and the thioxanthone catalyst **7** (2.5 mol %) in the given solvent was irradiated by 16 fluorescent lamps with an emission maximum at $\lambda$ = 420 nm in a Duran glass phototube (outer Ø = 1 cm). [b]Calculated from the ratio of enantiomers **8a**/*ent*-**8a** as determined by chiral HPLC analysis (Daicel Chiralpak, AD-H). [c]Yield of isolated product after column chromatography. [d]The yield was not determined.

The absolute configuration of the major enantiomer was assigned based on its calculated specific rotation. For this purpose, we computed the specific rotation by means of time-dependent DFT calculations at the BHLYP/def2-TZVPD +COSMO level of theory as the Boltzmann average for the three lowest conformers (see SI). This yields a computed specific rotation of $[\alpha]_D^{\text{comput.}} = -89.8$.[20e,h,i,27] The experimentally determined specific rotation for the major enantiomer obtained from the deracemization experiment was $[\alpha]_D^{20} = -50.0$ ($CHCl_3$).

Although a careful monitoring of the ee with time (see the SI for further details) had revealed that the reaction *rac*-**8a** → **8a** in trifluorotoluene reached a photostationary state after 5 h, all allene amides were irradiated under optimized conditions (Table 1, entry 9) for 7 h. For synthetic reasons, most substrates were arylmethyl-substituted in the 2-position of the 2,3-butadienamide (Scheme 4). The wide range of alkyl and functional groups (products **8b**−**8l**) tolerated in this part of the substrate emphasizes the mild conditions under which the reaction takes place. Interestingly, the substitution at the phenyl ring had an influence on the enantioselectivity. The highest selectivities (≥90% ee) were found for substrates with a polyhalogenated phenyl ring (**8g**, **8j**) or a trifluoromethyl substituent (**8i**). Product yields were in general high (≥74%), in some cases even quantitative clearly ruling out that the enantioselectivity was due to a photodestruction of one enantiomer. Other tertiary alkyl groups but *tert*-butyl in 4-position gave similarly high enantioselectivities (products **8m**, **8n**), but the ee dropped when the group size decreased (products **8o**, **8p**). The lower ee for product **8q** is likely due to fact that the reaction had to be conducted at ambient temperature for solubility reasons. The 2-allyl- and the 2-methyl-substituted allene amides **8r** and **8s** gave lower yields than the 2-benzylated substrate **8a**.



https://doi.org/10.1021/jacs.1c05286
J. Am. Chem. Soc. 2021, 143, 11209−11217

**Scheme 4. Photochemical Isomerization of Racemic Allene Amides *rac*-8 to Enantioenriched Products 8**

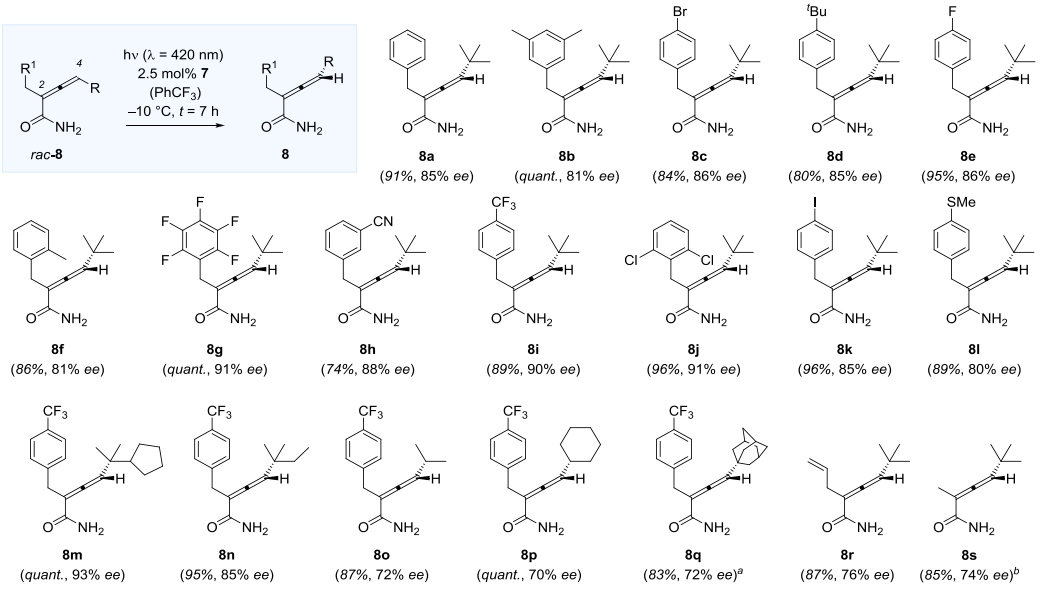


[a]Reaction performed at room temperature. [b]Reaction performed in MeCN.

Consistently, all major enantiomers obtained from the deracemization experiments were found to be levorotatory, and the assignment of the absolute configuration was based on the analogy to product **8a**.

**Association Data and Triplet Energies.** As explained before, one important aspect for the success of the deracemization is the preferential binding of one of the enantiomers of the allene amides to chiral photocatalyst **7** when compared to the other. In order to determine the association constants of the allene enantiomers **8** and *ent*-**8** with catalyst **7**, we performed NMR titration experiments (benzene-$d_6$ solution).[28] For practical reasons, allene amide **8l** was employed as a model substrate for these experiments. Its separation by semipreparative chiral HPLC conditions could be readily accomplished, and both enantiomers **8l** and *ent*-**8l** were isolated in adequate quantity and optical purity (>99% ee). The values of the dimerization and both association constants are shown in Scheme 5 (see the SI for detailed information on the data analysis). Remarkably, the dimerization constant ($K_{dim}$) of racemic allene **8l** was determined to be 10.2 L·mol$^{-1}$, which is lower than the value determined for the corresponding cyclic allene lactam analogues in a previous study, where $K_{dim}$ was found to be 32 L·mol$^{-1}$.[12] For propionamide, which is a comparable primary amide, a value for $K_{dim}$ = 27 ± 5 L·mol$^{-1}$ had been obtained by dielectric constant measurement in benzene solution at 30 °C.[29]

**Scheme 5. Association Data Obtained for Allene Amide 8l and Its Enantiomer *ent*-8l by NMR Titration in Benzene-$d_6$**

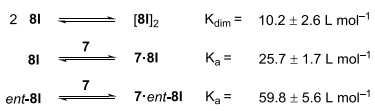


The determination of the association constants of the allene enantiomers with chiral sensitizer **7** revealed that *ent*-**8l** features a higher binding constant ($K_a$ = 59.8 L·mol$^{-1}$) to **7** than does **8l** ($K_a$ = 25.7 L·mol$^{-1}$). However, the difference in association constants $K_a$ cannot solely explain the high enantioselectivity in the observed deracemization, and additional synergistic effects—most notably unequal sensitization efficiencies of catalyst **7** to each of the allene enantiomers **8** and *ent*-**8** in the bound complex (*vide infra*)—must play a key role.

The association data agree well with DFT calculations,[20c−i] which show a negative association energy of −93.8 and −97.1 kJ mol$^{-1}$ for the complexes of **7**·**8a** and **7**·*ent*-**8a**, respectively. The association energy gets almost completely compensated by solvation and particularly entropic contributions to the free energy (see SI). This leads to slightly positive association free energies of 3.5 kJ mol$^{-1}$ and 2.5 kJ mol$^{-1}$ for **7**·**8a** and **7**·*ent*-**8a** at room temperature. Lowering the temperature can increase the concentration of reactive complexes in solution, while a lower solubility may compromise the beneficial effect on the reactivity. The computed association free energies for **8a** and *ent*-**8a** with **7** are slightly too positive as compared to the experimentally determined values for **8l** and *ent*-**8l**, which is likely due to inaccuracies of the *ansatz*, in particular, the implicit treatment of solvation effects (see the SI for further details). Deviations of about 10−12 kJ mol$^{-1}$ have been reported before for similarly sized systems.[30] However, this is more a systematic shift, and the difference in computed association free energies of ∼1 kJ mol$^{-1}$ for the two enantiomers is in reasonable agreement with the experimental difference of ∼2 kJ mol$^{-1}$.

The structures calculated at the PBEh-3c level of theory[20c] of the two complexes **7**•**8a** and **7**•*ent*-**8a** revealed significant,



https://doi.org/10.1021/jacs.1c05286
J. Am. Chem. Soc. 2021, 143, 11209−11217

unexpected differences regarding the position of the allene amide (Figure 2) relative to the thioxanthone chromophore.

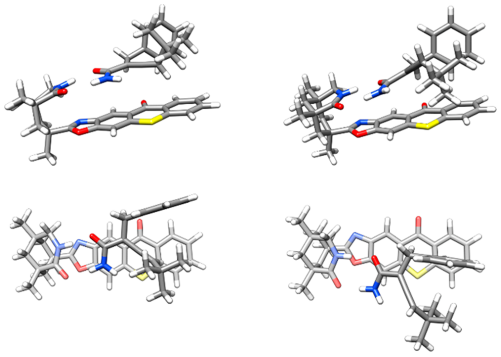

**Figure 2.** Calculated structures of the complexes **7**•*ent*-**8a** (left) and **7**•**8a** (right) in the ground state as seen from the side and from the top.[31] In both cases, a CH−$\pi$ interaction is notable. In the latter case, the *ortho* C−H bond of the arene is involved, and in the former case, the terminal C−H bond of the allene is involved. In the views from the top, the thioxanthone is depicted more transparently for better visibility.

In complex **7**•**8a**, the *ortho* C−H bond of the phenyl group is directed perfectly perpendicular to the $\pi$ system of the thioxanthone ring. The dispersion interaction[32] forces the allene moiety away from the chromophore, elongating significantly the spacing to the thioxanthone chromophore. Indeed, the distance of the internal sp-hybridized allene carbon atom to the thioxanthone carbonyl carbon atom was found to be 570 pm. In complex **7**•*ent*-**8a**, the hydrogen-bonding event places the C−H bond at the terminal allene carbon atom in a position which is ideal for a CH−$\pi$ interaction,[33] forcing the allene in close proximity to the thioxanthone. The distance of the internal allene sp-hybridized carbon atom to the thioxanthone carbonyl carbon atom is found to be only 357 pm. The calculations clarify the fact that the observed association constants **7**•**8l** and **7**•*ent*-**8l** do not differ significantly. A much lower association constant might be expected for **7**•**8l** due to the Pauli repulsion of the *tert*-butyl group with the thioxanthone. The difference was found to be much less pronounced ($\Delta K_a \cong 30$ L·mol$^{-1}$) than anticipated, which can be readily understood since the Pauli repulsion is mitigated by the larger distance between the allene to the thioxanthone in **7**•**8l** and simultaneously compensated by the attractive and more long-ranged dispersion interaction.[32]

**Insights from the Computational Investigation.** By means of DFT studies[20c−i] of the singlet ground and first excited triplet states of thioxanthone **7**, we obtain a value of 278 kJ mol$^{-1}$ for the energy difference between the $S_0$ and $T_1$ states of **7**, which is in good agreement with the aforementioned experimentally determined triplet energy of about 263 kJ mol$^{-1}$. The computed adiabatic energy difference for **8a** is found to be 201 kJ mol$^{-1}$. Hence, the triplet energy transfer is expected to be thermodynamically favored, once the chiral sensitizer reaches the $T_1$ state. Details on these calculations can be found in the SI. Phosphorescence data obtained for compound **8c** allowed to determine the triplet energy experimentally.[34,35] A delayed emission was detected at $\lambda = 461$ nm, and the emission falls off to a value below $\lambda = 400$ nm. For the determination of the triplet energy, a notable shoulder was tentatively assigned as the (0,0) transition, which results for **8c** in a triplet energy $E_T = 272$ kJ mol$^{-1}$ (77 K, EtOH). The value was verified by subjecting compound **8a** to racemization reactions in the presence of achiral sensitizers with defined triplet energies (see the SI for further details). Racemization ceased if the triplet energy of the sensitizer fell below $E_T \leq 250$ kJ mol$^{-1}$. The deviation from the theoretical value can be rationalized from the finding that the vertical triplet excitation energy of the allenes is found at comparably high energies at the ground-state minimum structure. Calculations at the linear response CC2/aug-cc-pVDZ level of theory[36] show that the lowest vertical triplet excitation of **8a** occurs at 4.25 eV (410 kJ mol$^{-1}$). Thus, this state becomes inaccessible if the sensitizer triplet energy is becoming too small.

The structure of the triplet intermediate ($T_1$) was assessed by DFT calculations.[20c−i] They suggest the intermediate to be achiral since the chirality axis gets distorted. The central allene carbon atom which is sp-hybridized in the ground state and displays a bond angle of 180° to its two substituents becomes bent, and the bond angle decreases to 142°. In line with previous suggestions to the structure of a triplet allene,[37] the two unpaired electrons in $T_1$ (**8a**) are found in the $\pi$ system formed by the three previous allene carbon atoms and in an orbital which is closest to sp$^2$ hybridization and which is located at the central allene carbon atom (Figure 3). Although the intermediate is

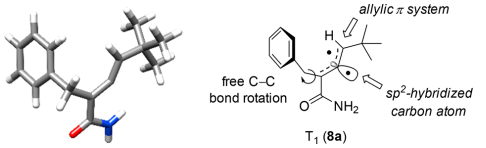


**Figure 3.** Calculated structure of the first excited triplet state $T_1$ of allene **8a** and its valence bond structure. The chirality axis is lost, and the allene adopts a bent structure with two unpaired electrons.

chiral, there is no significant barrier for racemization which can easily occur by rotation around the indicated single bond. Relaxation of intermediate $T_1$ (**8a**) leads to both enantiomers **8a** and *ent*-**8a** under the likely provision that it is sufficiently long-lived to dissociate from catalyst **7** (*vide infra*).

Assuming that the energy transfer takes place in the triplet manifold, a Dexter-type energy transfer is expected to occur, which strongly (exponentially) depends on the intermolecular separation between the two chromophores (thioxanthone carbonyl group/allene double bond).[38] In the previous section, it has already been mentioned that this distance is remarkably different for the two diastereomeric complexes. Complex **7**•*ent*-**8** does not only benefit from the higher association constant but the CH−$\pi$ interaction of the allene C−H bond also forces the two chromophores in close distance, providing an ideal setting for rapid energy transfer benefit (Scheme 6). In the diastereomeric complex **7**•**8**, there is a repulsive interaction between the R substituent at the terminal allene carbon atom but even more importantly an attractive interaction between $R^1$ and the thioxanthone. The two chromophores are forced apart, and triplet energy transfer is retarded. The interaction is most pronounced for $R^1$ = aryl due to the C−H $\pi$ interaction. In some cases (substrates **8g**, **8j**), an even stronger C−halogen $\pi$ interaction[39] might be the reason for an improved enantioselectivity.



https://doi.org/10.1021/jacs.1c05286
J. Am. Chem. Soc. 2021, 143, 11209−11217

**Scheme 6. Two Diastereomeric Complexes of the Two Allene Amide Enantiomers *ent*-8 and 8 to Sensitizer 7: The Smaller Distance of the Chromophores (Orange Dots) Facilitates a Fast Energy Transfer in Complex 7·*ent*-8**

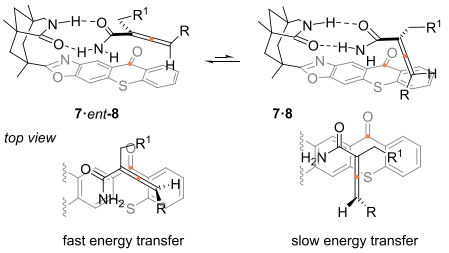


DFT calculations[20c−i] confirm that for the triplet complexes, that is, when **7** is in its $T_1$ state $T_1$(**7**), the intermolecular distances remain similar to the ground-state complexes. The lowest structure found for $T_1$(**7**)·*ent*-**8a** shows a distance of about 474 pm between the central allene carbon and the carbonyl carbon atom, while another accessible conformation (3.3 kJ mol$^{-1}$ higher in free energy) computed for the triplet $T_1$(**7**)·*ent*-**8a** is structurally almost identical to **7**·*ent*-**8a** (Figure 2). As a consequence, the conformations computed for the triplet $T_1$(**7**)·*ent*-**8a** place the central allene carbon atom much closer to the carbonyl carbon atom than the conformation found for $T_1$(**7**)·**8a**. Hence, a much faster energy transfer to *ent*-**8a** occurs, and once the energy has been transferred, the allene is expected to planarize almost instantly. Due to the excess energy that results from the energy transfer, we expect the weakly bound complex to dissociate quickly. The now achiral triplet form of the allene will eventually decay to the $S_0$ state and end up in either of the two chiral forms (**8** and *ent*-**8**). Due to the slightly stronger binding of *ent*-**8** to **7** and, more importantly, the faster energy transfer within complex $T_1$(**7**)·*ent*-**8**, enantiomer **8** accumulates in the photostationary state.

In order to possibly quantify the faster energy transfer by computations, we searched for the minimum energy conical intersections (MECIs) between the two low-lying triplet states in both diastereomeric complexes. Toward this goal, we employed the floating occupation molecular orbital-complete active space configuration interaction (FOMO-CASCI) method[40] in combination with a (4,4) active space and the def2-SV(P) basis set.[20e] The D3(BJ) London dispersion correction was employed, and the active electrons were smeared out evenly over the active orbital space. These optimizations were carried out in the TeraChem electronic structure program.[41] The obtained MECI geometries are shown in Figure 4. After identifying the respective MECI geometries with this approach, single point calculations at the Tamm−Dancoff-approximated TD-DFT level[42] were computed in combination with the PBEh-3c[20c] method (see SI for more details).

At these geometries, the $T_1$ and $T_2$ states, which correspond to the triplet states localized on the allene triplet state and the sensitizer, respectively, are exactly degenerate. We find that the MECI geometry is decidedly lower for $T_1$(**7**)·*ent*-**8a** (+52 kJ mol$^{-1}$) than for $T_1$(**7**) **8a** (+79 kJ mol$^{-1}$) relative to its respective triplet minimum. Since it is expected that the energy-transfer process takes place via population transfer through this conical intersection seam, our calculation predicts a much faster energy transfer for the *ent*-**8a** enantiomer (by ca. 5 orders of magnitude

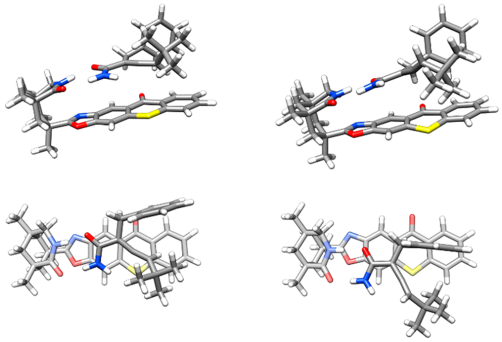

**Figure 4.** Minimum energy conical intersection structures at which the two low-lying triplet states become degenerate. Structures are shown for $T_1$(**7**)·*ent*-**8a** (left) and $T_1$(**7**)·**8a** (right) as seen from the side and from the top.[31] These two triplet states correspond to the individual triplet states that are responsible for the triplet energy transfer. The geometries were obtained at the FOMO-CASCI(4,4)-D3(BJ)/def2-SV(P) level. In the views from the top, the thioxanthone is depicted more transparently for better visibility.

faster than for **8a**). We can therefore conclude that the differential photochemical behavior that is observed for both enantiomers is not primarily due to different association constants. Instead, the energy-transfer pathway is less favored for **8a**, which we could identify from differences in the complex geometries and, analogously, from the energetic positioning of the relevant conical intersection geometry. This finding corroborates previous assumptions regarding the distance dependence of energy transfer within complexes of sensitizer **7**,[13a,15b] and it allows for the first time to approximate the effect quantitatively. The results are summarized in Figure 5 which compares the relative energies of the involved states for both complexes **7**·**8a** (right) and **7**·*ent*-**8a**.

## CONCLUSION

In summary, allene amides have been shown to undergo a photochemical deracemization reaction when irradiated with visible light ($\lambda$ = 420 nm) in the presence of a chiral sensitizer (2.5 mol %). Two noncovalent interactions have been identified as crucial for the success of the reaction: (1) Hydrogen bonding between the catalyst and the substrate established the spatial proximity that is required for an efficient energy transfer. One enantiomer binds less efficiently to the catalyst than the other. However, as seen from the association constants, the extent of the different binding properties is relatively small. (2) More importantly and not previously recognized, attractive dispersion interactions between the allene and the $\pi$ system of the thioxanthone have been revealed by quantum chemical calculations. In the case of the major allene enantiomer, either a C−H or a C−halogen bond is oriented perpendicular to the $\pi$ system which forces the allene away from the thioxanthone chromophore. In the case of the minor allene enantiomer, an attractive CH−$\pi$ interaction between the C−H bond at the terminal allene carbon atom and the external benzene ring of the thioxanthone brings the allene in close proximity to the chromophore. The strong distance dependence of energy transfer manifests itself in a different energetic positioning of the conical intersections that funnel the triplet population transfer from the sensitizer to the allene. This effect is


https://doi.org/10.1021/jacs.1c05286
J. Am. Chem. Soc. 2021, 143, 11209−11217

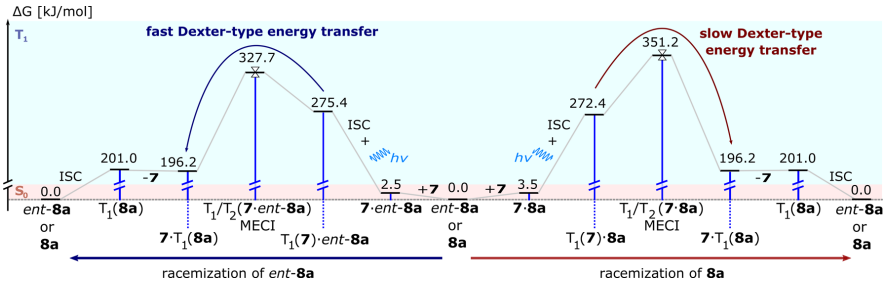


**Figure 5.** Computed free energy reaction profile for the photocatalytic deracemization preferring **8a** (right) over *ent*-**8a** (left). All free energies are computed at the PW6B95-D3(BJ)/def2-QZVP//PBEh-3c electronic structure level of theory. Zero-point vibrational energies and thermal gas-phase free energies are computed in the modified rigid-rotor-harmonic oscillator approximation[43] based on PBEh-3c geometries and harmonic frequencies (scaled by 0.95). The solvation free energies are computed at the semiempirical GFN2-xTB level with a generalized Born model with solvent accessible surface terms.[44] The MECI energies are computed at the TDA-PBEh-3c//FOMO-CASCI(4,4) D3(BJ)/def2-SV(P) level, and their relative energies are obtained as purely electronic energy differences referenced to the energy of $7{\cdot}T_1$(**8a**) computed at the same level of theory.

responsible for a photostationary state in which the enantiomer that is close to the chromophore is processed with a much higher rate, which in turn leads to an equilibrium in which the allene enantiomer, that binds less efficiently and displays a larger distance to the chromophore, is formed in large excess (up to 93% ee). The study provides evidence that dispersion interactions can serve as a useful handle to increase the enantioselectivity of a photochemical reaction, and it serves as an excellent starting point for the future design of enantioselective light-induced transformations.

## ■ ASSOCIATED CONTENT

### Supporting Information

The Supporting Information is available free of charge at https://pubs.acs.org/doi/10.1021/jacs.1c05286.

Detailed experimental procedures, characterization data for new compounds, coordinates for all computed structures, applied computational methods, luminescence spectra, racemization experiments, NMR titration experiments, chiral HPLC traces, NMR spectra for new compounds, including Figures S5.1−S6.2 (PDF)

NMR data (ZIP)

Optimized geometries of the molecules considered in the computational study (ZIP)

## ■ AUTHOR INFORMATION


### Corresponding Authors

**Thorsten Bach** − *Department Chemie and Catalysis Research Center (CRC), Technische Universität München, D-85747 Garching, Germany*; orcid.org/0000-0002-1342-0202; Email: thorsten.bach@ch.tum.de

**Christoph Bannwarth** − *Institute of Physical Chemistry, RWTH Aachen University, D-52056 Aachen, Germany*; orcid.org/0000-0003-3242-496X; Email: bannwarth@pc.rwth-aachen.de

### Authors

**Manuel Plaza** − *Department Chemie and Catalysis Research Center (CRC), Technische Universität München, D-85747 Garching, Germany*; orcid.org/0000-0002-5058-5321

**Johannes Großkopf** − *Department Chemie and Catalysis Research Center (CRC), Technische Universität München, D-85747 Garching, Germany*

**Stefan Breitenlechner** − *Department Chemie and Catalysis Research Center (CRC), Technische Universität München, D-85747 Garching, Germany*; orcid.org/0000-0001-5519-1922

Complete contact information is available at: https://pubs.acs.org/10.1021/jacs.1c05286

### Author Contributions

‖These authors contributed equally.


### Notes

The authors declare no competing financial interest.

## ■ ACKNOWLEDGMENTS

Financial support by the Deutsche Forschungsgemeinschaft (Ba 1372/24) and the Fonds der Chemischen Industrie (Kekulé fellowship to J.G.) is gratefully acknowledged. C.B. acknowledges funding by the Federal Ministry of Education and Research (BMBF) and the Ministry of Culture and Science of the German State of North Rhine-Westphalia under the Excellence Strategy of the Federal Government and the Länder. We thank O. Ackermann (TU München) for his help with the HPLC analyses and C. Hagemann (TU München) for synthetic assistance. Simulations were performed with computing resources granted by RWTH Aachen University under project rwth0721.

## ■ REFERENCES

(1) (a) Arunan, E.; Desiraju, G. R.; Klein, R. A.; Sadlej, J.; Scheiner, S.; Alkorta, I.; Clary, D. C.; Crabtree, R. H.; Dannenberg, J. J.; Hobza, P.; Kjaergaard, H. G.; Legon, A. C.; Mennucci, B.; Nesbitt, D. J. Defining the hydrogen bond: An account (IUPAC Technical Report). *Pure Appl. Chem.* **2011**, *83*, 1619−1636. (b) *An Introduction to Hydrogen Bonding*; Jeffrey, G. A., Ed.; Oxford University Press: Oxford, 1997. (c) *Hydrogen Bonding in Biological Structures*; Jeffrey, G. A., Saenger, W., Eds.; Springer: New York, 1991.

(2) Recent general reviews: (a) Fanourakis, A.; Docherty, P. J.; Chuentragool, P.; Phipps, R. J. Recent Developments in Enantioselective Transition Metal Catalysis Featuring Attractive Noncovalent Interactions between Ligand and Substrate. *ACS Catal.* **2020**, *10*, 10672−10714. (b) Burg, F.; Bach, T. Lactam Hydrogen Bonds as Control Elements in Enantioselective Transition-Metal-Catalyzed and Photochemical Reactions. *J. Org. Chem.* **2019**, *84*, 8815−8836. (c) Mote, N. R.; Chikkali, S. H. Hydrogen-Bonding-Assisted Supramolecular Metal Catalysis. *Chem. - Asian J.* **2018**, *13*, 3623−

3646. (d) Raynal, M.; Ballester, P.; Vidal-Ferran, A.; van Leeuwen, P. W. N. M. Supramolecular catalysis. Part 1: non-covalent interactions as a tool for building and modifying homogeneous catalysts. *Chem. Soc. Rev.* **2014**, *43*, 1660−1733. (e) See also: *Hydrogen Bonding in Organic Synthesis*; Pikho, P. M., Ed.; Wiley-VCH: Weinheim, 2009.

(3) For a recent review on the use of peptide backbones in asymmetric catalysis, see: Metrano, A. J.; Chinn, A. J.; Shugrue, C. R.; Stone, E. A.; Kim, B.; Miller, S. J. Asymmetric Catalysis Mediated by Synthetic Peptides, Version 2.0: Expansion of Scope and Mechanisms. *Chem. Rev.* **2020**, *120*, 11479−11615.

(4) Ippolito, J. A.; Alexander, R. S.; Christianson, D. W. Hydrogen Bond Stereochemistry in Protein Structure and Function. *J. Mol. Biol.* **1990**, *215*, 457−471.

(5) For some key references to the use of hydrogen bonds in photochemical reactions, see the cited literature in ref 2b and see also: (a) Vallavoju, N.; Selvakumar, S.; Jockusch, S.; Sibi, M. P.; Sivaguru, J. Enantioselective Organo-Photocatalysis Mediated by Atropisomeric Thiourea Derivatives. *Angew. Chem., Int. Ed.* **2014**, *53*, 5604−5608. (b) Vallavoju, N.; Selvakumar, S.; Jockusch, S.; Prabhakaran, M. T.; Sibi, M. P.; Sivaguru, J. Evaluating Thiourea Architecture for Intramolecular [2 + 2] Photocycloaddition of 4-Alkenylcoumarins. *Adv. Synth. Catal.* **2014**, *356*, 2763−2768. (c) Skubi, K. L.; Kidd, J. B.; Jung, H.; Guzei, I. A.; Baik, M.-H.; Yoon, T. P. Enantioselective Excited-State Photoreactions Controlled by a Chiral Hydrogen-Bonding Iridium Sensitizer. *J. Am. Chem. Soc.* **2017**, *139*, 17186−17192.

(6) (a) Eberhardt, E. S.; Raines, R. T. Amide-Amide and Amide-Water Hydrogen Bonds: Implications for Protein Folding and Stability. *J. Am. Chem. Soc.* **1994**, *116*, 2149−2150. (b) Moynihan, H. A.; Hayes, J. A.; Eccles, K. S.; Coles, S. J.; Lawrence, S. E. Hydrogen bonding in crystal forms of primary amide functionalized glucose and cellobiose. *Carbohydr. Res.* **2013**, *374*, 29−39.

(7) (a) Kapitán, P.; Bach, T. Template-Induced Enantioselectivity in the Reductive Radical Cyclization of 3-(3-Iodopropyloxy)propenoic Acid Derivatives and its Derivatives Depending on the Binding Motif. *Synthesis* **2008**, *2008*, 1559−1564. (b) Fackler, P.; Huber, S. M.; Bach, T. Enantio- and Regioselective Epoxidation of Olefinic Double Bonds in Quinolones, Pyridones, and Amides Catalyzed by a Ruthenium Porphyrin Catalyst with a Hydrogen Bonding Site. *J. Am. Chem. Soc.* **2012**, *134*, 12869−12878.

(8) Seo, M.; Park, J.; Kim, S. Y. Self-assembly driven by an aromatic primary amide motif. *Org. Biomol. Chem.* **2012**, *10*, 5332−5342.

(9) Dressel, M.; Bach, T. Chirality Multiplication and Efficient Chirality Transfer in *exo*- and *endo*-Radical Cyclization Reactions of 4-(4′-Iodobutyl)quinolones. *Org. Lett.* **2006**, *8*, 3145−3147.

(10) Bergmann, H.; Grosch, B.; Sitterberg, S.; Bach, T. An Enantiomerically Pure 1,5,7-Trimethyl-3-azabicyclo[3.3.1]nonan-2-one as $^{1}$H NMR Shift Reagent for the ee Determination of Chiral Lactams, Quinolones, and Oxazolidinones. *J. Org. Chem.* **2004**, *69*, 970−973.

(11) Reviews: (a) Yang, C.; Inoue, Y. An exciting tool for asymmetric synthesis. *Nature* **2018**, *564*, 197−199. (b) Shi, Q.; Ye, J. Deracemization Enabled by Visible-Light Photocatalysis. *Angew. Chem., Int. Ed.* **2020**, *59*, 4998−5001.

(12) For a pioneering study on allene deracemization reactions (up to 3.4% ee), see: Drucker, C. S.; Toscano, V. G.; Weiss, R. G. General Method for the Determination of Steric Effects during Collisional Energy Transfer. Partial Photoresolution of Penta-2,3-diene. *J. Am. Chem. Soc.* **1973**, *95*, 6482−6484.

(13) (a) Hölzl-Hobmeier, A.; Bauer, A.; Silva, A. V.; Huber, S. M.; Bannwarth, C.; Bach, T. Catalytic deracemization of chiral allenes by sensitized excitation with visible light. *Nature* **2018**, *564*, 240−243. (b) Plaza, M.; Jandl, C.; Bach, T. Photochemical Deracemization of Allenes and Subsequent Chirality Transfer. *Angew. Chem., Int. Ed.* **2020**, *59*, 12785−12788.

(14) Wimberger, L.; Kratz, T.; Bach, T. Photochemical Deracemization of Chiral Sulfoxides Catalyzed by a Hydrogen-Bonding Xanthone Sensitizer. *Synthesis* **2019**, *51*, 4417−4424.

(15) (a) Tröster, A.; Bauer, A.; Jandl, C.; Bach, T. Enantioselective Visible-Light-Mediated Formation of 3-Cyclopropylquinolones by Triplet-Sensitized Deracemization. *Angew. Chem., Int. Ed.* **2019**, *58*, 3538−3541. (b) Li, X.; Kutta, R. J.; Jandl, C.; Bauer, A.; Nuernberger, P.; Bach, T. Photochemically Induced Ring Opening of Spirocyclopropyl Oxindoles: Evidence for a Triplet 1,3-Diradical Intermediate and Deracemization by a Chiral Sensitizer. *Angew. Chem., Int. Ed.* **2020**, *59*, 21640−21647.

(16) For reviews on chiral allenes and their use in synthesis, see: (a) Yu, S.; Ma, S. Allenes in Catalytic Asymmetric Synthesis and Natural Product Syntheses. *Angew. Chem., Int. Ed.* **2012**, *51*, 3074−3112. (b) *Cumulenes and Allenes, Science of Synthesis*; Krause, N., Ed.; Thieme Chemistry: Stuttgart, 2008; Vol. *44*. (c) *Modern Allene Chemistry*; Krause, N., Hashmi, A. S. K., Eds.; Wiley-VCH: Weinheim, 2004.

(17) For nonphotochemical deracemization approaches to chiral allenes, see: (a) Naruse, Y.; Watanabe, H.; Ishiyama, Y.; Yoshida, T. Enantiomeric Enrichment of Allenedicarboxylates by a Chiral Organoeuropium Reagent. *J. Org. Chem.* **1997**, *62*, 3862−3866. (b) Varghese, J. P.; Zouev, I.; Aufauvre, L.; Knochel, P.; Marek, I. Carbocupration/Zinc Carbenoid Homologation and $\beta$-Elimination Reactions for a New Synthesis of Allenes − Application to the Enantioselective Synthesis of Chiral Allenes by Deracemization of $sp^3$-Organometallic Derivatives. *Eur. J. Org. Chem.* **2002**, *2002*, 4151−4158. (c) Ye, J.; Ma, S. Conquering three-carbon axial chirality of allenes. *Org. Chem. Front.* **2014**, *1*, 1210−1224.

(18) In a conceptually different approach, cyclic imidazolidinones were photochemically deracemized: Shin, N. Y.; Ryss, J. M.; Zhang, X.; Miller, S. J.; Knowles, R. R. Light-driven deracemization enabled by excited-state electron transfer. *Science* **2019**, *366*, 364−369.

(19) For a review, see: Soriano, E.; Fernández, I. Allenes and computational chemistry: from bonding situations to reaction mechanisms. *Chem. Soc. Rev.* **2014**, *43*, 3041−3105.

(20) (a) Pracht, P.; Bohle, F.; Grimme, S. Automated exploration of the low-energy chemical space with fast quantum chemical methods. *Phys. Chem. Chem. Phys.* **2020**, *22*, 7169−7192. (b) Bannwarth, C.; Ehlert, S.; Grimme, S. GFN2-xTB—An Accurate and Broadly Parametrized Self-Consistent Tight-Binding Quantum Chemical Method with Multipole Electrostatics and Density-Dependent Dispersion Contributions. *J. Chem. Theory Comput.* **2019**, *15*, 1652−1671. (c) Grimme, S.; Brandenburg, J. G.; Bannwarth, C.; Hansen, A. Consistent structures and interactions by density functional theory with small atomic orbital basis sets. *J. Chem. Phys.* **2015**, *143*, 054107. (d) Zhao, Y.; Truhlar, D. G. Design of Density Functionals That Are Broadly Accurate for Thermochemistry, Thermochemical Kinetics, and Nonbonded Interactions. *J. Phys. Chem. A* **2005**, *109*, 5656−5667. (e) Weigend, F.; Ahlrichs, R. Balanced basis sets of split valence, triple zeta valence and quadruple zeta valence quality for H to Rn: Design and assessment of accuracy. *Phys. Chem. Chem. Phys.* **2005**, *7*, 3297−3305. (f) Grimme, S.; Antony, J.; Ehrlich, S.; Krieg, H. A consistent and accurate ab initio parametrization of density functional dispersion correction (DFT-D) for the 94 elements H-Pu. *J. Chem. Phys.* **2010**, *132*, 154104. (g) Grimme, S.; Ehrlich, S.; Goerigk, L. Effect of the damping function in dispersion corrected density functional theory. *J. Comput. Chem.* **2011**, *32*, 1456−1465. (h) Furche, F.; Ahlrichs, R.; Hättig, C.; Klopper, W.; Sierka, M.; Weigend, F. Turbomole. *Wiley Interdiscip. Rev.: Comput. Mol. Sci.* **2014**, *4*, 91−100. (i) *TURBOMOLE*, version 7.4.1. Program Package For Electronic Structure Calculations; TURBOMOLE GmbH: Karlsruhe, Germany. https://www.turbomole.org/ (accessed 2021-07-03).

(21) Wittig, G.; Haag, W. Über Triphenyl-phosphin-methylene als olefinbildende Reagenzien. *Chem. Ber.* **1955**, *88*, 1654−1666.

(22) Britto, N.; Gore, V. G.; Mali, R. S.; Ranade, A. C. A Convenient Synthesis of 3-Benzyl, 3-Benzyl-4-Substituted Coumarins and Their Benzo Derivatives. *Synth. Commun.* **1989**, *19*, 1899−1910.

(23) Wang, G.; Liu, X.; Chen, Y.; Yang, J.; Li, J.; Lin, L.; Feng, X. Diastereoselective and Enantioselective Alleno-aldol Reaction of Allenoates with Isatins to Synthesis of Carbinol Allenoates Catalyzed by Gold. *ACS Catal.* **2016**, *6*, 2482−2486.

(24) Montalbetti, C. A. G. N.; Falque, V. Amide bond formation and peptide coupling. *Tetrahedron* **2005**, *61*, 10827−10852.



https://doi.org/10.1021/jacs.1c05286
*J. Am. Chem. Soc.* 2021, 143, 11209−11217

(25) Iyer, A.; Clay, A.; Jockusch, S.; Sivaguru, J. Evaluating brominated thioxanthones as organo-photocatalysts. *J. Phys. Org. Chem.* **2017**, *30*, e3738.
(26) It was pointed out by one reviewer that the erosion of selectivity could be entropy related. For a treatise on entropy control in photochemistry, see: Inoue, Y.; Sugahara, N.; Wada, T. Vital Role of Entropy in Photochirogenesis. *Pure Appl. Chem.* **2001**, *73*, 475−480.
(27) (a) Becke, A. D. A new mixing of Hartree−Fock and local density-functional theories. *J. Chem. Phys.* **1993**, *98*, 1372−1377. (b) Rappoport, D.; Furche, F. Property-optimized Gaussian basis sets for molecular response calculations. *J. Chem. Phys.* **2010**, *133*, 134105. (c) Klamt, A.; Schüürmann, G. COSMO: a new approach to dielectric screening in solvents with explicit expressions for the screening energy and its gradient. *J. Chem. Soc., Perkin Trans. 2* **1993**, 799−805.
(28) (a) Fielding, L. Determination of association constants (*Ka*) from solution NMR data. *Tetrahedron* **2000**, *56*, 6151−6170. (b) Thordarson, P. Determining association constants from titration experiments in supramolecular chemistry. *Chem. Soc. Rev.* **2011**, *40*, 1305−1323.
(29) Hobbs, M. E.; Bates, W. W. The determination of the association constants of some acid amides in benzene solution. *J. Am. Chem. Soc.* **1952**, *74*, 746−749.
(30) Bannwarth, C.; Hansen, A.; Grimme, S. The Association of Two "Frustrated" Lewis Pairs by State-of-the-Art Quantum Chemical Methods. *Isr. J. Chem.* **2015**, *55*, 235−242.
(31) Molecular graphics images were produced using the UCSF Chimera package from the Resource for Biocomputing, Visualization, and Informatics at the University of California, San Francisco: Pettersen, E. F.; Goddard, T. D.; Huang, C. C.; Couch, G. S.; Greenblatt, D. M.; Meng, E. C.; Ferrin, T. E. UCSF Chimera - A Visualization System for Exploratory Research and Analysis. *J. Comput. Chem.* **2004**, *25*, 1605−1612.
(32) (a) For a pertinent review, see: Wagner, J. P.; Schreiner, P. R. London Dispersion in Molecular Chemistry—Reconsidering Steric Effects. *Angew. Chem., Int. Ed.* **2015**, *54*, 12274−12296. (b) For a recent study, see: Eschmann, C.; Song, L.; Schreiner, P. R. London Dispersion Interactions Rather than Steric Hindrance Determine the Enantioselectivity of the Corey−Bakshi−Shibata Reduction. *Angew. Chem., Int. Ed.* **2021**, *60*, 4823−4832.
(33) (a) Nishio, M. The CH/$\pi$ hydrogen bond in chemistry. Conformation, supramolecules, optical resolution and interactions involving carbohydrates. *Phys. Chem. Chem. Phys.* **2011**, *13*, 13873−13900. (b) Nishio, M.; Umezawa, Y.; Fantini, J.; Weiss, M. S.; Chakrabarti, P. CH−$\pi$ hydrogen bonds in biological macromolecules. *Phys. Chem. Chem. Phys.* **2014**, *16*, 12648−12683.
(34) Compound **8c** benefits from an increased ISC rate due to the heavy atom effect: Koziar, J. C.; Cowan, D. O. Photochemical heavy-atom effects. *Acc. Chem. Res.* **1978**, *11*, 334−341.
(35) For some selected references on the triplet energy of allenes, see: (a) Gotthardt, H.; Hammond, G. S. Zur Photochemie des Allens. *Chem. Ber.* **1975**, *108*, 657−663. (b) Kamphuis, J.; Bos, H. J. T.; Visser, R. J.; Huizer, B. H.; Varma, C. A. G. O. An extremely short-lived 1,4-biradical as intermediate in the photo-cycloaddition reactions of triplet state aromatic thiones with allenes. *J. Chem. Soc., Perkin Trans. 2* **1986**, 1867−1874. (c) Tsuno, T.; Hoshino, H.; Sugiyama, K. Allenyl(vinyl)-methane photochemistry. Photochemistry of 4,4,7-trimethyl-5-phenyl-2,5,6-octatrienate derivatives. *Tetrahedron Lett.* **1997**, *38*, 1581−1584. (d) Alcaide, B.; Almendros, P.; Aragoncillo, C. Exploiting [2 + 2] cycloaddition chemistry: achievements with allenes. *Chem. Soc. Rev.* **2010**, *39*, 783−816.
(36) (a) Hättig, C.; Weigend, F. CC2 excitation energy calculations on large molecules using the resolution of the identity approximation. *J. Chem. Phys.* **2000**, *113*, 5154−5161. (b) Dunning, T. H., Jr. Gaussian basis sets for use in correlated molecular calculations. I. The atoms boron through neon and hydrogen. *J. Chem. Phys.* **1989**, *90*, 1007−1023. (c) Kendall, R. A.; Dunning, T. H.; Harrison, R. J. Electron affinities of the first-row atoms revisited. Systematic basis sets and wave functions. *J. Chem. Phys.* **1992**, *96*, 6796−6806.
(37) Bucher, G.; Mahajan, A. A.; Schmittel, M. The Photochemical $C^2$-$C^6$ Cyclization of Enyne-Allenes: Interception of the Fulvene Diradical with a Radical Clock Ring Opening. *J. Org. Chem.* **2009**, *74*, 5850−5860.
(38) (a) Turro, N. J.; Ramamurthy, V.; Scaiano, J. C. *Modern Molecular Photochemistry of Organic Molecules*; University Science: Sausalito, 2010; pp 383−481. (b) Dexter, D. L. A Theory of Sensitized Luminescence in Solids. *J. Chem. Phys.* **1953**, *21*, 836−850. (c) Klán, P.; Wirz, J. *Photochemistry of Organic Compounds*; Wiley: Chichester, 2009; pp 57−60.
(39) Prasanna, M.; Row, T. G. C−halogen···$\pi$ interactions and their influence on molecular conformation and crystal packing: a database study. *Cryst. Eng.* **2000**, *3*, 135−154.
(40) (a) Slavíček, P.; Martínez, T. J. Ab initio floating occupation molecular orbital-complete active space configuration interaction: An efficient approximation to CASSCF. *J. Chem. Phys.* **2010**, *132*, 234102. (b) Hohenstein, E. G.; Bouduban, M. E. F.; Song, C.; Luehr, N.; Ufimtsev, I. S.; Martínez, T. J. Analytic first derivatives of floating occupation molecular orbital-complete active space configuration interaction on graphical processing units. *J. Chem. Phys.* **2015**, *143*, 014111. (c) Hohenstein, E. G. Analytic formulation of derivative coupling vectors for complete active space configuration interaction wavefunctions with floating occupation molecular orbitals. *J. Chem. Phys.* **2016**, *145*, 174110.
(41) Seritan, S.; Bannwarth, C.; Fales, B. S.; Hohenstein, E. G.; Isborn, C. M.; Kokkila-Schumacher, S. I. L.; Li, X.; Liu, F.; Luehr, N.; Snyder, J. W., Jr.; Song, C.; Titov, A. V.; Ufimtsev, I. S.; Wang, L.-P.; Martínez, T. J. TeraChem: A graphical processing unit-accelerated electronic structure package for large-scale ab initio molecular dynamics. *Wiley Interdiscip. Rev.: Comput. Mol. Sci.* **2021**, *11*, e1494.
(42) (a) Hirata, S.; Head-Gordon, M. Time-dependent density functional theory within the Tamm−Dancoff approximation. *Chem. Phys. Lett.* **1999**, *314*, 291−299. (b) Casida, M. E. Time-Dependent Density Functional Response Theory for Molecules. In *Recent Advances in Density Functional Methods*; Chong, D. P., Ed.; World Scientific: Singapore, 1995; pp 155−192.
(43) Grimme, S. Supramolecular Binding Thermodynamics by Dispersion-Corrected Density Functional Theory. *Chem. - Eur. J.* **2012**, *18*, 9955−9964.
(44) Ehlert, S.; Stahn, M.; Spicher, S.; Grimme, S. Robust and Efficient Implicit Solvation Model for Fast Semiempirical Methods. *J. Chem. Theory Comput.* **2021**, in press. DOI: 10.1021/acs.jctc.1c00471.

## NOTE ADDED AFTER ASAP PUBLICATION

Due to a production error, Scheme 1 was replaced incorrectly on July 19, 2021. The corrected version was reposted on July 19, 2021.


https://doi.org/10.1021/jacs.1c05286
J. Am. Chem. Soc. 2021, 143, 11209−11217

# 7 Photochemical Deracemization at sp$^3$-Hybridized Carbon Centers *via* a Reversible Hydrogen Atom Transfer

**Title:** "Photochemical Deracemization at sp$^3$-Hybridized Carbon Centers *via* a Reversible Hydrogen Atom Transfer"

**Status:** Communication, published online December 13, 2021

**Journal:** *Journal of the American Chemical Society* **2021**, *143*, 21241–21245.

**Publisher:** American Chemical Society

**DOI:** 10.1021/jacs.1c11266

**Authors:** Johannes Großkopf*, Manuel Plaza*, Antonia Seitz*, Stefan Breitenlechner, Golo Storch, Thorsten Bach (*These authors contributed equally.)

**Content**: This communication reports the successful development of a novel type of deracemization mechanism based on hydrogen atom transfer. By using a chiral benzophenone catalyst with a two-point hydrogen bonding site, an array of structurally different hydantoins (27 examples) was successfully deracemized. Only 5 mol% of catalyst were sufficient to induce an enantiomeric excess of up to 99% *ee* with up to quantitative yield. Mechanistic investigations, including kinetic isotope effect (KIE) studies, deuterium scrambling, radical clock experiments and ground-state DFT calculations, suggest a selective HAT event. Due to precise positioning of the substrates within the catalyst array, it was concluded that only the enantiomer, whose hydrogen atom at the stereogenic center points towards the benzophenone moiety, is processed by the catalyst. By passing a transient carbon centered radical and subsequent back HAT, the reformation of the stereogenic center by an unselective pathway is achieved, resulting in the prevalence of the desired enantiomer in the photostationary state.

J. Großkopf and T. Seitz initiated the project and optimized the reaction conditions. J. Großkopf and M. Plaza performed all scope experiments. J. Großkopf conducted all synthetic mechanistic investigations. G. Storch performed the DFT calculations. J. Großkopf and T. Bach wrote the manuscript. S. Breitenlechner helped with KIE experiments and proof reading of the manuscript. All work was performed under the supervision of T. Bach.

JACS
JOURNAL OF THE AMERICAN CHEMICAL SOCIETY
pubs.acs.org/JACS
Communication

# Photochemical Deracemization at sp$^3$-Hybridized Carbon Centers via a Reversible Hydrogen Atom Transfer

Johannes Großkopf,[‡] Manuel Plaza,[‡] Antonia Seitz,[‡] Stefan Breitenlechner, Golo Storch, and Thorsten Bach*

Cite This: *J. Am. Chem. Soc.* 2021, 143, 21241−21245
Read Online
ACCESS | Metrics & More | Article Recommendations | Supporting Information

**ABSTRACT:** A photochemical deracemization of 5-substituted 3-phenylimidazolidine-2,4-diones (hydantoins) is reported (27 examples, 69%-quant., 80−99% *ee*). The reaction is catalyzed by a chiral diarylketone which displays a two-point hydrogen bonding site. Mechanistic evidence (DFT calculations, radical clock experiments, H/D labeling) suggests the reaction to occur by selective hydrogen atom transfer (HAT). Upon hydrogen binding, one substrate enantiomer displays the hydrogen atom at the stereogenic center to the photoexcited catalyst allowing for a HAT from the substrate and eventually for its conversion into the product enantiomer. The product enantiomer is not processed by the catalyst and is thus enriched in the photostationary state.

A remarkable feature of most compounds generated and utilized by nature is the fact that they are homochiral, i.e. that only a single enantiomer is present.[1] The encounter with another chiral entity leads to diastereomeric interactions which means that nature can discriminate between enantiomers.[2] As a consequence, the selective synthesis of enantiopure compounds has received tremendous attention and became a flourishing research area within recent decades.[3] Still, the production and unselective synthesis of racemates is sometimes unavoidable or less expensive than the selective synthesis of one enantiomer. While it is thermodynamically impossible to achieve the conversion of a racemate into an enantiomer under equilibrium conditions,[4−6] photochemical deracemization reactions are viable with the light energy compensating the entropic penalty of the process.[7] Although envisioned for over 50 years,[8] highly selective photochemical deracemization reactions have only recently been realized.[9−13]

Three approaches have so far been reported. One approach, taken by our group, rests on the fact that a photolabile stereogenic unit is equilibrated by triplet energy transfer. Selective excitation of one enantiomer is achieved by a chiral sensitizer. The method has been applied successfully to allenes,[9] sulfoxides,[10] and cyclopropanes.[11] In a different approach, Knowles, Miller, and co-workers employed a three-component catalytic system composed of an achiral iridium complex, a chiral phosphoric acid, and a chiral cysteine-based tetrapeptide to deracemize ureas in a sequence of electron, proton, and hydrogen-atom transfer steps.[12] Very recently, the groups of Meggers and Chen reported a deracemization of 2-pyridylketones based on a photoredox process in the course of which a chiral-at-metal rhodium enolate is stereoselectively protonated.[13]

In Scheme 1 ($c$ = concentration), the interconversion between two enantiomers *ent*-**I** and **I** of a chiral $\alpha$-amino acid derivative is depicted occurring by a reversible hydrogen atom transfer (HAT) via radical **II**.[14] We hypothesized that a photochemical deracemization might be possible in this scenario by a single catalyst which would discriminate between *ent*-**I** and **I**. If HAT from **I** to the chiral photoexcited catalyst was retarded vs *ent*-**I** (blue) or in the extreme case nonexistent, enantiomer **I** would prevail, ideally with 100% enantiomeric excess (*ee*). We now report on the successful realization of this idea in the context of imidazolidine-2,4-dione (hydantoin) deracemization. Hydantoins belong to the most frequently used heterocyclic scaffolds in the pharmaceutical industry, and there is a large demand for their preparation in enantiopure form.[15]

**Scheme 1. Mechanistic Scenario for a Deracemization at a Stereogenic Center in Amino Acid Derivatives by Hydrogen Atom Transfer (HAT)**

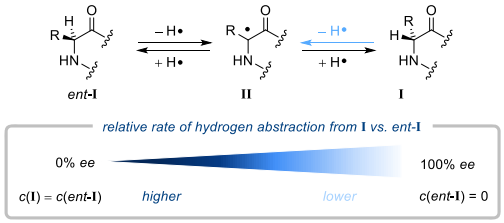


In preliminary DFT calculations we explored the option of removing the hydrogen atom at the stereogenic center of *tert*-leucin-derived hydantoins **1a** and *ent*-**1a** (Figure 1). The known benzophenone **2**[16] was considered as a suitable organocatalyst[17] which might discriminate between the two

**Received:** October 25, 2021
**Published:** December 13, 2021





https://doi.org/10.1021/jacs.1c11266
*J. Am. Chem. Soc.* 2021, 143, 21241−21245

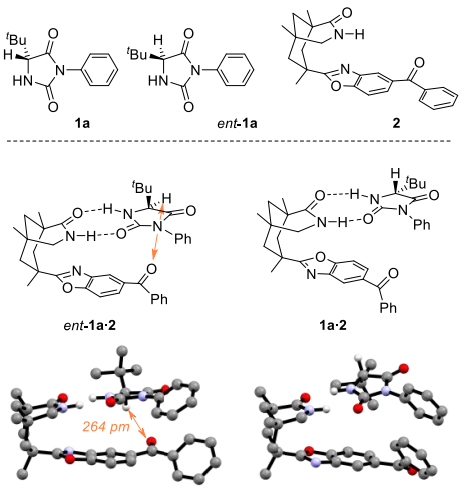


**Figure 1.** Structures of the enantiomeric hydantoins **1a** and *ent*-**1a** and of ketone **2** (top). Binding of ketone **2** to compounds *ent*-**1a** and **1a** via two hydrogen bonds (bottom). In complex *ent*-**1a·2** the close proximity of the hydrogen atom at the stereogenic center to the carbonyl oxygen atom invites a HAT upon excitation of ketone **2** while no hydrogen atom is accessible in any conformer of the diastereomeric complex **1a·2** (the lowest energy conformer is depicted).

enantiomers by hydrogen bonding. It is well established that photoexcited benzophenones are capable of abstracting hydrogen atoms from $sp^3$-hybridized carbon centers.[14,18] The calculations revealed that complex *ent*-**1a·2** can access a ground-state conformation in which the carbonyl oxygen atom is only 264 pm remote from the hydrogen atom at the stereogenic center (see the Supporting Information (SI) for the conformational analysis). Upon excitation, a HAT should occur readily in contrast to complex **1a·2**, in which the hydrogen atom is located in an inaccessible position at the opposite side of the hydantoin ring.

Although we had initially speculated that an additive would be required to shuttle the hydrogen atom after the HAT back to the substrate, preliminary studies with benzophenone **2** and leucine-derived hydantoin *rac*-**1b** showed this not to be necessary (Table S3 in the SI). A deracemization was possible simply by employing 5 mol % of photocatalyst **2** upon irradiation at $\lambda$ = 366 nm. Further optimization revealed that $\alpha,\alpha,\alpha$-trifluorotoluene was the optimal solvent, and a concentration of $c$ = 10 mM gave the best results in this instance. Irradiation at a shorter wavelength ($\lambda$ = 350 nm) or in polar solvents ($CH_2Cl_2$, MeCN) led to inferior enantioselectivities. Product **1b** was eventually isolated (Table 1) in a yield of 86% and with 93% *ee*. The absolute configuration was assigned as (*R*) based on comparison with authentic material prepared from (*R*)- and (*S*)-leucine. A kinetic analysis (Figure S1 in the SI) revealed that the *ee* increased steadily until it reached a plateau after 10 h. When the scope of the reaction was being investigated, the reactions were typically run overnight (13 h) at ambient temperature. The racemic hydantoins were readily synthesized[15] from commercially available racemic amino acids by treatment of the respective methyl ester with phenyl isocyanate and subsequent condensation.[19] In all other instances the hydantoins *rac*-**1** were prepared from the respective aldehydes by a Bucherer–Bergs reaction[20] and a subsequent regioselective *N*-arylation of the hydantoin.[21] In order to avoid complications with diastereoisomers, only hydantoins with a single stereogenic center were employed.

**Table 1. Product Scope for the Photochemical Deracemization of Hydantoins *rac*-1 by Chiral Ketone 2**

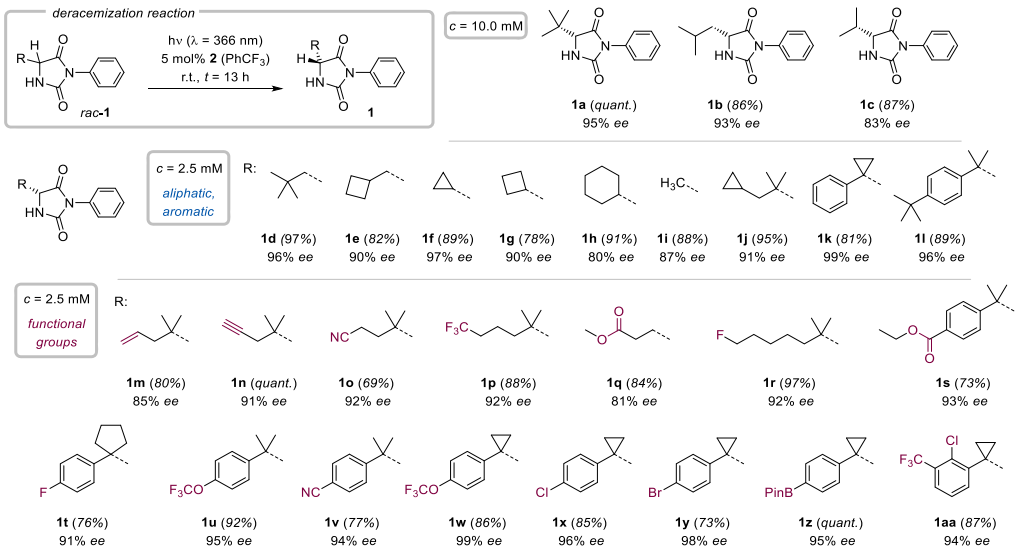




https://doi.org/10.1021/jacs.1c11266
J. Am. Chem. Soc. 2021, 143, 21241−21245

**Scheme 2. Mechanistic Experiments and Potential Key Intermediates of the Deracemization Reaction**

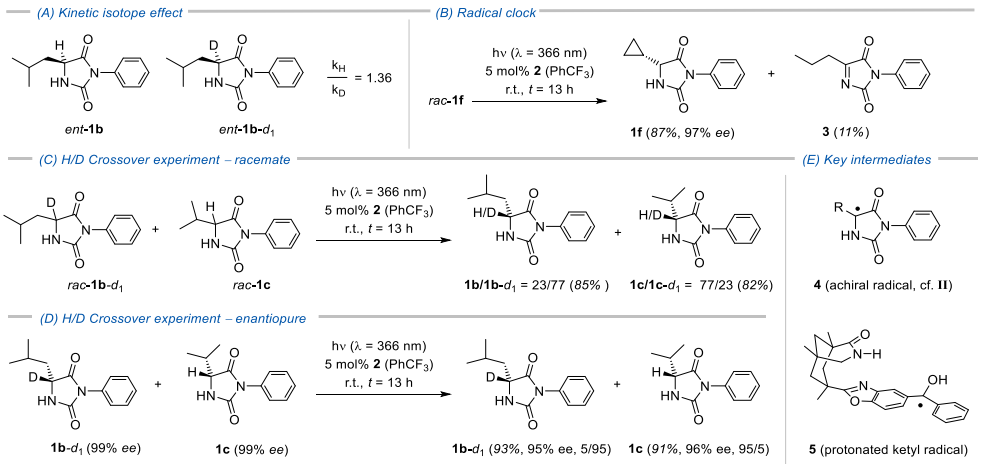


For solubility reasons most reactions were performed at a concentration of $c$ = 2.5 mM. A total of 27 hydantoins **1** were prepared in enantioselectivities of 80−99% *ee*. In the aliphatic substrate series, it is worthy to note that the *ee* does not correlate with the size of the substituent R (*vide infra*). For example, primary alkyl groups (**1b**, **1e**) gave in some cases better results than secondary alkyl groups (**1c**, **1h**). Even the alanine-derived hydantoin with a small methyl group at the stereogenic center could be deracemized successfully (**1i**).

Regarding functional groups, a broad range of multiple bonds and hetero atoms were tolerated including olefins (**1m**), alkynes (**1n**), nitriles (**1o**, **1v**), esters (**1q**, **1s**), ethers (**1u**, **1w**), halogen atoms (**1r**, **1t**, **1x**, **1y**, **1aa**), and boronates (**1z**, pin = pinacolate). Due to the oxidizing properties of the photoexcited ketone, hydantoins with oxidation sensitive groups (amines, sulfides, selenides) could not be used or gave low *ee*'s. If the substituent R stabilizes a negative charge in the $\alpha$-position, e.g. phenyl, the hydantoins are configurationally unstable and racemize readily.[18] Other *N*-aryl- and *N*-alkyl-substituted hydantoins gave lower enantioselectivities than the *N*-phenyl compounds or featured solubility issues (see Table S4 in the SI). Reactions were typically run on a scale of 0.05 mmol due to the limited supply of catalyst. For two products, we showed exemplarily that reactions on a larger scale (1.0 mmol) delivered comparable results at a slightly elongated irradiation time ($t$ = 15 h). Hydantoin **1a** was obtained in 96% yield with 95% *ee*, and hydantoin **1r**, in 75% yield with 93% *ee*.

Preliminary mechanistic experiments were performed to decipher the nature of the intermediates involved in the deracemization reaction. While the rate of the deracemization from *rac*-**1** cannot be determined, the initial rate for the formation of **1b** from *ent*-**1b** could be measured and a primary kinetic isotope effect ($k_H/k_D$) of 1.36 was found (Scheme 2A). The low value may indicate that the C−H(D) bond is broken *via* a nonlinear transition state,[22] and it is likely that an achiral radical **4** (R = isobutyl) is formed. The latter notion was corroborated by the fact that the cyclopropyl-substituted hydantoin *rac*-**1f** not only delivered product **1f** but also a ring-opened product to which we assigned structure **3** (Scheme 2B). The rate for ring opening of a cyclopropylmethyl to a but-3-enyl radical[23] is in the order of $10^8$ $s^{-1}$ which allows for a preliminary assessment of the lifetime of radical **4**. In a crossover experiment with racemic compounds *rac*-**1b**-$d_1$ and *rac*-**1c**, it was found that H/D scrambling occurs in the range of ca. 25% (Scheme 2C). If enantiopure compounds with defined (*R*)-configuration were employed there was practically no H/D scrambling (Scheme 2D). If the starting materials were used exclusively as (*S*)-enantiomers, H/D scrambling reached a value of ca. 50% (see the Supporting Information for details). Regarding the nature of the excited state, it is well established that benzophenones populate their lowest lying triplet state $T_1$ by excitation and subsequent intersystem crossing with quantum yields close to unity.[17,24]

Taken the mechanistic studies and previous work together, it appears as if ketone **2** can differentiate between the two hydantoin enantiomers **1** and *ent*-**1** as suggested by the calculations (Figure 1). Upon excitation, a HAT occurs only at (*S*)-configured hydantoins *ent*-**1** but not at compounds **1** with the (*R*)-configuration (e.g., **1b**-$d_1$ and **1c**, Scheme 2D). Hydrogen abstraction leads to achiral radical **4** and protonated ketyl radical **5** (Scheme 2E). Remarkably, the back HAT from **5** to **4** appears to be preferred over any C−C bond forming events and dimers of **4** and **5** were not detected. In addition, back HAT occurs with statistical H/D scrambling (cf. Scheme 2C and the Supporting Information) which suggests it to be an intermolecular process that occurs after dissociation of **4** from **5**. The question whether back HAT generates **1** and *ent*-**1** with a preference for either enantiomer and how the process works in detail remains to be elucidated. If back HAT occurs to the oxygen atom of radical **4**, the intermediate enols could be responsible for H/D scrambling and racemization. In either case, for any molecule of *ent*-**1**, the HAT cycle is restarted as long as ketone **2** is available. Reactions that do not deliver high enantioselectivities very likely suffer from catalyst decomposition which in turn retards the progress of the reaction. This hypothesis explains the relative low enantioselectivity obtained for **1c** and **1h**, with both displaying an abstractable hydrogen atom at a tertiary carbon atom next to the stereogenic center.



https://doi.org/10.1021/jacs.1c11266
J. Am. Chem. Soc. 2021, 143, 21241−21245

In both cases, prolonged irradiation did not lead to improved enantioselectivity. However, addition of another 5 mol % of catalyst **2** after 13 h led to an enantioselectivity increase from 83% *ee* to 94% *ee* in the reaction *rac*-**1c** → **1c**. The yield remained unchanged.

In summary, a conceptually new method for a photochemical deracemization has been established which relies on a selective HAT to the photocatalyst. It enables the conversion of racemic mixtures into a single enantiomer by reverting the configuration at a $sp^3$-hybridized carbon center. Studies are ongoing to elucidate the nature of the intermediates and to obtain detailed information on their lifetime. It is envisioned that other compounds with a two-point hydrogen bonding site will also be amenable to deracemization by catalyst **2**.

## ■ ASSOCIATED CONTENT

### Supporting Information

The Supporting Information is available free of charge at https://pubs.acs.org/doi/10.1021/jacs.1c11266.

Experimental procedures, analytical data and NMR spectra for all new compounds, HPLC traces of all hydantoins (racemates, enantioenriched products), optimization and mechanistic experiments, details of the DFT calculations (PDF)

NMR data for compounds **1**, **3**−**9** (ZIP)

## ■ AUTHOR INFORMATION


### Corresponding Author

**Thorsten Bach** − *School of Natural Sciences, Department Chemie, and Catalysis Research Center (CRC), Technische Universität München, 85747 Garching, Germany;* orcid.org/0000-0002-1342-0202; Email: thorsten.bach@ch.tum.de

### Authors

**Johannes Großkopf** − *School of Natural Sciences, Department Chemie, and Catalysis Research Center (CRC), Technische Universität München, 85747 Garching, Germany*

**Manuel Plaza** − *School of Natural Sciences, Department Chemie, and Catalysis Research Center (CRC), Technische Universität München, 85747 Garching, Germany;* orcid.org/0000-0002-5058-5321

**Antonia Seitz** − *School of Natural Sciences, Department Chemie, and Catalysis Research Center (CRC), Technische Universität München, 85747 Garching, Germany*

**Stefan Breitenlechner** − *School of Natural Sciences, Department Chemie, and Catalysis Research Center (CRC), Technische Universität München, 85747 Garching, Germany;* orcid.org/0000-0001-5519-1922

**Golo Storch** − *School of Natural Sciences, Department Chemie, and Catalysis Research Center (CRC), Technische Universität München, 85747 Garching, Germany;* orcid.org/0000-0002-6747-3035

Complete contact information is available at: https://pubs.acs.org/10.1021/jacs.1c11266

### Author Contributions

‡J.G., M.P., and A.S. contributed equally to this work.


### Notes

The authors declare no competing financial interest.

## ■ ACKNOWLEDGMENTS

The project was funded by the Deutsche Forschungsgemeinschaft (DFG, German Research Foundation) by Grants Ba 1372/23, Ba 1372/24 and within TRR 325 (444632635). G.S. is the recipient of an Emmy Noether fellowship granted by the DFG (Sto 1175/3), and J.G. is supported by a Kekulé fellowship from the *Fonds der Chemischen Industrie*. The authors gratefully acknowledge the Leibniz Supercomputing Centre for funding this project by providing computing time on its Linux-Cluster. They thank O. Ackermann, L. Koser, and F. Pecho (all TU München) for help with the HPLC analyses.

## ■ REFERENCES

(1) (a) Mason, S. F. Origins of biomolecular handedness. *Nature* **1984**, *311*, 19−23. (b) Meierhenrich, U. *Amino Acids and the Asymmetry of Life*; Springer: 2008. (c) Hein, J. E.; Blackmond, D. G. On the Origin of Amino Acids and Sugars in Biogenesis. *Acc. Chem. Res.* **2012**, *45*, 2045−2054.

(2) (a) Bentley, R. Diastereoisomerism, contact points, and chiral selectivity: a four-site saga. *Arch. Biochem. Biophys.* **2003**, *414*, 1−12. (b) Brooks, W. H.; Guida, W. C.; Daniel, K. G. The Significance of Chirality in Drug Design and Development. *Curr. Top Med. Chem.* **2011**, *11*, 760−770.

(3) (a) Carreira, E. M.; Yamamoto, H., Eds.; *Comprehensive Chirality*; Academic Press, 2012. (b) Calcaterra, A.; D'Acquarica, I. The market of chiral drugs: Chiral switches versus de novo enantiomerically pure compounds. *J. Pharm. Biomed. Anal.* **2018**, *147*, 323−340.

(4) For a review on the separation of enantiomers, see: Lorenz, H.; Seidel-Morgenstern, A. Processes to Separate Enantiomers. *Angew. Chem., Int. Ed.* **2014**, *53*, 1218−1250.

(5) For reviews on deracemization by dynamic kinetic resolution: (a) Bhat, V.; Welin, E. R.; Guo, X.; Stoltz, B. M. Advances in Stereoconvergent Catalysis from 2005 to 2015: Transition-Metal-Mediated Stereoablative Reactions, Dynamic Kinetic Resolutions, and Dynamic Kinetic Asymmetric Transformations. *Chem. Rev.* **2017**, *117*, 4528−4561. (b) Rachwalski, M.; Vermue, N.; Rutjes, F. P. J. T. Recent advances in enzymatic and chemical deracemisation of racemic compounds. *Chem. Soc. Rev.* **2013**, *42*, 9268−9282.

(6) For reviews on deracemization by crystallization: (a) Buhse, T.; Cruz, J.-M.; Noble-Terán, M. E.; Hochberg, D.; Ribó, J. M.; Crusats, J.; Micheau, J.-C. Spontaneous Deracemizations. *Chem. Rev.* **2021**, *121*, 2147−2229. (b) Palmans, A. R. A. Deracemisations under kinetic and thermodynamic control. *Mol. Syst. Des. Eng.* **2017**, *2*, 34−46.

(7) (a) Yang, C.; Inoue, Y. An exciting tool for asymmetric synthesis. *Nature* **2018**, *564*, 197−199. (b) Shi, Q.; Ye, J. Deracemization Enabled by Visible-Light Photocatalysis. *Angew. Chem., Int. Ed.* **2020**, *59*, 4998−5001.

(8) Examples: (a) Hammond, G. S.; Cole, R. S. Asymmetric Induction during Energy Transfer. *J. Am. Chem. Soc.* **1965**, *87*, 3256−3257. (b) Drucker, C. S.; Toscano, V. G.; Weiss, R. G. A General Method for the Determination of Steric Effects during Collisional Energy Transfer. Partial Photoresolution of Penta-2,3-diene. *J. Am. Chem. Soc.* **1973**, *95*, 6482−6484. (c) Ouannès, C.; Beugelmans, R.; Roussi, G. Asymmetric Induction during Transfer of Triplet Energy. *J. Am. Chem. Soc.* **1973**, *95*, 8472−8474. (d) Balavoine, G.; Jugé, S.; Kagan, H. B. Photoactivation optique du methyl p-tolyl sulfoxyde racemique par emploi d'un sensibilisateur chiral. *Tetrahedron Lett.* **1973**, *14*, 4159−4162.

(9) (a) Hölzl-Hobmeier, A.; Bauer, A.; Silva, A. V.; Huber, S. M.; Bannwarth, C.; Bach, T. Catalytic deracemization of chiral allenes by sensitized excitation with visible light. *Nature* **2018**, *564*, 240−243. (b) Plaza, M.; Großkopf, J.; Breitenlechner, S.; Bannwarth, C.; Bach, T. Photochemical Deracemization of Primary Allene Amides by Triplet Energy Transfer: A Combined Synthetic and Theoretical Study. *J. Am. Chem. Soc.* **2021**, *143*, 11209−11217.

(10) Wimberger, L.; Kratz, T.; Bach, T. Photochemical Deracemization of Chiral Sulfoxides Catalyzed by a Hydrogen-Bonding Xanthone Sensitizer. *Synthesis* **2019**, *51*, 4417−4424.
(11) (a) Tröster, A.; Bauer, A.; Jandl, C.; Bach, T. Enantioselective Visible-Light-Mediated Formation of 3-Cyclopropylquinolones by Triplet-Sensitized Deracemization. *Angew. Chem., Int. Ed.* **2019**, *58*, 3538−3541. (b) Li, X.; Kutta, R. J.; Jandl, C.; Bauer, A.; Nuernberger, T.; Bach, T. Photochemically Induced Ring Opening of Spirocyclopropyl Oxindoles: Evidence for a Triplet 1,3-Diradical Intermediate and Deracemization by a Chiral Sensitizer. *Angew. Chem., Int. Ed.* **2020**, *59*, 21640−21647.
(12) Shin, N. Y.; Ryss, J. M.; Zhang, X.; Miller, S. J.; Knowles, R. R. Light-driven deracemization enabled by excited-state electron transfer. *Science* **2019**, *366*, 364−369.
(13) Zhang, C.; Gao, A. Z.; Nie, X.; Ye, C.-X.; Ivlev, S. I.; Chen, S.; Meggers, E. Catalytic α-Deracemization of Ketones Enabled by Photoredox Deprotonation and Enantioselective Protonation. *J. Am. Chem. Soc.* **2021**, *143*, 13393−13400.
(14) For reviews on photochemical HAT, see: (a) Capaldo, L.; Ravelli, D.; Fagnoni, M. Direct Photocatalyzed Hydrogen Atom Transfer (HAT) for Aliphatic C−H Bonds Elaboration. *Chem. Rev.* **2021**, *121*, in press; DOI: 10.1021/acs.chemrev.1c00263. (b) Capaldo, L.; Quadri, L. L.; Ravelli, D. Photocatalytic hydrogen atom transfer: the philosopher's stone for late-stage functionalization? *Green Chem.* **2020**, *22*, 3376−3396. (c) Stateman, L. M.; Nakafuku, K. M.; Nagib, D. A. Remote C−H Functionalization via Selective Hydrogen Atom Transfer. *Synthesis* **2018**, *50*, 1569−1586.
(15) Konnert, L.; Lamaty, F.; Martinez, J.; Colacino, E. Recent Advances in the Synthesis of Hydantoins: The State of the Art of a Valuable Scaffold. *Chem. Rev.* **2017**, *117*, 13757−13809.
(16) Bauer, A.; Westkämper, F.; Grimme, S.; Bach, T. Catalytic enantioselective reactions driven by photoinduced electron transfer. *Nature* **2005**, *436*, 1139−1140.
(17) Reviews: (a) Genzink, M. J.; Kidd, J. B.; Swords, W. B.; Yoon, T. P. Chiral Photocatalyst Structures in Asymmetric Photochemical Synthesis. *Chem. Rev.* **2021**, *121*, in press; DOI: 10.1021/acs.chemrev.1c00467. (b) Silvi, M.; Melchiorre, P. Enhancing the potential of enantioselective organocatalysis with light. *Nature* **2018**, *554*, 41−49.
(18) Dormán, G.; Nakamura, H.; Pulsipher, A.; Prestwich, G. D. The Life of Pi Star: Exploring the Exciting and Forbidden Worlds of the Benzophenone Photophore. *Chem. Rev.* **2016**, *116*, 15284−15398.
(19) Bischoff, A. J.; Nelson, B. M.; Niemeyer, Z. L.; Sigman, M. S.; Movassaghi, M. Quantitative Modeling of Bis(pyridine)silver(I) Permanganate Oxidation of Hydantoin Derivatives: Guidelines of Predicting the Site of Oxidation in Complex Substrates. *J. Am. Chem. Soc.* **2017**, *139*, 15539−15547.
(20) Bucherer, H. T.; Lieb, V. A. Über die Bildung substituierter Hydantoine aus Aldehyden und Ketonen. *J. Prakt. Chem.* **1934**, *141*, 5−43.
(21) Saikia, R. A.; Barman, D.; Dutta, A.; Thakur, A. J. $N^1$- and $N^3$-Arylations of Hydantoins Employing Diaryliodonium Salts via Copper(I) Catalysis at Room Temperature. *Eur. J. Org. Chem.* **2021**, *2021*, 400−410.
(22) O'Ferrall, R. A. M. Model calculations of hydrogen isotope effects for non-linear transition states. *J. Chem. Soc. B* **1970**, *1970*, 785−790.
(23) Nonhebel, D. C. The chemistry of cyclopropylmethyl and related radicals. *Chem. Soc. Rev.* **1993**, *22*, 347−359.
(24) Marazzi, M.; Mai, S.; Roca-Sanjuán, D.; Delcey, M. G.; Lindh, R.; González, L.; Monari, A. Benzophenone Ultrafast Triplet Population: Revisiting the Kinetic Model by Surface-Hopping Dynamics. *J. Phys. Chem. Lett.* **2016**, *7*, 622−626.


https://doi.org/10.1021/jacs.1c11266
*J. Am. Chem. Soc.* 2021, 143, 21241−21245

# 8 Multifaceted View on the Mechanism of a Photochemical Deracemization Reaction

**Title:** "Multifaceted View on the Mechanism of a Photochemical Deracemization Reaction"

**Status:** Article, published online January 20, 2023

**Journal:** *Journal of the American Chemical Society* **2023**, *145*, 2354–2363.

**Publisher:** American Chemical Society

**DOI:** 10.1021/jacs.2c11265

**Authors:** Roger Jan Kutta*, Johannes Großkopf*, Nils van Staalduinen, Antonia Seitz, Philipp Pracht, Stefan Breitenlechner, Christoph Bannwarth, Patrick Nürnberger, Thorsten Bach (*These authors contributed equally.)

**Content**: The mechanism of the deracemization of hydantoins by hydrogen atom transfer using a chiral benzophenone catalyst was studied thoroughly by a set of mechanistic experiments. These included preparative investigations, excited-state DFT calculations and the use of TA spectroscopy. By NMR titration experiments a difference in the association behavior of the two enantiomers was observed. Calculations showed that in one of the diastereomeric complexes, the hydrogen atom of the stereogenic center is suitably positioned for HAT by the benzophenone catalyst upon excitation. By detection of the protonated ketyl radical, TA spectroscopy confirmed that only one enantiomer is processed by the catalyst. The further procession of the transient carbon-centered substrate radical was elucidated by excited-state DFT calculations, which visualized that the hydrogen atom is not donated back to the carbon atom but to the adjacent carbonyl oxygen. The achiral enol was spectroscopically detected. It was shown that tautomerization leads to both enantiomers, of which only one re-enters the catalytic cycle.

J. Großkopf performed all preparative experiments. R. J. Kutta conducted all TA measurements. N. v. Staalduinen, P. Pracht and C. Bannwarth performed all DFT calculations. A. Seitz and S. Breitenlechner helped with synthetic and KIE experiments and with proof reading of the manuscript. J. Großkopf, R. J. Kutta, C. Bannwarth, P. Nürnberger and T. Bach wrote the manuscript. All work was performed under the supervision of T. Bach.

JACS
JOURNAL OF THE AMERICAN CHEMICAL SOCIETY
pubs.acs.org/JACS
Article

# Multifaceted View on the Mechanism of a Photochemical Deracemization Reaction

Roger Jan Kutta,[⊥] Johannes Großkopf,[⊥] Nils van Staalduinen, Antonia Seitz, Philipp Pracht, Stefan Breitenlechner, Christoph Bannwarth,* Patrick Nuernberger,* and Thorsten Bach*

Cite This: J. Am. Chem. Soc. 2023, 145, 2354−2363

Read Online

ACCESS | Metrics & More | Article Recommendations | Supporting Information

**ABSTRACT:** Upon irradiation in the presence of a chiral benzophenone catalyst (5 mol %), a racemic mixture of a given chiral imidazolidine-2,4-dione (hydantoin) can be converted almost quantitatively into the same compound with high enantiomeric excess (80−99% *ee*). The mechanism of this photochemical deracemization reaction was elucidated by a suite of mechanistic experiments. It was corroborated by nuclear magnetic resonance titration that the catalyst binds the two enantiomers by two-point hydrogen bonding. In one of the diastereomeric complexes, the hydrogen atom at the stereogenic carbon atom is ideally positioned for hydrogen atom transfer (HAT) to the photoexcited benzophenone. Detection of the protonated ketyl radical by transient absorption revealed hydrogen abstraction to occur from only one but not from the other hydantoin enantiomer. Quantum chemical calculations allowed us to visualize the HAT within this complex and, more importantly, showed that the back HAT does not occur to the carbon atom of the hydantoin radical but to its oxygen atom. The achiral enol formed in this process could be directly monitored by its characteristic transient absorption signal at $\lambda \cong 330$ nm. Subsequent tautomerization leads to both hydantoin enantiomers, but only one of them returns to the catalytic cycle, thus leading to an enrichment of the other enantiomer. The data are fully consistent with deuterium labeling experiments and deliver a detailed picture of a synthetically useful photochemical deracemization reaction.

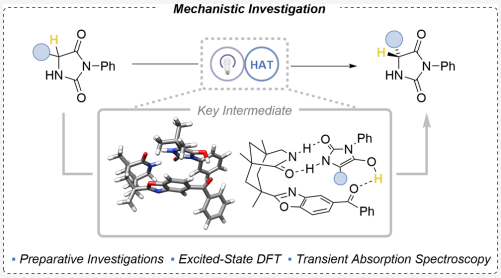


## INTRODUCTION

Enantiomerically pure compounds, i.e., chiral compounds sold as single enantiomers, represent a huge class of chemicals with sales exceeding 100 billion US-$ per year.[1] The market for enantiomerically pure drugs displays even higher sales figures.[2] Although research in enantioselective (asymmetric) catalysis has led to remarkably efficient processes for the syntheses of chiral compounds,[3] it is frequently less expensive and more efficient to prepare chiral compounds as a racemic mixture and to separate the enantiomers subsequently.[4] The latter approach is particularly appealing if both enantiomers of a chiral compound are required. If this is not the case, e.g., in many pharmaceutical applications, the unwanted enantiomer is a waste product, and it is desirable to find ways of proper recycling or to generate enantiomerically pure compounds from their racemates. In the latter context, deracemization reactions have received considerable attention,[5] and most methods to perform deracemization have until recently relied on the stoichiometric conversion of the respective racemate into an achiral intermediate, which is subsequently or in situ converted by a chiral reagent to the desired enantiomer. A key requirement for a deracemization reaction is the existence of two distinct steps which are not simply the reversal of each other. In an equilibrium situation, the racemate is entropically favored, and this preference cannot be overcome in a closed catalytic system violating the principle of microscopic reversibility.[6] Based on pioneering efforts in the 1960s and 1970s,[7] photochemical deracemization reactions have been studied more closely in the last five years.[8] The key idea is to decouple a thermal reaction step from a photochemical event, enabling the enrichment of a single enantiomer (Scheme 1). Two different approaches may be considered: (1) A chiral photocatalyst can be used to differentiate between the two substrate enantiomers and to form an achiral intermediate from which the respective substrate is formed thermally in an unselective fashion. If this cycle is continuously repeated, the enantiomer that is not or only slowly processed in the photochemical step will be enriched. (2) Alternatively, the photochemical step can occur unselectively, and a chiral

Received: October 24, 2022
Published: January 20, 2023





https://doi.org/10.1021/jacs.2c11265
J. Am. Chem. Soc. 2023, 145, 2354−2363

**Scheme 1. Photochemical Deracemization by a Chiral Catalyst: Enrichment of a Single Enantiomer Is Possible by Selective Excitation or by a Selective Reaction of the Intermediate**

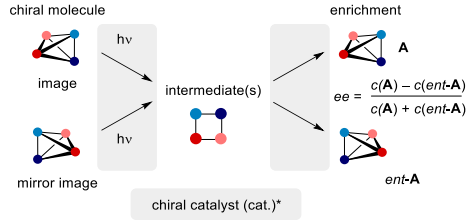


catalyst can be used to form one of the substrate enantiomers in an enantioselective fashion. In the latter scenario, it is desirable that the thermal step is compatible with the photochemical step.[9] If not, the reaction might be preferably performed in two separate steps and bears the characteristics of an enantioselective catalytic reaction but not of a deracemization.[10]

In 2018, our group reported the first photochemical deracemization reaction that delivered chiral organic compounds in high yields and enantioselectivities.[11] Chiral allene lactams were successfully employed as substrates, and a chiral triplet sensitizer (2.5 mol %) was utilized to differentiate between the two substrate enantiomers (17 examples, 52−99% yield, 89−97% *ee*). Achiral diradical **IN1** was postulated as a triplet intermediate based on analogy to known allene triplets,[12] corroborated by subsequent calculations on the deracemization of chiral 2,3-butadienamides.[13] Since then, we have studied several reactions in which achiral intermediates **IN** are selectively formed from a chiral precursor by triplet sensitization according to approach (1) mentioned above (Figure 1). Putative triplet intermediates include diradicals **IN2** (sulfoxide deracemization),[14] **IN3** (cyclopropane deracemization),[15] and **IN4** (alkene deracemization).[16] Knowles, Miller, and co-workers reported in 2019 a dual catalysis approach, in which radical intermediates like **IN5** were formed by a selective photocatalytic reaction and further converted to the cyclic urea substrates by a second enantioselective step on the ground state (15 examples, 90−99% yield, 62−92% *ee*).[17] A chiral phosphoric acid (5 mol %) was employed to allow for differentiation in the first step (radical formation) and a chiral thiol (5 mol %) for the selective hydrogen atom transfer (HAT).

More recently, Meggers and co-workers reported on the formation of chiral enolate intermediates in an unselective photochemical step which were subsequently protonated diastereoselectively via chiral-at-metal rhodium (*[Rh]) enolate **IN6**.[18] In a related approach, taken by Luo and co-workers,[19] a chiral amine was used as the catalyst to promote an enantioselective protonation of (*Z*)-enamine **IN7** which was diastereoselectively generated by triplet-sensitized *E*/*Z*-isomerization.[20] Also in this case, the protonation step is responsible for the preferential formation of a major enantiomer. So far, only the 1,3-diradical **IN3** was observed by transient absorption spectroscopy,[15b] whereas all other intermediates **IN** were postulated and their immediate detection has not been reported.

While all our previous work had focused on the generation of achiral intermediates by triplet sensitization,[11,13−16] we have recently started to investigate different modes of action by which chiral substrates would be differentiated in a photochemical step. In a first study, benzophenone (+)-**2** was found to deliver high enantioselectivities in the photochemical deracemization of hydantoins *rac*-**1** (Scheme 2).[21] A high

**Scheme 2. Photochemical Deracemization of Hydantoins *rac*-1 Catalyzed by Chiral Benzophenone (+)-2**

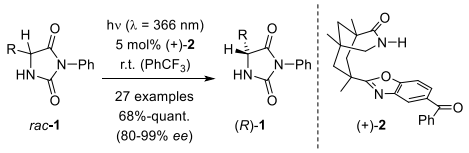


preference for the respective (*R*)-enantiomers (*R*)-**1** was recorded, and circumstantial evidence was collected, which suggested that photoexcited benzophenone (+)-**2** enables a selective HAT[22] from one of the two hydantoins.

Although the first step of the reaction appeared intuitive, the further fate of the intermediate remained unclear. In particular, the thermal pathway which leads to the formation of the hydantoin after HAT required further studies. We have now undertaken a suite of mechanistic experiments to shed light on the course of the deracemization reaction. Based on quantum chemical calculations and supported by the spectroscopic detection of intermediates, a clear picture of the reaction pathway has evolved which we present in this manuscript.

## RESULTS AND DISCUSSION

**Side Reactions, Association Constants, and Labeling Experiments.** For reasons of compound supply, most studies of this section and all transient absorption experiments (vide infra) were performed with benzophenone (−)-**2** (Figure 2).

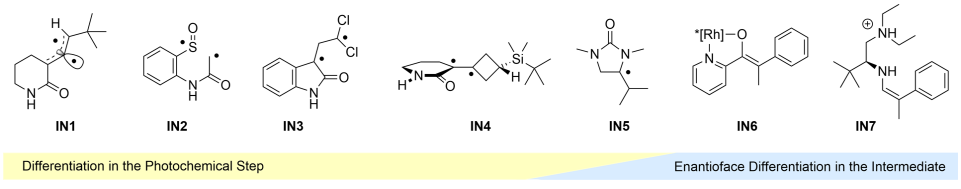


**Figure 1.** Typical intermediates **IN1**−**IN7** invoked in photochemical deracemization reactions: Intermediates **IN1**−**IN4** are generated predominantly from one substrate enantiomer while intermediates **IN6** and **IN7** react enantioselectively. For intermediate **IN5**, both modes of action operate (two chiral catalysts).



https://doi.org/10.1021/jacs.2c11265
J. Am. Chem. Soc. 2023, 145, 2354−2363

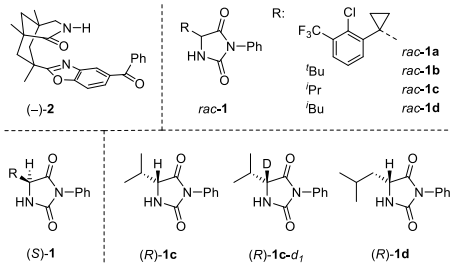


**Figure 2.** Structure of the chiral catalyst (−)-**2** and of hydantoins *rac*-**1** used in this study. The use of catalyst (−)-**2** leads to the preferred formation of (*S*)-configured hydantoins (*S*)-**1** in the deracemization reaction. Enantiomerically pure (*R*)-hydantoins were used for kinetic experiments.

Expectedly, the catalyst favors in the photochemical reaction the opposite enantiomers compared to benzophenone (+)-**2**, i.e., not the (*R*)-hydantoins but the respective (*S*)-enantiomers are formed. This was verified by performing the deracemization of hydantoin *rac*-**1a** as a control experiment. In previous work, we had isolated the enantiomer (*R*)-**1a** with (+)-**2** as the catalyst in 87% yield and with 94% *ee*.[21] When the same reaction was conducted under identical conditions with catalyst (−)-**2**, the (*S*)-enantiomer (*S*)-**1a** was isolated in 86% yield and with 94% *ee*.

The use of compound *rac*-**1a** or its enantiomers for several of the mechanistic investigations was due to its high solubility in trifluorotoluene which is the preferred solvent for the deracemization experiments. To simplify the nature of the substituent R, the *tert*-butyl-substituted hydantoin **1b** was the preferred model compound for the computational studies (vide infra). Further mechanistic experiments were performed with the valine- and leucine-derived hydantoins **1c** and **1d**.

A key feature of the deracemization experiments performed with benzophenone **2** relies on its propensity for hydrogen abstraction[23] in the excited triplet $n\pi^*$ state.[24] A prerequisite for the HAT to be selective is the formation of the respective 1:1 complex with the individual enantiomers. We therefore studied these complexes by nuclear magnetic resonance (NMR) titration in benzene-$d_6$ at ambient temperature (20 °C).[25] Indeed, it was confirmed that both enantiomers of hydantoin **1a**, (*R*)-**1a** and (*S*)-**1a**, undergo association to (−)-**2** via two hydrogen bonds (for details see the Supporting Information). The binding constants are not identical, reflecting the fact that the formation of (−)-**2** · (*S*)-**1a** is hampered by Pauli repulsion of the bulky hydantoin substituent and the benzoyl group of the catalyst. Formation of (−)-**2** · (*R*)-**1a** is preferred for steric reasons. Within this complex, the hydrogen atom at the stereogenic center (indicated in bold in Figure 3) is close to the carbonyl group of the benzophenone. In complex (−)-**2** · (*S*)-**1a**, an intramolecular HAT at the stereogenic center has too high a barrier to become kinetically relevant.

Hydrogen abstraction by catalyst (−)-**2** was monitored in kinetic experiments with deuterated and nondeuterated hydantoins. Since the reaction of enantiopure (*R*)-enantiomers leads to a complete inversion of the stereogenic center, the reaction can be followed kinetically by recording the enantiomeric purity over time. In separate experiments, the kinetics were monitored for the reaction of (*R*)-**1** → (*S*)-**1** and

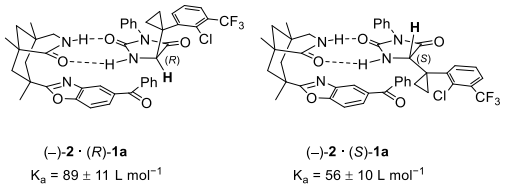


**Figure 3.** Complexes of chiral benzophenone (−)-**2** with the two enantiomers of hydantoin **1a**: The preferably formed enantiomer (*S*)-**1a** displays a smaller binding constant than its antipode (*R*)-**1a**. Rotation around single bonds is possible at the benzoxazole core, and the conformation is depicted, in which the complex of (−)-**2** and substrates (*R*)-**1** has been found to be the most stable (vide infra).

for (*R*)-**1**-$d_1$→ (*S*)-**1**-$d_1$. The rate of conversion was linear within the first 10 min and a kinetic isotope effect $k_H/k_D$ = 1.4 was determined (see the Supporting Information for details). In an intermolecular competition experiment, the inversion of compounds (*R*)-**1** and (*R*)-**1**-$d_1$ was studied. The observed value was not significantly higher ($k_H/k_D$ = 1.8), which, at first sight, suggested that the HAT has little influence on the rate and selectivity.[26] However, the computational results revealed an equally low kinetic isotope effect (vide infra) which potentially indicates that the HAT step is turnover limiting.

Previous work with deuterated hydantoins had revealed that H/D cross-over occurs during deracemization employing catalyst (+)-**2**.[21] With an equimolar mixture of deuterated, leucine-derived hydantoin **1d**-$d_1$ and non-deuterated valine-derived hydantoin **1c**, the products also displayed non-deuterated **1d** and deuterated **1c**-$d_1$ in varying amounts. If a complete inversion was performed, e.g., by going from (*S*)-**1** to (*R*)-**1**, a ca. 50% H/D cross-over was noted. If the starting materials were racemic, the cross-over was ca. 25%, and if the starting material already possessed the correct configuration, there was no cross-over. If one assumes that the deracemization occurs via the protonated (or deuterated) ketyl radical (−)-**3** (Figure 4), the results appeared to suggest that the re-

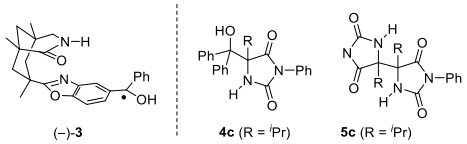


**Figure 4.** Structure of putative intermediate (−)-**3** and reaction products **4c** and **5c** obtained upon irradiation of a sample containing parent benzophenone (BP) and the valine-derived hydantoin **1c** (2 equiv, $\lambda$ = 350 nm, $PhCF_3$).

delivery of the hydrogen or deuterium atom occurs not always to the same molecule it had been abstracted from. Radical-radical coupling products were not detected, however. In contrast, when using parent benzophenone (PhCOPh, BP) to induce a racemization reaction in valine-derived hydantoin (*S*)-**1c**, significant amounts of coupling products **4c** and **5c** were observed.

Product **4c** is the 1:1 adduct of the protonated ketyl radical with the hydantoin radical formed by hydrogen abstraction. Product **5c** (isolated as a single diastereoisomer) is the product of a radical-radical combination between two hydantoin radicals. The results indicate that upon leaving the solvent


https://doi.org/10.1021/jacs.2c11265
J. Am. Chem. Soc. 2023, 145, 2354−2363

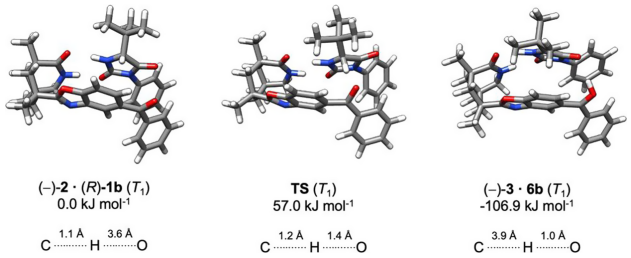


**Figure 5.** Calculated $T_1$ structures for (−)-**2** · (*R*)-**1b**, **TS**, and (−)-**3** · **6b** in the deracemization reaction of *rac*-**1b**. Free energies of the corresponding species are calculated relative to (−)-**2** · (*R*)-**1b** at the ωB97X-V/def2-QZVP//PBEh-3c level of theory (see the Supporting Information for details).[29,27] The hydrogen atom of hydantoin is transferred to the catalyst yielding a complex of the protonated ketyl radical (−)-**3** and the hydantoin radical **6b**.

cage, the radicals formed via hydrogen abstraction by photoexcited benzophenone may undergo free radical-radical recombination. To shed light on this issue, we investigated the reaction pathway leading to deracemization of compound *rac*-**1b** by quantum chemical calculations.

**Quantum Chemical Calculations on the Hydrogen Atom Transfer.** Based on the experimental analyses (NMR and kinetic studies, vide supra), we restricted the computational analysis to the configuration inversion of (*R*)-**1b** assisted by catalyst (−)-**2**. As starting geometry for the HAT in complex (−)-**2** · (*R*)-**1b**, we initially used the previously determined complex structure[21] from a conformational analysis that exhibited the shortest hydrogen−oxygen distance. However, we identified in this work a second, lower energetic conformation by conformational sampling of (−)-**2** · (*R*)-**1b**. Here, the benzoxazole core has undergone a rotation around the single bond to the azabicyclo[3.3.1]nonan-2-one backbone. In the following, we discuss exclusively the results for the energetically more stable conformer (called **min2** in the SI) but provide results for the other conformer (**min1**) in the Supporting Information. The final geometries on the triplet ($T_1$) state for (−)-**2** · (*R*)-**1b** and the identified HAT intermediate, (−)-**3** · **6b**, were obtained by structure optimization at the PBEh-3c level, which is a low-cost DFT composite method.[27] Intermediate **6b** is the hydantoin radical obtained by HAT from **1b**. The transition state for the HAT was determined by a nudged elastic band optimization with subsequent transition state (TS) optimization on the $T_1$ state employing the GFN2-xTB method.[28] The identified structure was then re-optimized also at the PBEh-3c level. Details for the optimization procedure can be found in the Supporting Information. The obtained $T_1$ species involved in the forward HAT are shown in Figure 5.

During the HAT, the proximal hydrogen atom of hydantoin (*R*)-**1b** is transferred to the catalyst, leading to the protonated ketyl radical (−)-**3** and the hydantoin radical **6b**. The distance of the involved hydrogen atom to the carbonyl oxygen atom of the catalyst decreases from 3.6 to 1.0 Å during the HAT. Simultaneously, the distance of the hydrogen atom to the hydantoin carbon increases from 1.1 to 3.9 Å at the chosen level of theory. At the transition state, the hydrogen atom is almost located halfway between the carbon atom (1.2 Å) and the oxygen atom (1.4 Å). Moreover, the initially chiral, tetrahedral carbon atom of (*R*)-**1b** planarizes as the hybridization changes from $sp^3$ to $sp^2$, leading to the achiral radical intermediate **6b**.

The low barrier of 57.0 kJ mol$^{-1}$ (ωB97X-V/def2-QZVP//PBEh-3c level[27,29]) found for the HAT confirms the experimentally observed rapid hydrogen transfer to occur at the $T_1$ state after photoexcitation and intersystem crossing (ISC). At the $T_1$ surface, the HAT toward (−)-**3** · **6b** is exergonic by −106.9 kJ mol$^{-1}$ relative to (−)-**2** · (*R*)-**1b**. Experimentally, a kinetic isotope effect $k_H/k_D$ = 1.4−1.8 was observed. To compute the theoretical kinetic isotope effect for the aforementioned HAT reaction, the nuclear thermal corrections[29a] to (−)-**2** · (*R*)-**1b** and **TS** were recalculated after changing the mass of the hydrogen involved in the HAT to 2.00141 u (see the Supporting Information for more details). For deuterium, the calculated HAT reaction barrier increases from 57.0 to 58.6 kJ mol$^{-1}$. This results in a theoretical kinetic isotope effect of 1.9 in good agreement with the experimental value (vide supra). It should be noted that for the higher lying conformer (**min1**, see SI), a lower barrier of 40.6 kJ mol$^{-1}$ was found, which, however, would result in a kinetic isotope effect around 4.7. Hence, based on the fact that conformer **min2** is more stable and reproduces the experimental kinetic isotope effect, we conclude that the photocatalyzed deracemization proceeds via the **min2** conformer and no rotation to the **min1** conformer occurs during the lifetime of the triplet state.

Given that (−)-**3** · **6b** is significantly lower in free energy on the triplet hypersurface than (−)-**2** · (*R*)-**1b**, the back HAT mechanism is expected to proceed in the singlet manifold after reverse ISC has taken place. The reaction is, hence, expected to involve a conical intersection between the open shell and closed shell ($S_0$) singlet state. The preceding ISC from $T_1$ to the open shell singlet is readily feasible, since for (−)-**3** · **6b**, the two states are found to be isoenergetic [−106.9 kJ mol$^{-1}$ relative to (−)-**2** · (*R*)-**1b**] and structurally indistinguishable. The energetically lowest $S_0/S_1$ minimum energy conical intersection (MECI) could be identified by a recently developed sampling algorithm[30] (see the Supporting Information for details). Remarkably, among all sampled structures, no precursor geometry could be identified that would correspond to a *direct* HAT to the prostereogenic carbon atom of radical intermediate **6b**. In conclusion, a back HAT directly forming the hydantoin **1b** can be ruled out. However, the lowest-lying complex structure in the ensemble shows a hydrogen bond between the hydrogen atom of the catalyst and the carbonyl oxygen atom of **6b**. It was found that the identified MECI structure is structurally very similar to another, lower-lying


https://doi.org/10.1021/jacs.2c11265
J. Am. Chem. Soc. 2023, 145, 2354−2363

minimum existing both on the open shell singlet and $T_1$ surface (Figure 6).

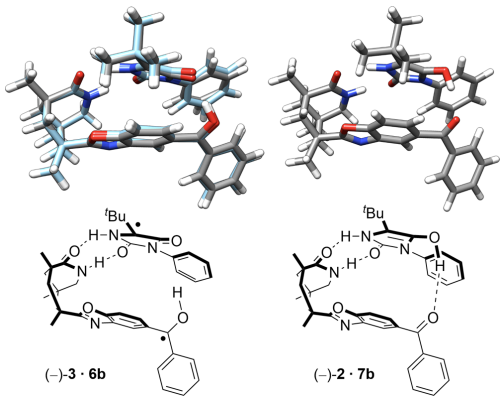


**Figure 6.** Left: MECI structure optimized at the FOMO-*hh*TDA-BHLYP-D3(BJ)/def2-SV(P) level of theory[31] (gray) and the proximate minimum structure (−)-**3** · **6b** in the open shell singlet (light-blue) optimized at the PBEh-3c[27] level of theory. Right: Ground state ($S_0$) structure (−)-**2** · **7b** after the back HAT optimized at the PBEh-3c[27] level of theory.

The computed association free energy between (−)-**3** and **6b** was found to be −38.8 kJ mol$^{-1}$, rendering the complex more stable than (−)-**2** · (*R*)-**1b** (see the Supporting Information for details). The dissociation into free radicals and coupling reactions as observed for BP (vide supra) are therefore avoided. Taken together with the fact that triplet and open shell singlet minima are isoenergetic for (−)-**3** · **6b**, ISC is expected to be easily feasible at this geometry. Once arrived at the singlet manifold, the reaction proceeds nearly barrierless through the MECI (see the Supporting Information). The final minimum structure after the back HAT on the singlet manifold was obtained by PBEh-3c optimizations[27] on the $S_0$ surface, leading to the noncovalent complex (−)-**2** · **7b** (Figure 6). Compound **7b** is the (achiral) enol[32] tautomer of hydantoin **1b**. The overall pathway for the deracemization process is comprehensively summarized in Figure 7.

The calculation delivered a fully coherent explanation for the abovementioned dichotomy regarding the deuterium scrambling and the side reactions observed with an achiral catalyst (Figure 4). Since the enol form **7** of the hydantoin is the intermediate via which the racemization occurs, scrambling does not occur in any of the intermolecular HAT processes but in the subsequent tautomerization step. The exchange of protons likely occurs in a bimolecular fashion[33] and is thus responsible for the observed H/D scrambling. From a stereochemical perspective, intermediate **7** will tautomerize to both enantiomers (*S*)-**1** and (*R*)-**1** with no preference for any of the two enantiomers. Enantiomer (*R*)-**1** is further processed in a catalytic cycle when bound to sensitizer (−)-**2** and will lead again via radical **6** to the respective enol **7** (Scheme 3). Enantiomer (*S*)-**1** is enriched because it does not display a suitable hydrogen atom for HAT and is found as the prevailing enantiomer if catalyst (−)-**2** is employed.

The introduction has already alluded to the fact that very few intermediates in deracemization reactions have been detected. With the mechanistic scheme outlined above already providing a plausible picture, we felt it crucial to experimentally identify the postulated intermediates by transient absorption spectroscopy. A key issue to be resolved related to the hypothesis that enantiomer (*S*)-**1** was not processed by benzophenone (−)-**2**. If detection of the protonated ketyl radical (−)-**3** was feasible, this question could be reliably answered.

**Transient Absorption Spectroscopy.** As benzophenone (PhCOPh; BP) is well known to undergo ISC to almost 100% on a ps time scale,[34] ISC will potentially outcompete a potential HAT and, therefore, the excited singlet $S_1$ of BP may not be relevant for a potential HAT. Accordingly, we focused

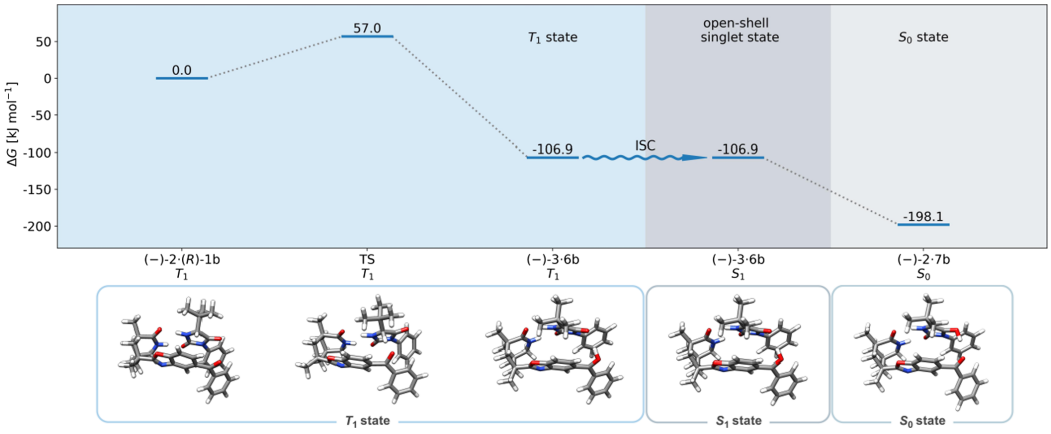


**Figure 7.** Computed free energy reaction profile for the photocatalytic deracemization of *rac*-**1b**. Electronic energies are calculated at the ωB97X-V/def2-QZVP//PBEh-3c[27,29] level of theory (see the Supporting Information for details on the thermal and solvation contributions). Relative energies are referenced to the free energy of (−)-**2** · (*R*)-**1b** in the $T_1$ state. A possible ISC step is indicated. Alternatively, triplet recombination is possible, which affords the diradical singlet complex as an intermediate.



https://doi.org/10.1021/jacs.2c11265
J. Am. Chem. Soc. 2023, 145, 2354−2363

**Scheme 3. Mechanistic Scheme for the Photochemical Deracemization of Hydantoins *rac*-1 Catalyzed by Chiral Benzophenone (−)-2**

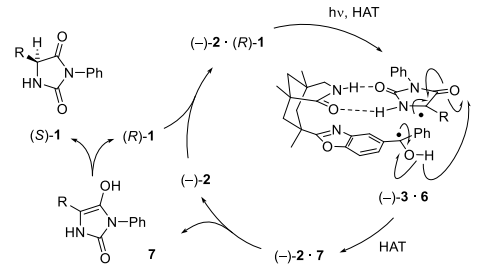


in this study on the triplet ($T_1$) and subsequent dynamics of the BP moiety on a ns to $\mu$s time scale. For acquiring reference spectra of the $T_1$ as well as the protonated ketyl radical, we initially recorded the transient absorption of BP in $PhCF_3$ and in a $PhCF_3$/cyclohexane (1.65 mM/8.17 M) mixture after excitation at 355 nm. Under the latter conditions, the radical formation should be observed after HAT from the aliphatic cyclohexane to BP.[24] In nondegassed $PhCF_3$, the well-known $T_1$ spectrum with its characteristic spectrum of two narrow absorption bands peaking at 321 and 525 nm and a shoulder at ca. 450 nm is observed within the duration of the excitation pulse, and decays monoexponentially with a lifetime of 240 ns obeying the pseudo-first order kinetics of diffusion-controlled quenching via energy transfer to molecular oxygen (Figure 8). With an abundance of an aliphatic molecule in the surrounding solvent layer, HAT from cyclohexane to the BP $T_1$ is observed, as evidenced by a tremendous $T_1$ lifetime reduction down to ca. 140 ns accompanied by the formation of a new species spectrum ascribed to the protonated BP ketyl radical ($^2$BP-H),[24,35] whose species-associated spectrum (SAS) is given in red in Figure 8d. From spectral (Figure 8d) and temporal (Figure 8f) decomposition of the data, an almost complete forward and back HAT for this system may be found (see the Supporting Information for a more detailed discussion on the analysis). As HAT occurs in the triplet spin system, the triplet-born spin-correlated radical pair will be spin-forbidden for back HAT. Accordingly, it is tempting to speculate that for cyclohexane the rate-limiting factor will be back ISC prior to back HAT (vide infra).

In the case of (−)-**2** in $PhCF_3$, the photophysical properties are totally dictated by the benzophenone moiety, as already seen by a very similar ground state $S_1 \leftarrow S_0$ transition with extinction coefficients in the range of 130 $M^{-1}$ $cm^{-1}$ (Supporting Information and Figure 9). Accordingly, after exciting at 355 nm, (−)-**2** also shows very efficient triplet formation to $^3$(−)-**2**, which subsequently decays with a lifetime of 206 ns in nondegassed solution (Figure 9a,d,g). As the substrate *rac*-**1a** itself absorbs at 355 nm, we separately recorded its transient absorption. It turned out that besides pump−pulse scatter at 355 nm, the fluorescence of *rac*-**1a** between 400 and 550 nm with a lifetime shorter than the instrumental response as well as a very small−barely detectable−broad absorption band with a lifetime of 470 ns is observed (Figure S8.1). Since this absorption signal is significantly smaller than the strong triplet absorption of $^3$(−)-**2**, it can be neglected in the transient absorption data obtained from (−)-**2** in the presence of either (*R*)-**1a** or (*S*)-**1a**.

While the presence of (*S*)-**1a** (40 mM) does not result in any changes of the $^3$(−)-**2** dynamics (Figure 9c,f,i), new spectral contributions in the transient data become evident in the presence of (*R*)-**1a** (40 mM) (Figure 9b). The initial

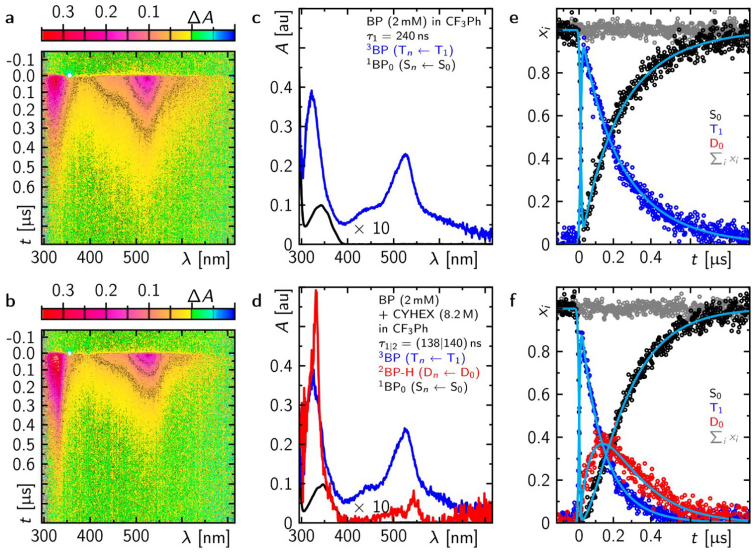


**Figure 8.** Transient absorption data of benzophenone (BP) in $PhCF_3$ (panels a,c,e) and in $PhCF_3$/cyclohexane (1.65 mM/8.2 M) mixture (panels b,d,f) after excitation at 355 nm. Panels a,b: Time-resolved spectra in false color representation. Panels c−f: Species-associated spectra (panels c,d) and the corresponding mole-fraction over time (together with the global fit shown in cyan) (panels e,f) that contribute to the data in panels a,b.



https://doi.org/10.1021/jacs.2c11265
J. Am. Chem. Soc. 2023, 145, 2354−2363

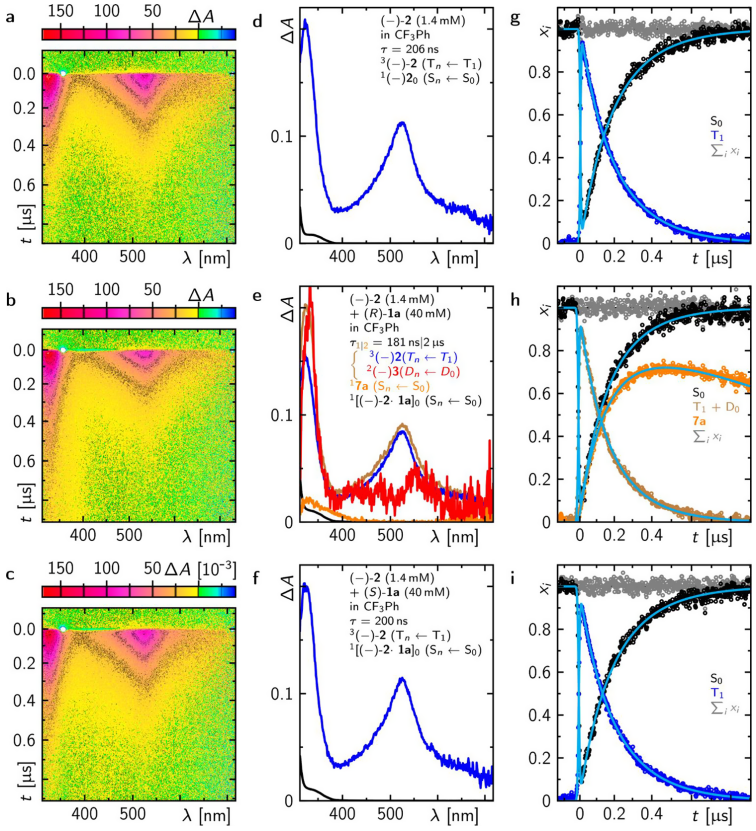


**Figure 9.** Transient absorption data of (−)-**2** in $PhCF_3$ (panels a,d,g) and in the presence of 40 mM concentration of either (*R*)-**1a** (panels b,e,h) or (*S*)-**1a** (panels c,f,i) after excitation at 355 nm. Panels a−c: Time-resolved spectra in false color representation. Panels d−i: Species-associated spectra (panels d−f) and the corresponding mole-fraction over time (together with the global fit shown in cyan; panels g−i) that contribute to the data in panels a−c. Note that $\sum_i x_i$ in panel h only includes contributions from $^3$(−)-**2**, $^2$(−)-**3**, and $^1$(−)-**2**. In panel e, the spectra of the triplet as well as of the ketyl radical are shown, which were obtained by subtracting 75% of the triplet spectrum (blue spectrum in panels d,f) from the spectrum at $t$ = 0 (sum of all DADS) and corresponding rescaling of the ketyl spectrum by (1−0.75).

transient spectrum formed within the excitation pulse shows in addition to the SAS of $^3$(−)-**2** further spectral contributions, and all spectral characteristics simultaneously decay with a slightly shorter lifetime of 181 ns compared to the pure $^3$(−)-**2** decay (compare brown and blue lines in Figure 9e). Subtraction of the $^3$(−)-**2** contribution (blue line) from this spectrum reveals the SAS of the protonated ketyl radical (−)-**3** as an intermediate (compare red lines in Figures 8d and 9e). The fact that only small signatures of (−)-**3** are observable and that only one lifetime can be determined indicates that the rather efficient radical pair formation after HAT from (*R*)-**1a** to $^3$(−)-**3** with an overall estimated yield of $\Phi_{HAT}$ = 1−181 ns/206 ns = 12% is followed by a faster back HAT so that no substantial concentration of the radical pair is detected.

Considering the concentration of (*R*)-**1a** as [(*R*)-**1a**] = 40 mM, the bimolecular rate constant for forward HAT may be estimated to $k_{HAT} = [(R)\text{-}\mathbf{1a}]^{-1}((181\ ns)^{-1} - (206\ ns)^{-1}) = 1.68 \times 10^7\ M^{-1}\ s^{-1}$. Comparison to the expected fully diffusion-controlled bimolecular rate constant in the order of $10^{10}\ M^{-1}\ s^{-1}$ demonstrates that a very specific diffusive encounter configuration is required for a successful HAT. The spectral features of the counter radical **6** (Scheme 3) are not observed, likely due to significantly lower extinction coefficients, as expected from quantum chemical calculations (compare panels a and b in Figure S8.3). Furthermore, as the back HAT is accompanied by a rise of a new absorption spectrum peaking at ca. 330 nm (orange line in Figure 9), the hydrogen atom is *not* transferred to the initially stereogenic carbon from where it originated. From quantum chemical calculations, it becomes evident that, on the one hand, the initially spin-correlated triplet-born radical pair $^3$[(−)-**3** · **6a**] first needs to undergo ISC to the singlet radical pair $^1$[(−)-**3** · **6a**] prior to back HAT and that subsequent back HAT occurs rather to the substrate's carbonyl group, leading to the formation of the enol form **7a** of the initial substrate **1a** and (−)-**2** (see Supporting Video on the molecular dynamics starting from the triplet-born radical pair and Figure S8.3 for comparing the experimental product spectrum with theoretical


https://doi.org/10.1021/jacs.2c11265
J. Am. Chem. Soc. 2023, 145, 2354−2363

spectra of putative **1a**-based intermediates and the corresponding discussion). On a μs timescale, keto-enol tautomerization[33] of enol **7a** will eventually reform (*S*)-**1a** and (*R*)-**1a** in equal amounts. Thus, the feasibility of the deracemization process via the matching combination of the chiral catalyst and substrate is directly reflected in the transient absorption data.

## CONCLUSIONS

In summary, a conclusive mechanistic picture has evolved for the photochemical deracemization of hydantoins *rac*-**1**. The reaction is initiated by HAT from the hydantoin to photoexcited benzophenone-based catalyst (−)-**2** or its enantiomer (+)-**2**. Transient absorption spectroscopy revealed unequivocally that HAT occurs only for one but not for the other enantiomer of *rac*-**1**. In the current study, using (−)-**2**, only the (*R*)-enantiomer (*R*)-**1** was processed. Quantum chemical calculations support the hypothesis that the abstracted hydrogen atom of (*R*)-**1** is the hydrogen atom at the stereogenic center, and the calculations delivered a coherent picture of the HAT within the hydrogen-bonded complex between (−)-**2** and (*R*)-**1**. Remarkably, the resulting radicals, protonated ketyl radical (−)-**3** and hydantoin-derived radical **6**, do not dissociate but retain their association via hydrogen bonds. Radical−radical side reactions, as observed for achiral benzophenone in the HAT with hydantoins, are consequently avoided. Instead, a clean back HAT is initiated, which occurs on the singlet hypersurface and which is not the reverse of the forward reaction that had occurred on the triplet hypersurface. Back HAT leads not immediately to the hydantoin but rather to their achiral enol **7**, which subsequently tautomerizes unselectively to either enantiomer (*R*)-**1** or (*S*)-**1**. Since the latter enantiomer is not processed, it is enriched and eventually obtained with high enantioselectivity. In cases where the enantioselectivity is low, the decomposition of the catalyst is likely responsible, inhibiting further conversion of (*R*)-**1**. Future catalyst design will have to take this issue into consideration. In general, however, the reversible HAT at a stereogenic center is an efficient and economical way to convert racemic mixtures into enantiomerically pure compounds by the use of a single chiral photocatalyst.

## ASSOCIATED CONTENT

### Supporting Information

The Supporting Information is available free of charge at https://pubs.acs.org/doi/10.1021/jacs.2c11265.

Detailed experimental procedures; characterization data for new compounds; NMR titration experiments; deuteration experiments; coordinates for all computed structures; details on the computational methods and procedures; UV/Vis spectra of (−)-**2**; time-resolved UV/vis absorption spectroscopy data; NMR spectra for new compounds; and chiral HPLC traces including Figures S3.1−S8.3 and Tables S3.1−S6.3 (PDF)

NMR spectra of novel compounds (ZIP)

Optimized geometries of the molecules considered in the computational study (ZIP)

Molecular dynamics (MP4)

## AUTHOR INFORMATION


### Corresponding Authors

**Christoph Bannwarth** − *Institut für Physikalische Chemie, RWTH Aachen University, D-52074 Aachen, Germany;* orcid.org/0000-0003-3242-496X; Email: bannwarth@pc.rwth-aachen.de

**Patrick Nuernberger** − *Institut für Physikalische und Theoretische Chemie, Universität Regensburg, Regensburg D-93053, Germany;* orcid.org/0000-0002-4690-0229; Email: Patrick.Nuernberger@chemie.uni-regensburg.de

**Thorsten Bach** − *Department Chemie and Catalysis Research Center (CRC), School of Natural Sciences, Technische Universität München, D-85747 Garching, Germany;* orcid.org/0000-0002-1342-0202; Email: thorsten.bach@ch.tum.de

### Authors

**Roger Jan Kutta** − *Institut für Physikalische und Theoretische Chemie, Universität Regensburg, Regensburg D-93053, Germany;* orcid.org/0000-0003-3368-9863

**Johannes Großkopf** − *Department Chemie and Catalysis Research Center (CRC), School of Natural Sciences, Technische Universität München, D-85747 Garching, Germany;* orcid.org/0000-0002-6540-3893

**Nils van Staalduinen** − *Institut für Physikalische Chemie, RWTH Aachen University, D-52074 Aachen, Germany*

**Antonia Seitz** − *Department Chemie and Catalysis Research Center (CRC), School of Natural Sciences, Technische Universität München, D-85747 Garching, Germany*

**Philipp Pracht** − *Institut für Physikalische Chemie, RWTH Aachen University, D-52074 Aachen, Germany; Yusuf Hamied Department of Chemistry, University of Cambridge, Cambridge CB2 1EW, United Kingdom*

**Stefan Breitenlechner** − *Department Chemie and Catalysis Research Center (CRC), School of Natural Sciences, Technische Universität München, D-85747 Garching, Germany;* orcid.org/0000-0001-5519-1922

Complete contact information is available at: https://pubs.acs.org/10.1021/jacs.2c11265


### Author Contributions

⊥R.J.K. and J.G. contributed equally. The manuscript was written through contributions of all authors.

### Notes

The authors declare no competing financial interest.

## ACKNOWLEDGMENTS

Financial support by the *Deutsche Forschungsgemeinschaft* (Ba 1372/23 and TRR 325; projects A5, B2; 444632635) and the *Fonds der Chemischen Industrie* (Kekulé fellowship to JG) is gratefully acknowledged. C.B. acknowledges funding by the Federal Ministry of Education and Research (BMBF) and the Ministry of Culture and Science of the German State of North Rhine-Westphalia under the Excellence Strategy of the Federal Government and the *Länder*. We thank O. Ackermann (TU München) for his help with the HPLC analysis and Dr. Golo Storch (TU München) for inspiring, helpful discussions. Parts of the simulations were performed with computing resources granted by RWTH Aachen University under project rwth0721.

## REFERENCES


(1) https://www.verifiedmarketresearch.com/product/chiral-chemicals-market/ (accessed Dec 16, 2022).

(2) Rouhi, A. M. Chiral Roundup. *Chem. Eng. News* **2002**, *80*, 43−50.

(3) (a) Akiyama, T.; Ojima, I. (Eds.) *Catalytic Asymmetric Synthesis*, 4th ed.; Weinheim, 2022. (b) Carreira, E. M.; Yamamoto, H. (Eds.) *Comprehensive Chirality*; Amsterdam, 2012. (c) Walsh, P. J.; Kozlowski, M. C.*Fundamentals of Asymmetric Catalysis*; Sausalito, 2009.

(4) Lorenz, H.; Seidel-Morgenstern, A. Processes to Separate Enantiomers. *Angew. Chem., Int. Ed.* **2014**, *53*, 1218−1250.

(5) Reviews: (a) Aranda, C.; Oksdath-Mansilla, G.; Bisogno, F. R.; de Gonzalo, G. Deracemisation Processes Employing Organocatalysis and Enzyme Catalysis. *Adv. Synth. Catal.* **2020**, *362*, 1233−1257. (b) Bhat, V.; Welin, E. R.; Guo, X.; Stoltz, B. M. Advances in Stereoconvergent Catalysis from 2005 to 2015: Transition-Metal-Mediated Stereoablative Reactions, Dynamic Kinetic Resolutions, and Dynamic Kinetic Asymmetric Transformations. *Chem. Rev.* **2017**, *117*, 4528−4561. (c) Palmans, A. R. A. Deracemisations under kinetic and thermodynamic control. *Mol. Syst. Des. Eng.* **2017**, *2*, 34−46. (d) Rachwalksi, M.; Vermue, N.; Rutjes, F. P. J. T. Recent advances in enzymatic and chemical deracemisation of racemic compounds. *Chem. Soc. Rev.* **2013**, *42*, 9268−9282. (e) Voss, C. V.; Gruber, C. C.; Kroutil, W. Deracemisation of Secondary Alcohols via Biocatalytic Stereoinversion. *Synlett* **2010**, 991−998.

(6) (a) Blackmond, D. G. "If Pigs Could Fly" Chemistry: A Tutorial on the Principle of Microscopic Reversibility. *Angew. Chem., Int. Ed.* **2009**, *48*, 2648−2654. (b) Kroutil, W.; Faber, K. Deracemization of compounds possessing a *sec*-alcohol or -amino group through a cyclic oxidation−reduction sequence: a kinetic treatment. *Tetrahedron: Asymmetry* **1998**, *9*, 2901−2913.

(7) (a) Hammond, G. S.; Cole, R. S. Asymmetric Induction during Energy Transfer. *J. Am. Chem. Soc.* **1965**, *87*, 3256−3257. (b) Drucker, C. S.; Toscano, V. G.; Weiss, R. G. General Method for the Determination of Steric Effects during Collisional Energy Transfer. Partial Photoresolution of Penta-2,3-diene. *J. Am. Chem. Soc.* **1973**, *95*, 6482−6484. (c) Ouannès, C.; Beugelmans, R.; Roussi, G. Asymmetric Induction during Transfer of Triplet Energy. *J. Am. Chem. Soc.* **1973**, *95*, 8472−8474.

(8) Reviews: (a) Yang, C.; Inoue, Y. An exciting tool for asymmetric synthesis. *Nature* **2018**, *564*, 197−199. (b) Shi, Q.; Ye, J. Deracemization Enabled by Visible-Light Photocatalysis. *Angew. Chem., Int. Ed.* **2020**, *59*, 4998−5001.

(9) Unselective photochemical reactions can also be combined with a kinetic resolution step. For a recent elegant example, see: Bierbaumer, S.; Schmermund, L.; List, A.; Winkler, C. K.; Glueck, S. M.; Kroutil, W. Synthesis of Enantiopure Sulfoxides by Concurrent Photocatalytic Oxidation and Biocatalytic Reduction. *Angew. Chem., Int. Ed.* **2022**, *61*, No. e202117103.

(10) Recent example: Zhang, Z.; Hu, X. Visible-Light-Driven Catalytic Deracemization of Secondary Alcohols. *Angew. Chem., Int. Ed.* **2021**, *60*, 22833−22838.

(11) (a) Hölzl-Hobmeier, A.; Bauer, A.; Silva, A. V.; Huber, S. M.; Bannwarth, C.; Bach, T. Catalytic deracemization of chiral allenes by sensitized excitation with visible light. *Nature* **2018**, *564*, 240−243. (b) Plaza, M.; Jandl, C.; Bach, T. Photochemical Deracemization of Allenes and Subsequent Chirality Transfer. *Angew. Chem., Int. Ed.* **2020**, *59*, 12785−12788.

(12) Bucher, G.; Mahajan, A. A.; Schmittel, M. The Photochemical $C^2$-$C^6$ Cyclization of Enyne-Allenes: Interception of the Fulvene Diradical with a Radical Clock Ring Opening. *J. Org. Chem.* **2009**, *74*, 5850−5860.

(13) Plaza, M.; Großkopf, J.; Breitenlechner, S.; Bannwarth, C.; Bach, T. Photochemical Deracemization of Primary Allene Amides by Triplet Energy Transfer: A Combined Synthetic and Theoretical Study. *J. Am. Chem. Soc.* **2021**, *143*, 11209−11217.

(14) Wimberger, L.; Kratz, T.; Bach, T. Photochemical Deracemization of Chiral Sulfoxides Catalyzed by a Hydrogen-Bonding Xanthone Sensitizer. *Synthesis* **2019**, *51*, 4417−4424.

(15) (a) Tröster, A.; Bauer, A.; Jandl, C.; Bach, T. Enantioselective Visible-Light-Mediated Formation of 3-Cyclopropylquinolones by Triplet-Sensitized Deracemization. *Angew. Chem., Int. Ed.* **2019**, *58*, 3538−3541. (b) Li, X.; Kutta, R. J.; Jandl, C.; Bauer, A.; Nuernberger, P.; Bach, T. Photochemically Induced Ring Opening of Spirocyclopropyl Oxindoles: Evidence for a Triplet 1,3-Diradical Intermediate and Deracemization by a Chiral Sensitizer. *Angew. Chem., Int. Ed.* **2020**, *59*, 21640−21647.

(16) Kratz, T.; Steinbach, P.; Breitenlechner, S.; Storch, G.; Bannwarth, C.; Bach, T. Photochemical Deracemization of Chiral Alkenes via Triplet Energy Transfer. *J. Am. Chem. Soc.* **2022**, *144*, 10133−10138.

(17) Shin, N. Y.; Ryss, J. M.; Zhang, X.; Miller, S. J.; Knowles, R. R. Light-driven deracemization enabled by excited-state electron transfer. *Science* **2019**, *366*, 364−369.

(18) Zhang, C.; Gao, A. Z.; Nie, X.; Ye, C.-X.; Ivlev, S. I.; Chen, S.; Meggers, E. Catalytic $\alpha$-Deracemization of Ketones Enabled by Photoredox Deprotonation and Enantioselective Protonation. *J. Am. Chem. Soc.* **2021**, *143*, 13393−13400.

(19) Huang, M.; Zhang, L.; Pan, T.; Luo, S. Deracemization through photochemical *E*/*Z* isomerization of enamines. *Science* **2022**, *375*, 869−874.

(20) Review: Neveselý, T.; Wienhold, M.; Molloy, J. J.; Gilmour, R. Advances in the E → Z Isomerization of Alkenes Using Small Molecule Photocatalysts. *Chem. Rev.* **2022**, *122*, 2650−2694.

(21) Großkopf, J.; Plaza, M.; Seitz, A.; Breitenlechner, S.; Storch, G.; Bach, T. Photochemical Deracemization at $sp^3$-Hybridized Carbon Centers via a Reversible Hydrogen Atom Transfer. *J. Am. Chem. Soc.* **2021**, *143*, 21241−21245.

(22) For related work employing a reversible HAT for the epimerization of diastereoisomers, see: (a) Wang, Y.; Carder, H. M.; Wendlandt, A. E. Synthesis of rare sugar isomers through site-selective epimerization. *Nature* **2020**, *578*, 403−408. (b) Oswood, C. J.; MacMillan, D. W. C. Selective Isomerization via Transient Thermodynamic Control: Dynamic Epimerization of trans to cis Diols. *J. Am. Chem. Soc.* **2022**, *144*, 93−98. (c) Zhang, Y.-A.; Gu, X.; Wendlandt, A. E. A Change from Kinetic to Thermodynamic Control Enables trans-Selective Stereochemical Editing of Vicinal Diols. *J. Am. Chem. Soc.* **2022**, *144*, 599−605. (d) Kazerouni, A. M.; Brandes, D. S.; Davies, C. C.; Cotter, L. F.; Mayer, J. M.; Chen, S.; Ellman, J. A. Visible Light-Mediated, Highly Diastereoselective Epimerization of Lactams from the Most Accessible to the More Stable Stereoisomer. *ACS Catal.* **2022**, *12*, 7798−7803.

(23) For reviews on photochemical HAT, see: (a) Capaldo, L.; Ravelli, D.; Fagnoni, M. Direct Photocatalyzed Hydrogen Atom Transfer (HAT) for Aliphatic C−H Bonds Elaboration. *Chem. Rev.* **2022**, *122*, 1875−1924. (b) Cao, H.; Tang, X.; Tang, H.; Yuan, Y.; Wu, J. Photoinduced intermolecular hydrogen atom transfer reactions in organic synthesis. *Chem. Catal.* **2021**, *1*, 523−598. (c) Capaldo, L.; Quadri, L. L.; Ravelli, D. Photocatalytic hydrogen atom transfer: the philosopher's stone for late-stage functionalization? *Green Chem.* **2020**, *22*, 3376−3396. (d) Stateman, L. M.; Nakafuku, K. M.; Nagib, D. A. Remote C−H Functionalization via Selective Hydrogen Atom Transfer. *Synthesis* **2018**, *50*, 1569−1586.

(24) (a) Porter, G.; Suppan, P. Primary photochemical processes in aromatic molecules. Part 12. − Excited states of benzophenone derivatives. *Trans. Faraday Soc.* **1965**, *61*, 1664−1673. (b) Godfrey, T. S.; Hilpern, W.; Porter, G. Triplet-triplet absorption spectra of benzophenone and its derivatives. *Chem. Phys. Lett.* **1967**, *1*, 490−492. (c) Dormán, G.; Nakamura, H.; Pulsipher, A.; Prestwich, G. D. The Life of Pi Star: Exploring the Exciting and Forbidden Worlds of the Benzophenone Photophore. *Chem. Rev.* **2016**, *116*, 15284−15398.

(25) (a) Fielding, L. Determination of association constants (*Ka*) from solution NMR data. *Tetrahedron* **2000**, *56*, 6151−6170. (b) Thordarson, P. Determining association constants from titration experiments in supramolecular chemistry. *Chem. Soc. Rev.* **2011**, *40*,




https://doi.org/10.1021/jacs.2c11265
*J. Am. Chem. Soc.* 2023, 145, 2354−2363

1305−1323. (c) Bakowski, A.; Dressel, M.; Bauer, A.; Bach, T. Enantioselective radical cyclisation reactions of 4-substituted quinolones mediated by a chiral template. *Org. Biomol. Chem.* **2011**, *9*, 3516−3529.
(26) Simmons, E. M.; Hartwig, J. F. On the Interpretation of Deuterium Kinetic Isotope Effects in C-H Bond Functionalizations by Transition-Metal Complexes. *Angew. Chem., Int. Ed.* **2012**, *51*, 3066−3072.
(27) (a) Grimme, S.; Brandenburg, J. G.; Bannwarth, C.; Hansen, A. Consistent structures and Interactions by density functional theory with small atomic orbital basis sets. *J. Chem. Phys.* **2015**, *143*, No. 054107. (b) Neese, F. The ORCA program system. *WIREs Comput. Mol. Sci.* **2012**, *2*, 73−78. (c) Neese, F. Software update: the ORCA program system, version 4.0. *WIREs Comput. Mol. Sci.* **2018**, *8*, No. e1327.
(28) (a) Bannwarth, C.; Ehlert, S.; Grimme, S. GFN2-xTB: An Accurate and Broadly Parametrized Self-Consistent Tight-Binding Quantum Chemical Method with Multipole Electrostatics and Density-Dependent Dispersion Contributions. *J. Chem. Theory Comput.* **2019**, *15*, 1652−1671. (b) Asgeirsson, V.; Birgisson, B. O.; Bjornsson, R.; Becker, U.; Neese, F.; Riplinger, C.; Jonsson, H. Nudged Elastic Band Method for Molecular Reactions Using Energy − Weighted Springs Combined with Eigenvector Following. *J. Chem. Theory Comput.* **2021**, *17*, 4929−4945.
(29) (a) Grimme, S. Supramolecular Binding Thermodynamics by Dispersion-Corrected Density Functional Theory. *Chem. − Eur. J.* **2012**, *18*, 9955−9964. (b) Ehlert, S.; Stahn, M.; Spicher, S.; Grimme, S. Robust and Efficient Implicit Solvation Model for Fast Semi-empirical Methods. *J. Chem. Theory Comput.* **2021**, *17*, 4250−4261. (c) Weigend, F.; Ahlrichs, R. Balanced basis sets of split valence, triple zeta valence and quadruple zeta valence quality for H to Rn: Design and assessment of accuracy. *Phys. Chem. Chem. Phys.* **2005**, *7*, 3297−3305. (d) Mardirossian, N.; Head-Gordon, M. *ω*B97X-V: A 10-parameter, range23 separated hybrid, generalized gradient approximation density functional with nonlocalcorrelation, designed by a survival-of-the-fittest strategy. *Phys. Chem. Chem. Phys.* **2014**, *16*, 9904−9924.
(30) Pracht, P.; Bannwarth, C. Fast Screening of Minimum Energy Crossing Points with Semiempirical Tight-Binding Methods. *J. Chem. Theory Comput.* **2022**, *18*, 6370−6385.
(31) (a) Bannwarth, C.; Yu, J. K.; Hohenstein, E. G.; Martinez, T. J. Hole-hole Tamm-Dancoff Approximated density functional theory: A highly efficient electronic structure method incorporating dynamic and static correlation. *J. Chem. Phys.* **2020**, *153*, No. 024110. (b) Yu, J. K.; Bannwarth, C.; Hohenstein, E. G.; Martinez, T. J. Ab Initio Nonadiabatic Molecular Dynamics with Hole-Hole Tamm-Dancoff Approximated Density Functional Theory. *J. Chem. Theory Comput.* **2020**, *16*, 5499−5511. (c) Seritan, S.; Bannwarth, C.; Fales, B. S.; Hohenstein, E. G.; Isborn, C. M.; Kokkila- Schumacher, S. I. L.; Li, X.; Liu, F.; Luehr, N.; Snyder, J. W., Jr.; Song, C.; Titov, A. V.; Umtsev, I. S.; Wang, L.-P.; Martinez, T. J. TeraChem: A graphical processing unit-accelerated electronic structure package for large-scale ab initio molecular dynamics. *WIREs Comput. Mol. Sci.* **2021**, *11*, No. e1494.
(32) For some key references on the characterization of enols, see: (a) Haspra, P.; Sutter, A.; Wirz, J. Acidity of Acetophenone Enol in Aqueous Solution. *Angew. Chem., Int. Ed.* **1979**, *18*, 617−619. (b) Capon, B.; Guo, B. Simple enols. 5. (Z)- and (E)-1-Hydroxy-1,3-butadiene. *J. Am. Chem. Soc.* **1988**, *110*, 5144−5147. (c) Chiang, Y.; Kresge, A. J. Enols and Other Reactive Species. *Science* **1991**, *253*, 395−400. (d) Mardyukov, A.; Eckhardt, A. K.; Schreiner, P. R. 1,1-Ethenediol: The Long Elusive Enol of Acetic Acid. *Angew. Chem., Int. Ed.* **2020**, *59*, 5577−5580.
(33) Bandyopadhyay, B.; Pandey, P.; Banerjee, P.; Samanta, A. K.; Chakraborty, T. CH···O Interaction Lowers Hydrogen Transfer Barrier to Keto−Enol Tautomerization of *β*-Cyclohexanedione: Combined Infrared Spectroscopic and Electronic Structure Calculation Study. *J. Phys. Chem. A* **2012**, *116*, 3836−3845.
(34) (a) McGarry, P. F.; Doubleday, C. E.; Wu, C.-H.; Staab, H. A.; Turro, N. J. UV—Vis Absorption Studies of Singlet to Triplet Intersystem Crossing Rates of Aromatic Ketones: Effects of Molecular Geometry. *J. Photochem. Photobiol., A* **1994**, *77*, 109−117. (b) Cai, X.; Sakamoto, M.; Fujitsuka, M.; Majima, T. Higher Triplet Excited States of Benzophenones and Bimolecular Triplet Energy Transfer Measured by Using Nanosecond−Picosecond Two-Color/Two-Laser Flash Photolysis. *Chem. − Eur. J.* **2005**, *11*, 6471−6477. (c) Aloïse, S.; Ruckebusch, C.; Blanchet, L.; Réhault, J.; Buntinx, G.; Huvenne, J.-P. The Benzophenone $S_1(n,\pi^*) \rightarrow T_1(n,\pi^*)$ States Intersystem Crossing Reinvestigated by Ultrafast Absorption Spectroscopy and Multivariate Curve Resolution. *J. Phys. Chem. A* **2008**, *112*, 224−231. (d) Marazzi, M.; Mai, S.; Roca-Sanjuán, D.; Delcey, M. G.; Lindh, R.; González, L.; Monari, A. Benzophenone Ultrafast Triplet Population: Revisiting the Kinetic Model by Surface-Hopping Dynamics. *J. Phys. Chem. Lett.* **2016**, *7*, 622−626. (e) Zvereva, E.; Segarra-Martí, J.; Marazzi, M.; Brazard, J.; Nenov, A.; Weingart, O.; Léonard, J.; Garavelli, M.; Rivalta, I.; Dumont, E.; Assfeld, X.; Haacke, S.; Monari, A. The Effect of Solvent Relaxation in the Ultrafast Time-Resolved Spectroscopy of Solvated Benzophenone. *Photochem. Photobiol. Sci.* **2018**, *17*, 323−331. (f) Venkatraman, R. K.; Kayal, S.; Barak, A.; Orr-Ewing, A. J.; Umapathy, S. Intermolecular Hydrogen Bonding Controlled Intersystem Crossing Rates of Benzophenone. *J. Phys. Chem. Lett.* **2018**, *9*, 1642−1648. (g) Venkatraman, R. K.; Orr-Ewing, A. J. Photochemistry of Benzophenone in Solution: A Tale of Two Different Solvent Environments. *J. Am. Chem. Soc.* **2019**, *141*, 15222−15229.
(35) (a) Tsubomura, H.; Yamamoto, N.; Tanaka, S. Transient Absorption Spectra of Benzophenone Studied by the Flash Excitation. *Chem. Phys. Lett.* **1967**, *1*, 309−310. (b) Buettner, A. V.; Dedinas, J. Photoreduction of Benzophenone in Benzene. II. Flash Photolysis Study of Primary Photochemical Reactions. *J. Phys. Chem.* **1971**, *75*, 187−191. (c) Topp, M. R. Activation-Controlled Hydrogen Abstraction by Benzophenone Triplet. *Chem. Phys. Lett.* **1975**, *32*, 144−149. (d) Brede, O.; Helmstreit, W.; Mehnert, R. Nanosekunden-Pulsradiolyse und Laserphotolyse von Benzophenon in Benzol und Cyclohexan. *Z. Phys. Chem.* **1975**, *256*, 505−512. (e) Hayashi, H. Direct Observation of the 1,4-Biradical of Benzophenone with Cis-3-Methyl-2-Pentene Excited by the Fourth Harmonic of a Nd:YAG Laser. *Bull. Chem. Soc. Jpn.* **1980**, *53*, 2201−2204. (f) Bensasson, R. V.; Gramain, J.-C. Benzophenone Triplet Properties in Acetonitrile and Water. Reduction by Lactams. *J. Chem. Soc., Faraday Trans. 1* **1980**, *76*, 1801−1810. (g) Encinas, M. V.; Scaiano, J. C. Reaction of Benzophenone Triplets with Allylic Hydrogens. Laser Flash Photolysis Study. *J. Am. Chem. Soc.* **1981**, *103*, 6393−6397. (h) Nagarajan, V.; Fessenden, R. W. Flash Photolysis of Transient Radicals. Benzophenone Ketyl Radical. *Chem. Phys. Lett.* **1984**, *112*, 207−211. (i) Ramseier, M.; Senn, P.; Wirz, J. Photohydration of Benzophenone in Aqueous Acid. *J. Phys. Chem. A* **2003**, *107*, 3305−3315. (j) Sakamoto, M.; Cai, X.; Hara, M.; Tojo, S.; Fujitsuka, M.; Majima, T. Transient Absorption Spectra and Lifetimes of Benzophenone Ketyl Radicals in the Excited State. *J. Phys. Chem. A* **2004**, *108*, 8147−8150.


https://doi.org/10.1021/jacs.2c11265
*J. Am. Chem. Soc.* 2023, 145, 2354−2363

# 9 Summary

Within this dissertation, the development of novel deracemization approaches towards the diversification and improved applicability of mono-catalytic photochemical deracemizations was disclosed. Two main goals were met: the diversification of the substrate scope of deracemization reactions involving allenes by selective triplet transfer towards non-cyclic, open-chain allene amides *rac*-**69** as well as the proof of feasibility and application of a new deracemization strategy involving hydrogen atom transfer for addressing $sp^3$-hybridized tertiary carbon centers in hydantoins *rac*-**71**.

The first project was meant to prove that also acyclic substrates allow for an efficient differentiation by catalyst **38** in a deracemization reaction.[154] In order to get a defined conformation within the catalyst array, the substrate had to be designed in a way that a major conformation was adopted. It was observed that the introduction of a benzylic group at the 2-position of the substrate led to a preferred conformation, with the aryl group *anti*-periplanar to the primary amide and the amino group *syn*-periplanar to the allene. This allowed for an efficient discrimination of the two enantiomers of *rac*-**69** by only 2.5 mol% **38**, affording 19 enantiomerically enriched substrates **69** in up to quantitative yield and 93% *ee* (Scheme 31).

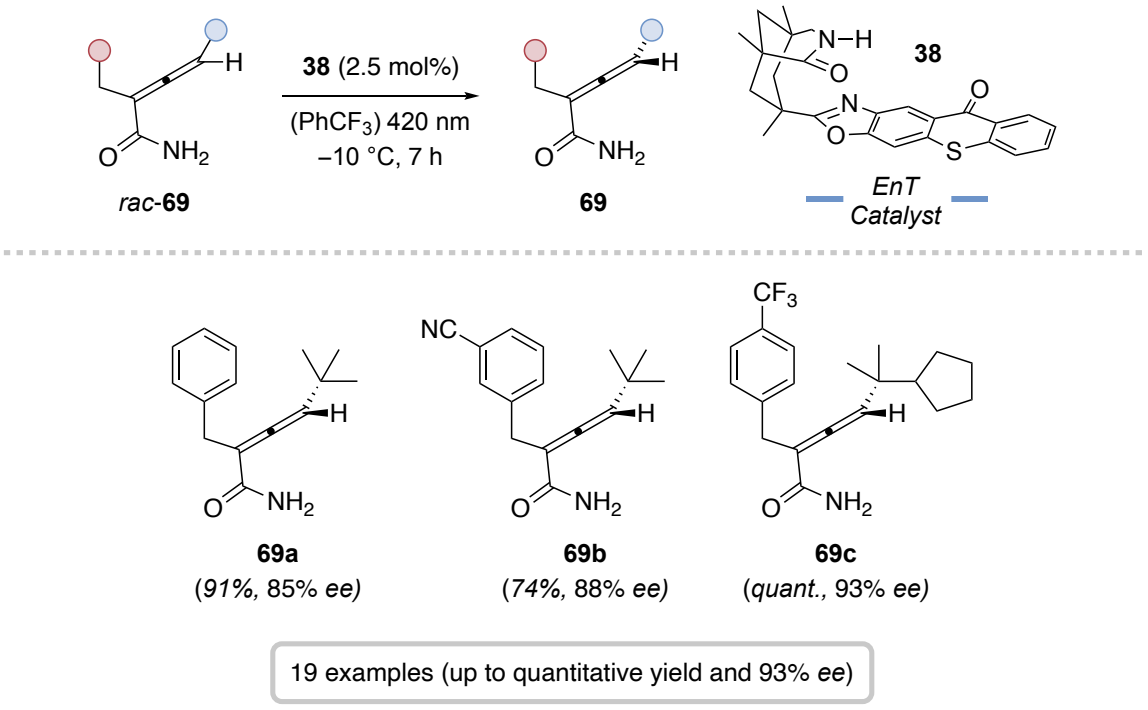


**Scheme 31.** Established conditions for the deracemization of primary allene amides *rac*-**69** and selected scope examples.

Profound DFT calculation revealed that the successful differentiation was rooted in the noncovalent interactions between the substrate and the catalyst. Apart from a slightly preferred binding of *ent*-**69**, attractive dispersion interactions between the allene moiety and the thioxanthone π-system governed the difference in the rate of triplet energy transfer. For *ent*-**69** an attractive CH–π interaction between the C($sp^2$)–H bond at the terminal allene carbon atom and the external thioxanthone benzene ring was detected, which brings the two chromophores in close proximity to each other resulting in fast energy transfer. In contrast, **69** places its benzyl moiety perpendicular to the catalyst π-system, which positions the allene farer away from the chromophore. This study underlined the vast potential of dispersion interactions to tune the enantioselectivity of photochemical reactions and the interplay of theoretical and synthetic chemistry for reaction development.

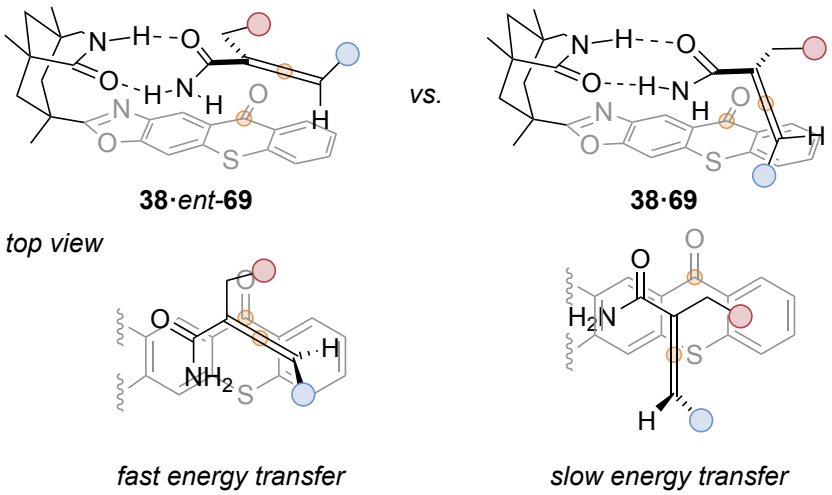


**Figure 7.** Difference in the coordination geometries of *ent*-**69** and **69** in an array with thioxanthone **38**, caused by attractive dispersion interactions. [Reprinted (adapted) with permission from *J. Am. Chem. Soc.* **2021**, *143*, 11209–11217. Copyright **2021** American Chemical Society]

The second project dealt with the development of a conceptually new method for the photochemical deracemization of abundant $sp^3$-hypridized carbon center by selective HAT.[155] As a first class of substrates, *α*-amino acid-derived hydantoins *rac*-**71** were chosen, which were amenable for deracemization by benzophenone-based catalyst **72**. In total 27 substrates could be transferred to enantiomerically enriched or even enantiopure compounds **71** with a catalyst loading of only 5 mol% (Scheme 32). It was shown that, in contrast to deracemizations based on triplet energy transfer, the steric bulk of the residue at the stereogenic center does not play a crucial role in the differentiation step as the positioning of the hydantoin in the diastereomeric complex only allows for the abstraction of the hydrogen atom of the *matched* enantiomer *ent*-**71**. Radical clock experiments

revealed the intermediacy of a carbon-centered radical and deuterium scrambling the existence of an intermolecular exchange of either a hydrogen atom or a proton between two hydantoin molecules.

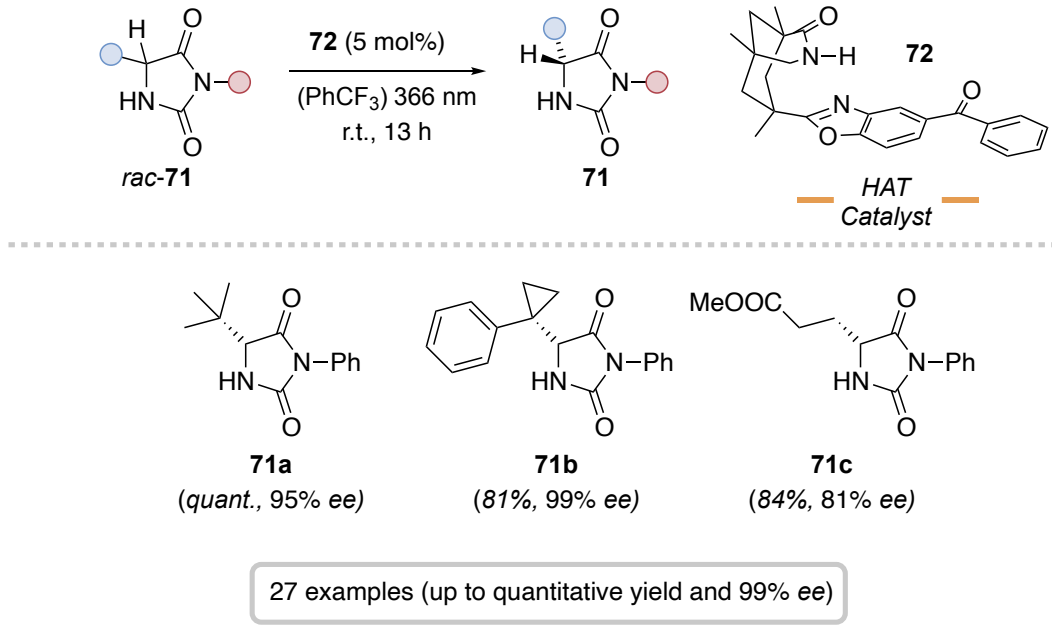


**Scheme 32.** Successful deracemization of hydantoins *rac*-**71** benzophenone-based HAT catalyst **72** furnishing an array of structurally different enantioenriched hydantoins **71**.

To deepen our understanding of the mode of action of the chiral benzophenone and to elucidate the nature of the intermediates involved in the deracemization, a collective study involving synthetic, spectroscopic and theoretical data was undertaken using *ent*-**72**.[156] A conclusive mechanistic picture was obtained that harmonized all previous findings (Scheme 33). TA spectroscopy proved that only one enantiomer is processed by *ent*-**72** by detecting a profound quenching of the triplet lifetime of the catalyst and the transient protonated ketyl radical *ent*-**73**, but only when **71** was used. Quantum chemical calculations revealed the structure of the involved complexes and showed that hydantoin-derived radical **72** does not dissociate from the catalyst but rather retains its association, explaining the absence of radical side reactions. The back HAT turned out to not directly lead to the hydantoin but to an achiral enol **74** by delivering the hydrogen atom to the adjacent carbonyl oxygen atom. The transient signal of this species could also be detected by spectroscopy. A final intermolecular tautomerization unselectively leads to the formation of both enantiomers out of which only the *matched* enantiomer re-enters the catalytic cycle.

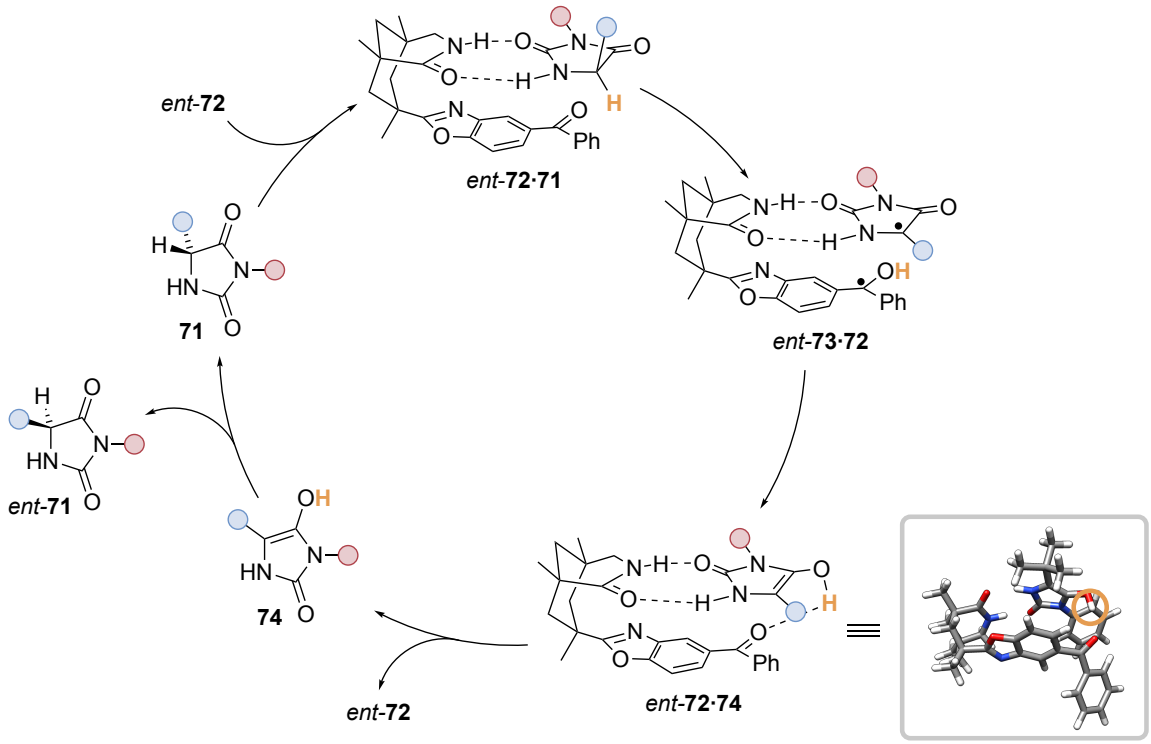


**Scheme 33.** Mechanism of the deracemization of hydantoins by chiral benzophenone *ent*-**71** elucidated by a combination of preparative, spectroscopic and theoretical investigations.

It could be shown that using reversible HAT as the selectivity governing element in deracemizations is a viable pathway of generating enantiopure compounds. Current investigations aim at the expansion of this deracemization method to other relevant substrate classes.

The presented examples as well as currently ongoing studies underline the mildness and versatility of deracemization reactions, paving the ground for further developments towards the general use of deracemizations for stereochemical editing in the synthesis of complex scaffolds.

## Abbreviations

| | |
|---|---|
| Ac | acetyl |
| Ad | adamantyl |
| Ar | aryl |
| Bn | benzyl |
| Boc | *tert*-butyloxycarbonyl |
| DFT | density functional theory |
| DNA | deoxyribonucleic acid |
| DT | decatungstate |
| *e.g.* | exempli gratia (lat.) / for example |
| *ee* | enantiomeric excess |
| *ent* | enantiomer |
| *epi* | epimer |
| Et | ethyl |
| FDA | Food and Drug Administration |
| *h* | *Planck* constant |
| HAT | hydrogen atom transfer |
| *i.e.* | id est (lat.) / that is |
| *k* | reaction rate constant |
| KIE | kinetic isotope effect |
| LA | *Lewis* acid |
| Me | methyl |
| *Mtr* | mRNA transport regulator |
| *n*-Bu | *n*-butyl |
| neop | neopentyl glycolate |
| NMR | nuclear magnetic resonance |
| PC | photocatalyst |
| PCET | proton-coupled electron transfer |
| Ph | phenyl |
| Pin | pinacolate |
| PMP | *para*-methoxyphenyl |
| r.t. | room temperature |
| *rac* | racemate |
| S | entropy |
| *sens.* | triplet energy sensitizer |

| | |
|---|---|
| *t*-Bu | tert-butyl |
| TA | transient absorption |
| TIPS | triisopropylsilyl |
| Trip | triisopropylbenzene |
| UV | ultraviolet |
| vis | visible |
| $\Delta G°$ | *Gibbs* free energy |
| λ | wavelength |
| ν | frequency |

## Licenses

The publication "*Photochemical Deracemization of Primary Allene Amides by Triplet Energy Transfer: A Combined Synthetic and Theoretical Study*" was included in this PhD thesis with permission of reference 154.

Copyright 2021 American Chemical Society. The respective license and additional information are presented here. The publication and corresponding background information can be found with following link:

https://pubs.acs.org/doi/abs/10.1021/jacs.1c05286

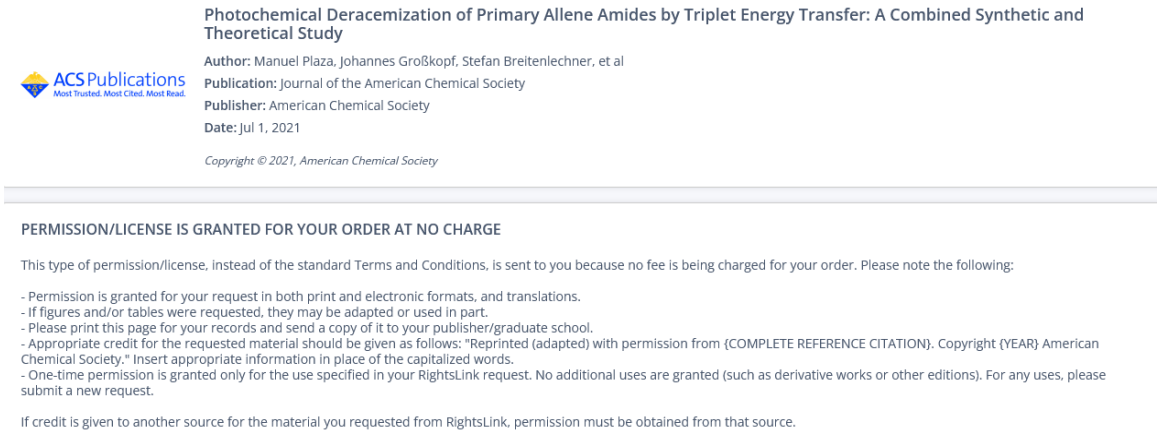

Photochemical Deracemization of Primary Allene Amides by Triplet Energy Transfer: A Combined Synthetic and Theoretical Study

**Author:** Manuel Plaza, Johannes Großkopf, Stefan Breitenlechner, et al
**Publication:** Journal of the American Chemical Society
**Publisher:** American Chemical Society
**Date:** Jul 1, 2021

*Copyright © 2021, American Chemical Society*

PERMISSION/LICENSE IS GRANTED FOR YOUR ORDER AT NO CHARGE

This type of permission/license, instead of the standard Terms and Conditions, is sent to you because no fee is being charged for your order. Please note the following:

- Permission is granted for your request in both print and electronic formats, and translations.
- If figures and/or tables were requested, they may be adapted or used in part.
- Please print this page for your records and send a copy of it to your publisher/graduate school.
- Appropriate credit for the requested material should be given as follows: "Reprinted (adapted) with permission from {COMPLETE REFERENCE CITATION}. Copyright {YEAR} American Chemical Society." Insert appropriate information in place of the capitalized words.
- One-time permission is granted only for the use specified in your RightsLink request. No additional uses are granted (such as derivative works or other editions). For any uses, please submit a new request.

If credit is given to another source for the material you requested from RightsLink, permission must be obtained from that source.

The publication "*Photochemical Deracemization at sp3-Hybridized Carbon Centers via a Reversible Hydrogen Atom Transfer*" was included in this PhD thesis with permission of reference 155.

Copyright 2021 American Chemical Society. The respective license and additional information are presented here. The publication and corresponding background information can be found with following link:

https://pubs.acs.org/doi/10.1021/jacs.1c11266

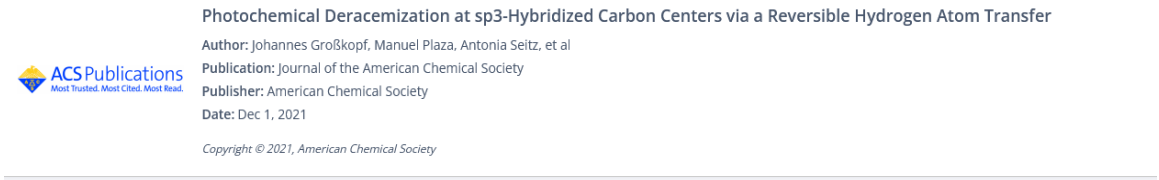

Photochemical Deracemization at sp3-Hybridized Carbon Centers via a Reversible Hydrogen Atom Transfer

**Author:** Johannes Großkopf, Manuel Plaza, Antonia Seitz, et al
**Publication:** Journal of the American Chemical Society
**Publisher:** American Chemical Society
**Date:** Dec 1, 2021

*Copyright © 2021, American Chemical Society*

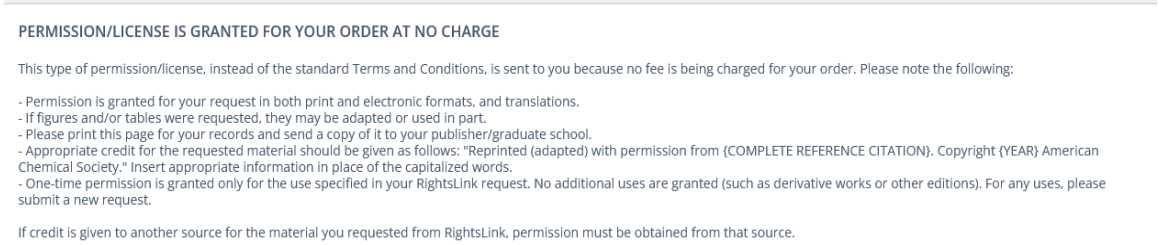

PERMISSION/LICENSE IS GRANTED FOR YOUR ORDER AT NO CHARGE

This type of permission/license, instead of the standard Terms and Conditions, is sent to you because no fee is being charged for your order. Please note the following:

- Permission is granted for your request in both print and electronic formats, and translations.
- If figures and/or tables were requested, they may be adapted or used in part.
- Please print this page for your records and send a copy of it to your publisher/graduate school.
- Appropriate credit for the requested material should be given as follows: "Reprinted (adapted) with permission from {COMPLETE REFERENCE CITATION}. Copyright {YEAR} American Chemical Society." Insert appropriate information in place of the capitalized words.
- One-time permission is granted only for the use specified in your RightsLink request. No additional uses are granted (such as derivative works or other editions). For any uses, please submit a new request.

If credit is given to another source for the material you requested from RightsLink, permission must be obtained from that source.

The publication "*Multifaceted View on the Mechanism of a Photochemical Deracemization Reaction*" was included in this PhD thesis with permission of reference 156.

Copyright 2023 American Chemical Society. The respective license and additional information are presented here. The publication and corresponding background information can be found with following link:

https://pubs.acs.org/doi/10.1021/jacs.2c11265

Multifaceted View on the Mechanism of a Photochemical Deracemization Reaction

**Author:** Roger Jan Kutta, Johannes Großkopf, Nils van Staalduinen, et al
**Publication:** Journal of the American Chemical Society
**Publisher:** American Chemical Society
**Date:** Feb 1, 2023

*Copyright © 2023, American Chemical Society*

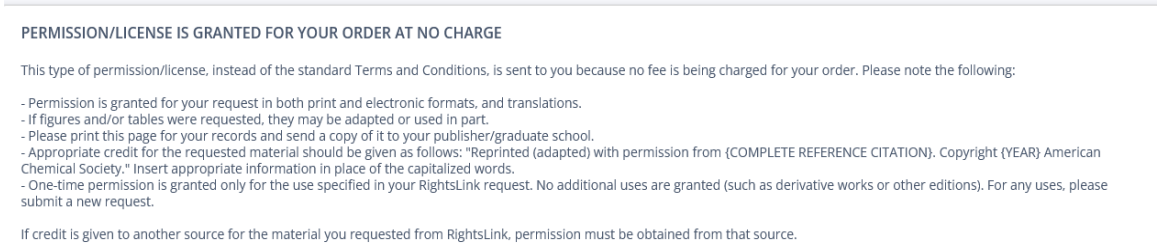

PERMISSION/LICENSE IS GRANTED FOR YOUR ORDER AT NO CHARGE

This type of permission/license, instead of the standard Terms and Conditions, is sent to you because no fee is being charged for your order. Please note the following:

- Permission is granted for your request in both print and electronic formats, and translations.
- If figures and/or tables were requested, they may be adapted or used in part.
- Please print this page for your records and send a copy of it to your publisher/graduate school.
- Appropriate credit for the requested material should be given as follows: "Reprinted (adapted) with permission from {COMPLETE REFERENCE CITATION}. Copyright {YEAR} American Chemical Society." Insert appropriate information in place of the capitalized words.
- One-time permission is granted only for the use specified in your RightsLink request. No additional uses are granted (such as derivative works or other editions). For any uses, please submit a new request.

If credit is given to another source for the material you requested from RightsLink, permission must be obtained from that source.

## References


(1) https://www.verifiedmarketresearch.com/product/chiral-chemicals-market/ (last accessed: March 28, 2023).

(2) Nguyen, L. A.; He, H.; Pham-Huy, C., Chiral drugs: an overview. *Int. J. Biomed. Sci.* **2006**, *2*, 85-100.

(3) Hancu, G.; Modroiu, A., Chiral Switch: Between Therapeutical Benefit and Marketing Strategy. *Pharmaceuticals* **2022**, *15*, 240.

(4) Singh, M.; Sethi, S.; Bhushan, R., Liquid chromatographic methods for separation, determination, and bioassay of enantiomers of etodolac: A review. *J. Sep. Sci.* **2020**, *43*, 18-30.

(5) Liu, A.; Han, J.; Nakano, A.; Konno, H.; Moriwaki, H.; Abe, H.; Izawa, K.; Soloshonok, V. A., New pharmaceuticals approved by FDA in 2020: Small-molecule drugs derived from amino acids and related compounds. *Chirality* **2022**, *34*, 86-103.

(6) Jarvis, L. M., FDA gives its nod to 53 new drugs in 2020. *Chem. Eng. News* **2021**, *99*.

(7) Ceramella, J.; Iacopetta, D.; Franchini, A.; De Luca, M.; Saturnino, C.; Andreu, I.; Sinicropi, M. S.; Catalano, A., A Look at the Importance of Chirality in Drug Activity: Some Significative Examples. *Applied Sciences* **2022**, *12*, 10909.

(8) Beasley, D. Gilead profit tops expectations despite lower COVID drug sales, outlook raised. https://www.reuters.com/business/healthcare-pharmaceuticals/gilead-reports-lower-3rd-quarter-profit-covid-drug-sales-slow-2022-10-27/ (last accessed: March 28, 2023).

(9) Bulik, B. S. Sunovion takes Urovant's overactive bladder med Gemtesa to primary care docs as promo partnership launches. https://www.fiercepharma.com/marketing/sunovion-calling-primary-care-docs-urovant-s-oab-med-gemtesa-as-promotion-partnership (last accessed: March 28, 2023).

(10) Radnor, p. Marinus Pharmaceuticals Reports Preliminary Fourth Quarter and Full Year 2022 ZTALMY® Net Product Revenue and Provides Business Update. https://www.businesswire.com/news/home/20230105005955/en/Marinus-Pharmaceuticals-Reports-Preliminary-Fourth-Quarter-and-Full-Year-2022-ZTALMY (last accessed: March 28, 2023).

(11) Sagonowsky, E. After delays, Pfizer's blockbuster-to-be eczema drug Cibinqo snags FDA nod. https://www.fiercepharma.com/pharma/pfizer-s-next-blockbuster-cibinqo-snags-fda-approval-to-challenge-sanofi-and-regeneron-s (last accessed: March 28, 2023).

(12) Mason, S. F., Origins of biomolecular handedness. *Nature* **1984**, *311*, 19-23.

(13) Hein, J. E.; Blackmond, D. G., On the origin of single chirality of amino acids and sugars in biogenesis. *Acc. Chem. Res.* **2012**, *45*, 2045-54.

(14) Meierhenrich, U., Tracing Life's Origin: From Amino Acids to Space Mission ROSETTA. In *Amino Acids and the Asymmetry of Life: Caught in the Act of Formation*, Meierhenrich, U., Ed. Springer Berlin Heidelberg: Berlin, Heidelberg, 2008; pp 1-16.

(15) H. Brooks, W.; C. Guida, W.; G. Daniel, K., The Significance of Chirality in Drug Design and Development. *Curr. Top. Med. Chem.* **2011**, *11*, 760-770.

(16) Chen, Y.; Ma, W., The origin of biological homochirality along with the origin of life. *PLoS Comput. Biol.* **2020**, *16*, e1007592.

(17) Senay, C.; Ferrari, P.; Rocher, C.; Rieger, K. J.; Winter, J.; Platel, D.; Bourne, Y., The Mtr2-Mex67 NTF2-like domain complex. Structural insights into a dual role of Mtr2 for yeast nuclear export. *J. Biol. Chem.* **2003**, *278*, 48395-403.

(18) Wigner, E., Einige Folgerungen aus der Schrödingerschen Theorie für die Termstrukturen. *Z. Phys.* **1927**, *43*, 624-652.

(19) Lee, T. D.; Yang, C. N., Question of Parity Conservation in Weak Interactions. *Phys. Rev.* **1956**, *104*, 254-258.

(20) Landau, L., On the conservation laws for weak interactions. *Nucl. Phys.* **1957**, *3*, 127-131.

(21) Meierhenrich, U., When Parity Falls: The Weak Nuclear Interaction. In *Amino Acids and the Asymmetry of Life: Caught in the Act of Formation*, Meierhenrich, U., Ed. Springer Berlin Heidelberg: Berlin, Heidelberg, 2008; pp 79-102.

(22) Ribó, J. M.; Hochberg, D.; Crusats, J.; El-Hachemi, Z.; Moyano, A., Spontaneous mirror symmetry breaking and origin of biological homochirality. *J. R. Soc. Interface* **2017**, *14*, 20170699.

(23) Ribó , J. M.; Blanco , C.; Crusats , J.; El-Hachemi , Z.; Hochberg, D.; Moyano, A., Absolute Asymmetric Synthesis in Enantioselective Autocatalytic Reaction Networks: Theoretical Games, Speculations on Chemical Evolution and Perhaps a Synthetic Option. *Chem. – Eur. J.* **2014**, *20*, 17250-17271.

(24) Hananel, U.; Ben-Moshe, A.; Diamant, H.; Markovich, G., Spontaneous and directed symmetry breaking in the formation of chiral nanocrystals. *Proc. Natl. Acad. Sci. USA* **2019**, *116*, 11159-11164.

(25) Meyerhoffer, W., Stereochemische Notizen. *Ber. Dtsch. Chem. Ges.* **1904**, *37*, 2604-2610.

(26) Vantomme, G.; Crassous, J., Pasteur and chirality: A story of how serendipity favors the prepared minds. *Chirality* **2021**, *33*, 597-601.

(27) Blackmond, D. G., Asymmetric autocatalysis and its implications for the origin of homochirality. *Proc. Natl. Acad. Sci. USA* **2004**, *101*, 5732-5736.

(28) Blackmond, D. G., Autocatalytic Models for the Origin of Biological Homochirality. *Chem. Rev.* **2020**, *120*, 4831-4847.

(29) Soai, K.; Kawasaki, T.; Matsumoto, A. Role of Asymmetric Autocatalysis in the Elucidation of Origins of Homochirality of Organic Compounds *Symmetry* **2019**, *11*, 694-713.

(30) Press Release: The Nobel Prize in Chemistry 2021. https://www.nobelprize.org/prizes/chemistry/2021/press-release/ (last accessed: March 28, 2023).

(31) Klussmann, M.; Iwamura, H.; Mathew, S. P.; Wells, D. H.; Pandya, U.; Armstrong, A.; Blackmond, D. G., Thermodynamic control of asymmetric amplification in amino acid catalysis. *Nature* **2006**, *441*, 621-623.

(32) List, B.; Lerner, R. A.; Barbas, C. F., Proline-Catalyzed Direct Asymmetric Aldol Reactions. *J. Am. Chem. Soc.* **2000**, *122*, 2395-2396.

(33) Ahrendt, K. A.; Borths, C. J.; MacMillan, D. W. C., New Strategies for Organic Catalysis: The First Highly Enantioselective Organocatalytic Diels−Alder Reaction. *J. Am. Chem. Soc.* **2000**, *122*, 4243-4244.

(34) Hajos, Z. G.; Parrish, D. R., Asymmetric synthesis of bicyclic intermediates of natural product chemistry. *J. Org. Chem.* **1974**, *39*, 1615-1621.

(35) Marzo, L.; Pagire, S. K.; Reiser, O.; König, B., Visible-Light Photocatalysis: Does It Make a Difference in Organic Synthesis? *Angew. Chem. Int. Ed.* **2018**, *57*, 10034-10072.

(36) Blackmond, D. G., "If Pigs Could Fly" Chemistry: A Tutorial on the Principle of Microscopic Reversibility. *Angew. Chem. Int. Ed.* **2009**, *48*, 2648-2654.

(37) Carey, F. A.; Sundberg, R. J., *Advanced Organic Chemistry: Part A: Structure and Mechanisms*. Springer US: 2007.

(38) Burwell, R. L., Jr.; Pearson, R. G., The Principle of Microscopic Reversibility. *J. Phys. Chem.* **1966**, *70*, 300-302.

(39) Tolman, R. C., The Principle of Microscopic Reversibility. *Proc. Natl. Acad. Sci. USA* **1925**, *11*, 436-439.

(40) Boyd, R. K., Detailed balance in chemical kinetics as a consequence of microscopic reversibility. *J. Chem. Phys.* **1974**, *60*, 1214-1222.

(41) Kathan, M.; Hecht, S., Photoswitchable molecules as key ingredients to drive systems away from the global thermodynamic minimum. *Chem. Soc. Rev.* **2017**, *46*, 5536-5550.

(42) Neveselý, T.; Wienhold, M.; Molloy, J. J.; Gilmour, R., Advances in the E → Z Isomerization of Alkenes Using Small Molecule Photocatalysts. *Chem. Rev.* **2022**, *122*, 2650-2694.

(43) Molloy, J. J.; Morack, T.; Gilmour, R., Positional and Geometrical Isomerisation of Alkenes: The Pinnacle of Atom Economy. *Angew. Chem. Int. Ed.* **2019**, *58*, 13654-13664.

(44) Ballard, A.; Narduolo, S.; Ahmed, H. O.; Keymer, N. I.; Asaad, N.; Cosgrove, D. A.; Buurma, N. J.; Leach, A. G., Racemisation in Chemistry and Biology. *Chem. – Eur. J.* **2020**, *26*, 3661-3687.

(45) Reist, M.; Testa, B.; Carrupt, P.-A.; Jung, M.; Schurig, V., Racemization, enantiomerization, diastereomerization, and epimerization: Their meaning and pharmacological significance. *Chirality* **1995**, *7*, 396-400.

(46) Harris, M. M.; Mitchell, R. K., 380. Activation energy and entropy in the racemisation of 2,2'-dibromobiphenyl-4,4'-dicarboxylic acid. *J. Chem. Soc.* **1960**, 1905-1908.

(47) Wolf, C., *Dynamic Stereochemistry of Chiral Compounds: Principles and Applications*. Royal Society of Chemistry: 2007.

(48) Fehr, C.; Galindo, J., Catalytic Enantioselective Protonation of Enolates. *Angew. Chem. Int. Ed.* **1994**, *33*, 1888-1889.

(49) Vedejs, E.; Lee, N.; Sakata, S. T., Deracemization via Highly Enantioselective Enolate Protonation Using a Chiral Aniline as the "Acid". *J. Am. Chem. Soc.* **1994**, *116*, 2175-2176.

(50) Ishihara, K.; Nakamura, S.; Kaneeda, M.; Yamamoto, H., First Example of a Highly Enantioselective Catalytic Protonation of Silyl Enol Ethers Using a Novel Lewis Acid-Assisted Brønsted Acid System. *J. Am. Chem. Soc.* **1996**, *118*, 12854-12855.

(51) Nakamura, S.; Kaneeda, M.; Ishihara, K.; Yamamoto, H., Enantioselective Protonation of Silyl Enol Ethers and Ketene Disilyl Acetals with Lewis Acid-Assisted Chiral Brønsted Acids: Reaction Scope and Mechanistic Insights. *J. Am. Chem. Soc.* **2000**, *122*, 8120-8130.

(52) Uraguchi, D.; Kinoshita, N.; Ooi, T., Catalytic Asymmetric Protonation of α-Amino Acid-Derived Ketene Disilyl Acetals Using P-Spiro Diaminodioxaphosphonium Barfates as Chiral Proton. *J. Am. Chem. Soc.* **2010**, *132*, 12240-12242.

(53) Cheon, C. H.; Kanno, O.; Toste, F. D., Chiral Brønsted Acid from a Cationic Gold(I) Complex: Catalytic Enantioselective Protonation of Silyl Enol Ethers of Ketones. *J. Am. Chem. Soc.* **2011**, *133*, 13248-13251.

(54) Mandrelli, F.; Blond, A.; James, T.; Kim, H.; List, B., Deracemizing α-Branched Carboxylic Acids by Catalytic Asymmetric Protonation of Bis-Silyl Ketene Acetals with Water or Methanol. *Angew. Chem. Int. Ed.* **2019**, *58*, 11479-11482.

(55) Zhang, C.; Gao, A. Z.; Nie, X.; Ye, C.-X.; vlev, S. I.; Chen, S.; Meggers, E., Catalytic α-Deracemization of Ketones Enabled by Photoredox Deprotonation and Enantioselective Protonation. *J. Am. Chem. Soc.* **2021**, *143*, 13393-13400.

(56) Kroutil, W.; Faber, K., Deracemization of compounds possessing a sec-alcohol or -amino group through a cyclic oxidation–reduction sequence: a kinetic treatment. *Tetrahedron: Asymmetry* **1998**, *9*, 2901-2913.

(57) Wang, H.; Tian, Y.-M.; König, B., Energy- and atom-efficient chemical synthesis with endergonic photocatalysis. *Nat. Rev. Chem.* **2022**, *6*, 745-755.

(58) Großkopf, J.; Kratz, T.; Rigotti, T.; Bach, T., Enantioselective Photochemical Reactions Enabled by Triplet Energy Transfer. *Chem. Rev.* **2022**, *122*, 1626-1653.

(59) Onsager, L., Reciprocal Relations in Irreversible Processes. I. *Phys. Rev.* **1931**, *37*, 405-426.

(60) Chapman, B.; Loiselle, D., Perspective – life and death of a photon: an intuitive non-equilibrium thermodynamic distinction between photochemistry and thermochemistry. *Photochem. Photobiol. Sci.* **2020**, *19*, 1623-1629.

(61) Ota, E.; Wang, H.; Frye, N. L.; Knowles, R. R., A Redox Strategy for Light-Driven, Out-of-Equilibrium Isomerizations and Application to Catalytic C–C Bond Cleavage Reactions. *J. Am. Chem. Soc.* **2019**, *141*, 1457-1462.

(62) Penocchio, E.; Rao, R.; Esposito, M., Nonequilibrium thermodynamics of light-induced reactions. *J. Chem. Phys.* **2021**, *155*, 114101.

(63) Wang, P.-Z.; Xiao, W.-J.; Chen, J.-R., Light-empowered contra-thermodynamic stereochemical editing. *Nat. Rev. Chem.* **2023**, *7*, 35-50.

(64) Turro, N. J.; Ramamurthy, V.; Cherry, W.; Farneth, W., The effect of wavelength on organic photoreactions in solution. Reactions from upper excited states. *Chem. Rev.* **1978**, *78*, 125-145.

(65) Fischer, E., Calculation of photostationary states in systems A .dblarw. B when only A is known. *J. Chem. Phys.* **1967**, *71*, 3704-3706.

(66) Dong, M.; Babalhavaeji, A.; Samanta, S.; Beharry, A. A.; Woolley, G. A., Red-Shifting Azobenzene Photoswitches for in Vivo Use. *Acc. Chem. Res.* **2015**, *48*, 2662-2670.

(67) Zhu, M.; Zhou, H., Azobenzene-based small molecular photoswitches for protein modulation. *Org. Biomol. Chem.* **2018**, *16*, 8434-8445.

(68) Bandara, H. M. D.; Burdette, S. C., Photoisomerization in different classes of azobenzene. *Chem. Soc. Rev.* **2012**, *41*, 1809-1825.

(69) Baroncini, M.; Ragazzon, G.; Silvi, S.; Venturi, M.; Credi, A., The eternal youth of azobenzene: new photoactive molecular and supramolecular devices. P*ure Appl. Chem.* **2015**, *87*, 537-545.

(70) An exeption is presented herein: Naskar, S.; Roy Chowdhury, S.; Mondal, S.; Maiti, D. K.; Mishra, S.; Das, I., Visible-Light-Activated Divergent Reactivity of Dienones: Dimerization in Neat Conditions and Regioselective *E* to *Z* Isomerization in the Solvent. *Org. Lett.* **2019**, *21*, 1578-1582.

(71) Kennedy, S. H.; Dherange, B. D.; Berger, K. J.; Levin, M. D., Skeletal editing through direct nitrogen deletion of secondary amines. *Nature* **2021**, *593*, 223-227.

(72) Jurczyk, J.; Lux, M. C.; Adpressa, D.; Kim, S. F.; Lam, Y.-h.; Yeung, C. S.; Sarpong, R., Photomediated ring contraction of saturated heterocycles. *Science* **2021**, *373*, 1004-1012.

(73) Jurczyk, J.; Woo, J.; Kim, S. F.; Dherange, B. D.; Sarpong, R.; Levin, M. D., Single-atom logic for heterocycle editing. *Nat. Synth.* **2022**, *1*, 352-364.

(74) Tan, G.; Glorius, F., Stereochemical Editing. *Angew. Chem. Int. Ed.* **2022**, *62*, e202217840.

(75) Siau, W.-Y.; Zhang, Y.; Zhao, Y., Stereoselective Synthesis of Z-Alkenes. In *Stereoselective Alkene Synthesis*, Wang, J., Ed. Springer Berlin Heidelberg: Berlin, Heidelberg, 2012; pp 33-58.

(76) Strieth-Kalthoff, F.; James, M. J.; Teders, M.; Pitzer, L.; Glorius, F., Energy transfer catalysis mediated by visible light: principles, applications, directions. *Chem. Soc. Rev.* **2018**, *47*, 7190-7202.

(77) Hammond, G. S.; Saltiel, J., Mechanisms of Photoreactions in Solution. XVIII. Energy Transfer with Nonvertical Transitions. *J. Am. Chem. Soc.* **1963**, *85*, 2516-2517.

(78) Hammond, G. S.; Saltiel, J.; Lamola, A. A.; Turro, N. J.; Bradshaw, J. S.; Cowan, D. O.; Counsell, R. C.; Vogt, V.; Dalton, C., Mechanisms of Photochemical Reactions in Solution. XXII.1 Photochemical cis-trans Isomerization. *J. Am. Chem. Soc.* **1964**, *86*, 3197-3217.

(79) Hammond, G. S.; Wyatt, P.; DeBoer, C. D.; Turro, N. J., Photosensitized Isomerization Involving Saturated Centers. *J. Am. Chem. Soc.* **1964**, *86*, 2532-2533.

(80) Saltiel, J.; Hammond, G. S., Mechanisms of Photochemical Reactions in Solution. XVII. cis-trans Isomerization of the Stilbenes by Excitation Transfer from Low Energy Sensitizers. *J. Am. Chem. Soc.* **1963**, *85*, 2515-2516.

(81) Gray, H. B.; Wrighton, M.; Hammond, G. S., Metal carbonyl photoassisted cis-trans isomerization of stilbene. *J. Am. Chem. Soc.* **1971**, *93*, 3285-3287.

(82) Arai, T.; Sakuragi, H.; Tokumaru, K., Photosensitized cis-trans Isomerization of β-Alkylstyrenes. *Bull. Chem. Soc. Jpn.* **1982**, *55*, 2204-2207.

(83) Arai, T.; Sakuragi, H.; Tokumaru, K., Unusual behaviour of *β-tert*-alkylstyrenes in photosensitized *cis–trans* isomerization. Structural effects on triplet energy trasnfer. *Chem. Lett.* **1980**, *9*, 261-264.

(84) Gai, F.; Hasson, K. C.; McDonald, J. C.; Anfinrud, P. A., Chemical Dynamics in Proteins: The Photoisomerization of Retinal in Bacteriorhodopsin. *Science* **1998**, *279*, 1886-1891.

(85) Hasson, K. C.; Gai, F.; Anfinrud, P. A., The photoisomerization of retinal in bacteriorhodopsin: Experimental evidence for a three-state model. *Proc. Natl. Acad. Sci. USA* **1996**, *93*, 15124-15129.

(86) Metternich, J. B.; Gilmour, R., A Bio-Inspired, Catalytic E → Z Isomerization of Activated Olefins. *J. Am. Chem. Soc.* **2015**, *137*, 11254-11257.

(87) Metternich, J. B.; Artiukhin, D. G.; Holland, M. C.; von Bremen-Kühne, M.; Neugebauer, J.; Gilmour, R., Photocatalytic E → Z Isomerization of Polarized Alkenes Inspired by the Visual Cycle: Mechanistic Dichotomy and Origin of Selectivity. *J. Org. Chem.* **2017**, *82*, 9955-9977.

(88) Livingstone, K.; Tenberge, M.; Pape, F.; Daniliuc, C. G.; Jamieson, C.; Gilmour, R., Photocatalytic E → Z Isomerization of β-Ionyl Derivatives. *Org. Lett.* **2019**, *21*, 9677-9680.

(89) Ramamurthy, V.; Bopp, T. T.; Liu, R. S. H., NMR studies of 7-cis-β-ionol and related compounds. Ring-chain conformational preference. *Tetrahedron Lett.* **1972**, *13*, 3915-3916.

(90) Ramamurthy, V.; Butt, Y.; Yang, C.; Yang, P.; Liu, R. S. H., Photochemistry of polyenes. III. Preparation of 7-cis-ionyl and ionylidene derivatives and other sterically hindered olefins by one-way sensitized geometric isomerization. *J. Org. Chem.* **1973**, *38*, 1247-1249.

(91) Ramamurthy, V.; Liu, R. S. H., Photochemistry of polyenes. VII. Preferred directions of photoisomerization of ionylideneacetaldehyde and the C18-tetraene ketone in the retinal series. Synthesis of the hindered 7-cis isomers. *J. Am. Chem. Soc.* **1974**, *96*, 5625-5627.

(92) Ramamurthy, V.; Tustin, G.; Yau, C. C.; Liu, R. S. H., Preparation of sterically hindered geometric isomers of 7-cis-β-ionyl and β-ionylidene derivatives in the vitamin A series. *Tetrahedron* **1975**, *31*, 193-199.

(93) Molloy, J. J.; Schäfer, M.; Wienhold, M.; Morack, T.; Daniliuc, C. G.; Gilmour, R., Boron-enabled geometric isomerization of alkenes via selective energy-transfer catalysis. *Science* **2020**, *369*, 302-306.

(94) Neveselý, T.; Molloy, J. J.; McLaughlin, C.; Brüss, L.; Daniliuc, C. G.; Gilmour, R., Leveraging the n→ $\pi$ * Interaction in Alkene Isomerization by Selective Energy Transfer Catalysis. *Angew. Chem. Int. Ed.* **2022**, *61*, e202113600.

(95) Ipatieff, V. N.; Pines, H.; Schaad, R. E., Isomerization of Normal Butenes. *J. Am. Chem. Soc.* **1934**, *56*, 2696-2698.

(96) Janssen-Müller, D.; Sahoo, B.; Sun, S.-Z.; Martin, R., Tackling Remote sp3 C−H Functionalization via Ni-Catalyzed "chain-walking" Reactions. *Isr. J. Chem.* **2020**, *60*, 195-206.

(97) Sommer, H.; Juliá-Hernández, F.; Martin, R.; Marek, I., Walking Metals for Remote Functionalization. *ACS Cent. Sci.* **2018**, *4*, 153-165.

(98) Meng, Q.-Y.; Schirmer, T. E.; Katou, K.; König, B., Controllable Isomerization of Alkenes by Dual Visible-Light-Cobalt Catalysis. *Angew. Chem. Int. Ed.* **2019**, *58*, 5723-5728.

(99) Kobayashi, T.; Yorimitsu, H.; Oshima, K., Cobalt-Catalyzed Isomerization of 1-Alkenes to (*E*)-2-Alkenes with Dimethylphenylsilylmethylmagnesium Chloride and Its Application to the Stereoselective Synthesis of (*E*)-Alkenylsilanes. *Chem. – Asian J.* **2009**, *4*, 1078-1083.

(100) Crossley, S. W. M.; Barabé, F.; Shenvi, R. A., Simple, Chemoselective, Catalytic Olefin Isomerization. *J. Am. Chem. Soc.* **2014**, *136*, 16788-16791.

(101) Henin, F.; Mortezaei, R.; Muzart, J.; Pete, J.-P., Enantioselective photodeconjugation of conjugated lactones induced by small amounts of a chiral inductor. *Tetrahedron Lett.* **1985**, *26*, 4945-4948.

(102) Piva, O.; Pete, J.-P., Highly enantioselective protonation of photodienols an unusual substituent effect on the induced chirality. *Tetrahedron Lett.* **1990**, *31*, 5157-5160.

(103) Morack, T.; Onneken, C.; Nakakohara, H.; Mück-Lichtenfeld, C.; Gilmour, R., Enantiodivergent Prenylation via Deconjugative Isomerization. *ACS Catal.* **2021**, *11*, 11929-11937.

(104) Noyori, R.; Inoue, H.; Kato, M., Photolysis of 1-acetylcyclooctene. Direct observation of dienol intermediate in photochemical deconjugation of .alpha.,.beta.-unsaturated ketone. *J. Am. Chem. Soc.* **1970**, *92*, 6699-6700.

(105) Zhao, K.; Knowles, R. R., Contra-Thermodynamic Positional Isomerization of Olefins. *J. Am. Chem. Soc.* **2022**, *144*, 137-144.

(106) Occhialini, G.; Palani, V.; Wendlandt, A. E., Catalytic, contra-Thermodynamic Positional Alkene Isomerization. *J. Am. Chem. Soc.* **2022**, *144*, 145-152.

(107) Fukuzumi, S.; Kochi, J. K., Mechanism of homolytic substitution (SH2) reactions. Radical chain cleavage of alkylmetals by photochemically generated iodine atoms. *J. Org. Chem.* **1980**, *45*, 2654-2662.

(108) Wang, Y.; Begley, T. P., Mechanistic Studies on CysS – A Vitamin B12-Dependent Radical SAM Methyltransferase Involved in the Biosynthesis of the tert-Butyl Group of Cystobactamid. *J. Am. Chem. Soc.* **2020**, *142*, 9944-9954.

(109) Liu, W.; Lavagnino, M. N.; Gould, C. A.; Alcazar, J.; MacMillan, D. W. C., A biomimetic $S_H2$ cross-coupling mechanism for quaternary $sp^3$-carbon formation. *Science* **2021**, *374*, 1258-1263.

(110) Dass Gupta, B.; Funabiki, T.; Johnson, M. D., Regiospecific homolytic displacement, with rearrangement, of cobaloxime(II) from allylcobaloxime(III) complexes by trichloromethyl radicals. *J. Am. Chem. Soc.* **1976**, *98*, 6697-6698.

(111) Johnson, M. D., Bimolecular homolytic displacement of transition-metal complexes from carbon. *Acc. Chem. Res.* **1983**, *16*, 343-349.

(112) Oswood, C. J.; MacMillan, D. W. C., Selective Isomerization via Transient Thermodynamic Control: Dynamic Epimerization of trans to cis Diols. *J. Am. Chem. Soc.* **2022**, *144*, 93-98.

(113) Wang, Y.; Carder, H. M.; Wendlandt, A. E., Synthesis of rare sugar isomers through site-selective epimerization. *Nature* **2020**, *578*, 403-408.

(114) Le, C.; Liang, Y.; Evans, R. W.; Li, X.; MacMillan, D. W. C., Selective $sp^3$ C–H alkylation via polarity-match-based cross-coupling. *Nature* **2017**, *547*, 79-83.

(115) Carder, H. M.; Wang, Y.; Wendlandt, A. E., Selective Axial-to-Equatorial Epimerization of Carbohydrates. *J. Am. Chem. Soc.* **2022**, *144*, 11870-11877.

(116) Zhang, Y.-A.; Palani, V.; Seim, A. E.; Wang, Y.; Wang, K. J.; Wendlandt, A. E., Stereochemical editing logic powered by the epimerization of unactivated tertiary stereocenters. *Science* **2022**, *378*, 383-390.

(117) Shen, Z.; Walker, M. M.; Chen, S.; Parada, G. A.; Chu, D. M.; Dongbang, S.; Mayer, J. M.; Houk, K. N.; Ellman, J. A., General Light-Mediated, Highly Diastereoselective Piperidine Epimerization: From Most Accessible to Most Stable Stereoisomer. *J. Am. Chem. Soc.* **2021**, *143*, 126-131.

(118) Pirkle, W. H.; Reno, D. S., Extension of chromatographically-derived molecular recognition concepts to first order asymmetric transformations. *J. Am. Chem. Soc.* **1987**, *109*, 7189-7190.

(119) Nakano, S.; Kozuka, K.; Minamino, Y.; Karasuda, H.; Hasebe, F.; Ito, S., Ancestral L-amino acid oxidases for deracemization and stereoinversion of amino acids. *Commun. Chem.* **2020**, *3*, 181.

(120) Aleku, G. A.; Mangas-Sanchez, J.; Citoler, J.; France, S. P.; Montgomery, S. L.; Heath, R. S.; Thompson, M. P.; Turner, N. J., Kinetic Resolution and Deracemization of Racemic Amines Using a Reductive Aminase. *ChemCatChem* **2018**, *10*, 515-519.

(121) Alexeeva, M.; Enright, A.; Dawson, M. J.; Mahmoudian, M.; Turner, N. J., Deracemization of α-Methylbenzylamine Using an Enzyme Obtained by In Vitro Evolution. *Angew. Chem. Int. Ed.* **2002**, *41*, 3177-3180.

(122) Hölzl-Hobmeier, A.; Bauer, A.; Silva, A. V.; Huber, S. M.; Bannwarth, C.; Bach, T., Catalytic deracemization of chiral allenes by sensitized excitation with visible light. *Nature* **2018**, *564*, 240-243.

(123) Plaza, M.; Jandl, C.; Bach, T., Photochemical Deracemization of Allenes and Subsequent Chirality Transfer. *Angew. Chem. Int. Ed.* **2020**, *59*, 12785-12788.

(124) Suarez, M.; Schuster, G. B., Photoresolution of an Axially Chiral Bicyclo[3.3.0]octan-3-one: Phototriggers for a Liquid-Crystal-Based Optical Switch. *J. Am. Chem. Soc.* **1995**, *117*, 6732-6738.

(125) Tejedor, R. M.; Oriol, L.; Serrano, J. L.; Sierra, T., Chiral photochemical induction in liquid crystals. *J. Mater. Chem.* **2008**, *18*, 2899-2908.

(126) Kratz, T.; Steinbach, P.; Breitenlechner, S.; Storch, G.; Bannwarth, C.; Bach, T., Photochemical Deracemization of Chiral Alkenes via Triplet Energy Transfer. *J. Am. Chem. Soc.* **2022**, *144*, 10133-10138.

(127) Shanshal, M., Contribution of the Walsh Orbitals to the Excited States of Conjugated Cyclopropyl Molecules (A PMO Treatment). *Z. Naturforsch. A* **1976**, *31*, 488-493.

(128) Hammond, G. S.; Cole, R. S., Asymmetric Induction during Energy Transfer1. *J. Am. Chem. Soc.* **1965**, *87*, 3256-3257.

(129) Ouannes, C.; Beugelmans, R.; Roussi, G., Asymmetric induction during transfer of triplet energy. *J. Am. Chem. Soc.* **1973**, *95*, 8472-8474.

(130) Li, X.; Kutta, R. J.; Jandl, C.; Bauer, A.; Nuernberger, P.; Bach, T., Photochemically Induced Ring Opening of Spirocyclopropyl Oxindoles: Evidence for a Triplet 1,3-Diradical Intermediate and Deracemization by a Chiral Sensitizer. *Angew. Chem. Int. Ed.* **2020**, *59*, 21640-21647.

(131) Tröster, A.; Bauer, A.; Jandl, C.; Bach, T., Enantioselective Visible-Light-Mediated Formation of 3-Cyclopropylquinolones by Triplet-Sensitized Deracemization. *Angew. Chem. Int. Ed.* **2019**, *58*, 3538-3541.

(132) Hammond, G. S.; Gotthardt, H.; Coyne, L. M.; Axelrod, M.; Rayner, D. R.; Mislow, K., Energy Transfer in the Racemization of Aryl Sulfoxides. *J. Am. Chem. Soc.* **1965**, *87*, 4959-4960.

(133) Jenks, W. S.; Lee, W.; Shutters, D., Photochemistry and Photophysics of Aromatic Sulfoxides. 1 Characterization of the Triplets at Cryogenic Temperatures. *J. Phys. Chem.* **1994**, *98*, 2282-2289.

(134) Wimberger, L.; Kratz, T.; Bach, T., Photochemical Deracemization of Chiral Sulfoxides Catalyzed by a Hydrogen-Bonding Xanthone Sensitizer. *Synthesis* **2019**, *51*, 4417-4416.

(135) Fu, N.; Zhang, L.; Li, J.; Luo, S.; Cheng, J.-P., Chiral Primary Amine Catalyzed Enantioselective Protonation via an Enamine Intermediate. *Angew. Chem. Int. Ed.* **2011**, *50*, 11451-11455.

(136) Huang, M.; Zhang, L.; Pan, T.; Luo, S., Deracemization through photochemical E/Z isomerization of enamines. *Science* **2022**, *375*, 869-874.

(137) Shin, N. Y.; Ryss, J. M.; Zhang, X.; Miller, S. J.; Knowles, R. R., Light-driven deracemization enabled by excited-state electron transfer. *Science* **2019**, *366*, 364-369.

(138) Gu, Z.; Zhang, L.; Li, H.; Cao, S.; Yin, Y.; Zhao, X.; Ban, X.; Jiang, Z., Deracemization through Sequential Photoredox-Neutral and Chiral Brønsted Acid Catalysis. *Angew. Chem. Int. Ed.* **2022**, *61*, e202211241.

(139) Lin, L.; Bai, X.; Ye, X.; Zhao, X.; Tan, C.-H.; Jiang, Z., Organocatalytic Enantioselective Protonation for Photoreduction of Activated Ketones and Ketimines Induced by Visible Light. *Angew. Chem. Int. Ed.* **2017**, *56*, 13842-13846.

(140) Yin, Y.; Dai, Y.; Jia, H.; Li, J.; Bu, L.; Qiao, B.; Zhao, X.; Jiang, Z., Conjugate Addition–Enantioselective Protonation of N-Aryl Glycines to α-Branched 2-Vinylazaarenes via Cooperative Photoredox and Asymmetric Catalysis. *J. Am. Chem. Soc.* **2018**, *140*, 6083-6087.

(141) Steinlandt, P. S.; Zuo, W.; Harms, K.; Meggers, E., Bis-Cyclometalated Indazole Chiral-at-Rhodium Catalyst for Asymmetric Photoredox Cyanoalkylations. *Chem. – Eur. J.* **2019**, *25*, 15333-15340.

(142) Gualandi, A.; Marchini, M.; Mengozzi, L.; Kidanu, H. T.; Franc, A.; Ceroni, P.; Cozzi, P. G., Aluminum(III) Salen Complexes as Active Photoredox Catalysts. *Eur. J. Org. Chem.* **2020**, *2020*, 1486-1490.

(143) Onneken, C.; Morack, T.; Sokolova, O.; Niemeyer, N.; Mück-Lichtenfeld, C.; Daniliuc, C.; Neugebauer, J.; Gilmour, R., Light-Enabled Deracemization of Cyclopropanes by Al-Salen Photocatalysis. *ChemRxiv* **2022** (last accessed: March 28, 2023).

(144) Moynihan, H. A.; Hayes, J. A.; Eccles, K. S.; Coles, S. J.; Lawrence, S. E., Hydrogen bonding in crystal forms of primary amide functionalised glucose and cellobiose. *Carbohydr. Res.* **2013**, *374*, 29-39.

(145) Eberhardt, E. S.; Raines, R. T., Amide-Amide and Amide-Water Hydrogen Bonds: Implications for Protein Folding and Stability. *J. Am. Chem. Soc.* **1994**, *116*, 2149-2150.

(146) Dressel, M.; Bach, T., Chirality Multiplication and Efficient Chirality Transfer in exo- and endo-Radical Cyclization Reactions of 4-(4‘-Iodobutyl)quinolones. *Org. Lett.* **2006**, *8*, 3145-3147.

(147) Lovering, F.; Bikker, J.; Humblet, C., Escape from Flatland: Increasing Saturation as an Approach to Improving Clinical Success. *J. Med. Chem.* **2009**, *52*, 6752-6756.

(148) Konnert, L.; Lamaty, F.; Martinez, J.; Colacino, E., Recent Advances in the Synthesis of Hydantoins: The State of the Art of a Valuable Scaffold. *Chem. Rev.* **2017**, *117*, 13757-13809.

(149) Luo, Y.-R., *Handbook of Bond Dissociation Energies in Organic Compounds*. CRC Press: Boca Raton, 2007.

(150) Bauer, A.; Westkämper, F.; Grimme, S.; Bach, T., Catalytic enantioselective reactions driven by photoinduced electron transfer. *Nature* **2005**, *436*, 1139-1140.

(151) Braeuchle, C.; Burland, D. M.; Bjorklund, G. C., Hydrogen abstraction by benzophenone studied by holographic photochemistry. *J. Phys. Chem.* **1981**, *85*, 123-127.

(152) Walling, C.; Gibian, M. J., Hydrogen Abstraction by the Triplet State of Benzophenone. *J. Am. Chem. Soc.* **1964**, *86*, 3902-3903.

(153) Capaldo, L.; Ravelli, D.; Fagnoni, M., Direct Photocatalyzed Hydrogen Atom Transfer (HAT) for Aliphatic C–H Bonds Elaboration. *Chem. Rev.* **2022**, *122*, 1875-1924.

(154) Plaza, M.; Großkopf, J.; Breitenlechner, S.; Bannwarth, C.; Bach, T., Photochemical Deracemization of Primary Allene Amides by Triplet Energy Transfer: A Combined Synthetic and Theoretical Study. *J. Am. Chem. Soc.* **2021**, *143*, 11209-11217.

(155) Großkopf, J.; Plaza, M.; Seitz, A.; Breitenlechner, S.; Storch, G.; Bach, T., Photochemical Deracemization at sp3-Hybridized Carbon Centers via a Reversible Hydrogen Atom Transfer. *J. Am. Chem. Soc.* **2021**, *143*, 21241-21245.

(156) Kutta, R. J.; Großkopf, J.; van Staalduinen, N.; Seitz, A.; Pracht, P.; Breitenlechner, S.; Bannwarth, C.; Nuernberger, P.; Bach, T., Multifaceted View on the Mechanism of a Photochemical Deracemization Reaction. *J. Am. Chem. Soc.* **2023**, *145*, 2354-2363.